Theses and Dissertations

12-15-2014

Design and Development of a Novel Class of Cell Cycle CDK Inhibitors Targeting the Cyclin Binding Groove Utilizing the Replace Strategy

Padmavathy Nandha Premnath
University of South Carolina - Columbia

Follow this and additional works at: http://scholarcommons.sc.edu/etd

DESIGN AND DEVELOPMENT OF A NOVEL CLASS OF CELL CYCLE CDK INHIBITORS TARGETING THE CYCLIN BINDING GROOVE UTILIZING THE REPLACE STRATEGY

by

Padmavathy Nandha Premnath

Bachelor of Pharmacy
The Tamilnadu Dr. MGR Medical University, 2000

Master of Pharmacy
The Tamilnadu Dr. MGR Medical University, 2003

_____

Submitted in Partial Fulfillment of the Requirements

For the Degree of Doctor of Philosophy in

Pharmaceutical Sciences

South Carolina College of Pharmacy

University of South Carolina

2014

Accepted by:

Campbell McInnes, Major Professor

James Chapman, Committee Member

Michael Wyatt, Committee Member

Thomas Dix, Committee Member

Lukasz Lebioda, Committee Member

Lacy Ford, Vice Provost and Dean of Graduate Studies

DEDICATION

I would like to dedicate this work to my grandmother who lost her life battling with

cancer.

ACKNOWLEDGEMENTS

ABSTRACT

Inhibition of CDK2 activity in G1 and S phases of the cell cycle can promote selective apoptosis of cancer cells through the E2F1 pathway. Currently available CDK inhibitors target the ATP binding pocket and result in lack of specificity for the cell cycle vs. the transcriptional CDKs. It has been shown that a peptide HAKRRLIF derived from the tumor suppressor p21 binds to the cyclin binding groove (CBG) and selectively inhibits cell cycle CDKs (CDK2/Cyclin A, CDK2/Cyclin E and CDK4/Cyclin D). The CBG is unique to cell cycle CDKs hence targeting this site avoids the inhibition of transcriptional CDKs can potentially lead to toxicity. The goal of this project is to iteratively convert potent cyclin groove inhibitory (CGI) peptides into more drug like molecules called FLIPs (Fragment ligated inhibitory peptides) using the REPLACE strategy (Replacement with Partial Ligand Alternatives through Computational Enrichment).

FLIPs were constructed by sequentially replacing key peptide binding determinants for RRLIF with fragment like small molecules in order to obtain a non-ATP competitive inhibitor of cell cycle CDKs with improved drug like properties. Fragment alternative capping groups were evaluated by docking, synthesis and testing of FLIPs in competitive binding and cellular viability assays. Partial Ligand Alternatives were identified which interacted with the main subsites of the N-terminal tetrapeptide of HAKRRLIF and were derivatives of phenyl heterocyclic carboxylic acids, furoic, picolinic and benzoic acids. The most effective Ncap was found to be 1-(3,5-

dichlorophenyl)-5-methyl-1H-1,2,4-triazole-3-carboxylic acid (35DCPT) ligated to RLIF. In a further iteration of REPLACE, the C-terminal motif was modified with β-homoleucine (βLeu) and N-Methyl Phe or 3-Thienylalanine in order to improve metabolic stability. The lead compound after Ncap and Ccap optimization was found to be 35DCPT-R{βLeu}{3TA}-NH$_2$ (SCCP5964) which has respectable antiproliferative activity and is also capable of inducing a G1 cell cycle arrest. The REPLACE strategy has therefore been further validated in the development of FLIPs molecules as non-ATP competitive CDK inhibitors. These cyclin groove inhibitors represent next generation CDK therapeutics having anti-tumor activity consistent with on target inhibition and demonstrated potential for drug development.

TABLE OF CONTENTS

LIST OF TABLES

LIST OF FIGURES

CHAPTER 1

INTRODUCTION

1.1.Cancer

Cancer is a group of diseases caused by uncontrolled proliferation of cells. There are more than 200 types of tumors originating from various types of cells affecting different organs. The major types of cancer are classified into broad categories including carcinomas, sarcomas, leukemias, lymphomas and cancers of the central nervous system. Carcinomas are types of cancer affecting skin or tissues covering internal organs, sarcomas originate in bones, cartilage, fat, muscle, blood vessels or connective tissues, leukemias arise in blood and bone marrow, lymphomas affects lympocytes and the CNS cancers are related to the brain and spinal cord[1]. Cancer is one of the greatest burdens on society and is one of the leading causes of death worldwide. In 2008, the global cancer mortality incidence was estimated to be 7.6 million and where this accounted for 13% of all deaths in that year. It has been predicted that annually, 13.1 million deaths will occur by 2030 due to cancer[2]. In the United States, one in four deaths is due to cancer and more than 1.66 million new cases and more than 0.56 million deaths occurred in 2014[2,3,4].

The most frequent deaths arise from the cancers of lung, stomach, liver, colon and breast. Cancer is caused by various factors which include among others chemicals, radiation, food, aging, hormones, infections, and tobacco. Some of the common preventable contributing factors include high body mass index, low fiber intake, lack of

physical activity, alcohol and smoking account which combined represent 30% of cancerdeaths. Tobacco alone contributes to 22% of global cancer deaths and 71% of all lung cancers. Cancer treatment methods include surgery, radiation and chemotherapy all of which are associated with significant negative outcomes. Surgery is generally not useful when cancer has metastasized to various parts of the body whereas chemotherapy and radiation therapy are not specific for cancer cells which results in side effects from toxicity on normal cells[2,3,5].

1.2 History of chemotherapy

Currently, there are about 200 drugs approved for cancer and hundreds more in clinical development[6]. Anti-cancer drug development has undergone many advances since the initial development of cytotoxic agents leading to the sophisticated targeted therapeutics available now[7],[8]. The development of chemotherapeutic agents started in the era of World War II in 1940s with the nitrogen mustards. At the outset, cancer drugs were based on cytotoxics that kill rapidly dividing cells and many of these drugs are widely used. The nitrogen mustards were studied and developed at Yale School of Medicine to treat non-Hodgkin's lymphoma. These compounds alkylate DNA on purine bases leading to crosslinking of strands and as a result inducing apoptosis[9]. The next step in chemotherapeutic agents was the development of antifolate treatments by Sidney Farber at the Harvard Medical School and at the Children's hospital at Boston. Methotrexate is an effective drug in the antimetabolite class and which was initially used in the treatment of acute lymphoblastic leukemia[10]. Later this drug was found to be effective in breast, ovary, bladder and head and neck cancers[7,11,12]. The antifolates bind to and inhibit dihydrofolate reductase which acts at the level of the building blocks of DNA and inhibits

the synthesis of thymidylate and purines leading to apoptosis[13]. Another example in this class is 6-Mercaptopurine (immunosuppressive agent)[14]. Vinca alkaloids are another class of drugs that act in mitosis causing spindle poisoning and also inhibit microtubule polymerization. These were developed by Eli Lilly and approved by the FDA in 1963. Prednisone (modifies gene transcription and affects the synthesis of various proteins) was developed in the 1950s and used for acute lymphoblastic leukemia, Non-Hodgkin lymphomas and multiple myeloma[7,8].

Drug resistance is major problem in cancer treatment as cancer cells mutate and become resistant to a single agent. Hence combination therapies were developed through the use of multiple drugs with different mechanism of action in attempts to overcome drug resistance problem. Combination therapies such as POMP (combination of methotrexate, vincristine, 6-MP and prednisone) and MOPP (combination of nitrogen mustard, vincristine, procarbazine and prednisone) regimens were validated in 1960s[15,16,17]. During the era of combination therapies, several natural product drugs such as the taxanes[18] (e.g. paclitaxel, an antimitotic agent) and camphothecins (topoisomerase inhibitor) were discovered which were later used for the treatment of ovarian and colon cancer respectively. Taxanes were discovered in the 1960s however not approved by the FDA until the 1990s[19]. Cisplatin, a platinum based drug was a serendipitous discovery in 1960s that was then approved for testicular cancer. Carboplatin was later developed as an improved and less toxic version of cisplatin. These drugs bind to DNA and interfere with DNA transcription and replication[20]. Many of the cancer therapeutics developed in early years of chemotherapy had serious drawbacks due to acute and long term toxicities affecting various parts of the body. These arise from the non-selectivity of conventional

3

therapeutics in targeting both cancer and normal cells. Molecular biology and genetics approaches helped in understanding the deregulation of signaling pathways and molecular defects in tumors. This lead to the development of drugs that target molecular pathways specific for cancer cells which marked the beginning of the new generation of targeted therapeutics in 1980s[7].

1.3 Targeted therapy

In targeted therapy, drugs are designed to specifically block the function of protein molecules that cause molecular defects ultimately leading to tumor growth and progression. Such defects are considered as important hallmarks of cancer and are mainly observed in proteins involved in signaling pathways and those responsible for regulating growth and division of cells. These include regulation of proliferative signaling, control of apoptotic pathways, angiogenesis, enabling of replicative immortality, activation of invasion and metastasis, deregulation of cellular energetics, control of genome stability and processes of tumor promoting inflammation[21,22]. Some examples of targeted drug discovery directed towards these pathways are shown in figure 1.1.

Clinically validated drugs in the category of targeted therapeutics are mostly based on small molecule enzyme inhibitors and biologic agents such as monoclonal antibodies and vaccines. A number of drugs targeting pathways mentioned above (figure 1.2) have been approved by the FDA. The first targeted therapeutics approved were the estrogen receptor modulators including tamoxifen and toremifene. Trastuzumab (Herceptin) was developed in 1998 acts at HER2/neu receptor, used in the treatment of breast cancer[23]. Imatinib Mesylate (Gleevac) developed by Novartis was the first small molecule drug and the first kinase inhibitor approved for use as targeted therapy and

which is capable of killing cancer cells specifically. Imatinib was approved by the FDA in 2001 for the treatment of chronic myeloid Leukemia (CML) acting on the tyrosine kinase (TYK) BCR-ABL which occurs only in the tumor and therefore provides a window of opportunity for selective targeting. Remarkable success was obtained with this drug when treating this disease in its early stages and further was shown to be effective in treating gastrointestinal tumors. Unfortunately cancers treated with imatinib develop resistance due to mutations in the catalytic site of BCR-ABL and which no longer bind the drug[24]. Subsequent advances in kinase targeted drug development include the epidermal growth factor receptor (EGFR) inhibitors gefitinib (Iressa) and the antibody cetuximab were approved by FDA in 2003 for the treatment of non-small cell lung cancer (NSCLC) and colon cancer. Erlotinib was then approved in 2005 following the failure of gefitinib for NSCLC[25].
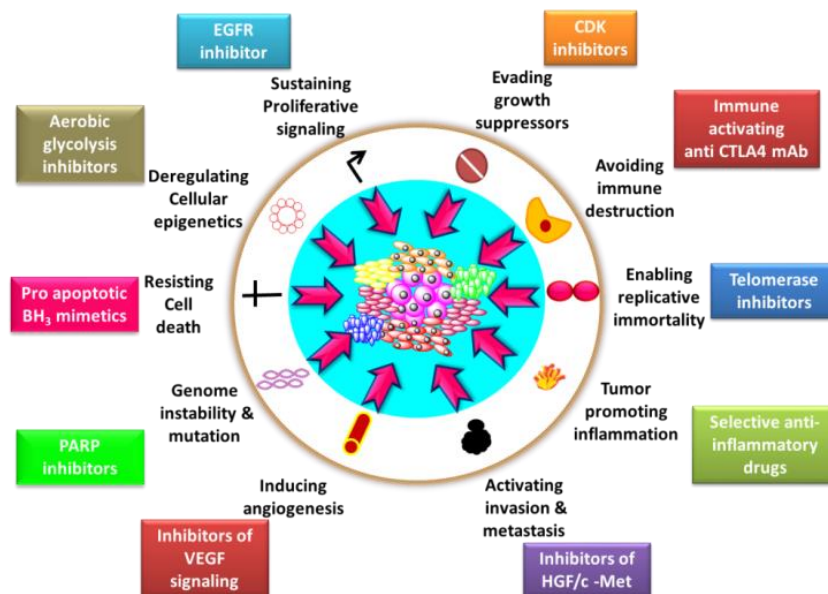
Figure 1.1 Therapeutic Targeting of the Hallmarks of Cancer

Additional drugs based on inhibition of tyrosine kinase inhibitors developed and approved by the FDA later include sorafenib (TYK- VEGFR (vascular endothelial growth factor receptor), PGDFR (Platelet derived growth factor)), sunitinib (TYK-VEGF, PGDFR, renal carcinoma), nilotinib (CML), pazopanib (VEGF) , vandetanib (inhibits EGFR, VEGF and RET), crizotinib (inhibits EML4-ALK), and axtitinib (VEGF, renal cell carcinoma). A common feature of these drugs is that they target different protein kinases which are deregulated in cancer[26, 27]. There are 519 proteins in this family, lack of drug selectivity, emergence of drug resistance may be problematic. Furthermore difficulty in drug target validation for particular disease settings may also be an issue[28, 29,30].

Hormones	Tamoxifen, toremifene, fulvestrant, Anastrozole, Exemestane, Letrozole
Growth factor/signal transduction	Imatinib, Dasatinib, Nilotinib, Bosutinib, Trastuzumab, Pertuzumab, Laptinib, Gefitinib, Erlotinib, Cetuximab, Panitumumab, Temsirolimus, Everolimus, Vandetanib, Vemurafenib, Crizotinib
Gene expression	Vorinostat, Romidepsin, Bexarotene, Alitretinoin, Tretinoin
Apoptosis	Bortezomib, Carfilzomib, Pralatrexate
Angiogenesis	Bevacizumab, Ziv-afliberecept, Sorafenib, Sunitinib, Pazopanib, Regorafenib, Cabozantinib
Immuno modulators	Rituximab, Alemtuzumab, Ofatumumab, Ipilimumab
Monoclonal antibodies	Trastuzumab, Tositumomab, Ibritumomab tiuxetan, Denileukin diftitox, Brentuximab vedotin,

Figure 1.2 FDA approved drugs for targeted cancer therapy (NIH data)[26]

6

1.4 Protein kinases

Protein kinases are a group of enzymes involved in phosphorylation of other substrates. Members of the kinome family constitute about 2% of all the human genes[28,29]. Kinases regulate many cellular pathways including those involved in signal transduction regulating growth and division of cells and therefore their deregulation frequently is associated with tumor formation. Kinase subfamilies implicated in cancer include the receptor tyrosine (RTK), cytoplasmic tyrosine (CTK), serine threonine (STK) and lipid kinases (LK)[27]. RTKs phosphorylate tyrosine residues on substrate proteins and generally function in transmembrane signaling. Various members of the RTK family have been shown to be mutated in cancer and include the EGF, IGF and PDGF receptors among others. Members of the CTKs regulate extracellular signaling e.g. the JAK-STAT pathway and include c-SRC, Abl and JAK-2 kinases. PI3K kinases are lipid kinases which modulate cell growth, proliferation, and intracellular trafficking, and phosphorylate phosphatidylinositol[31, 32]. ST kinases phosphorylate serine and threonine residues in various substrates that are required for controlling cell proliferation and survival in the presence of abnormal ploidy. Some examples of such enzymes include the cyclin dependent kinases (CDKs) that regulate cell cycle check points, the aurora kinases which are required for chromosome separation and the polo like kinases involved in numerous roles in mitosis and cytokinesis. CDKs play a significant role in cancer mechanisms including amplification or overexpression occurring in sarcoma, glioma, and melanoma. Mutations in CDK2 are not frequently observed however overexpression of its activator cyclin E and the inactivation of p21 and p27 inhibitory proteins can lead to excessive CDK2 activity in tumors. Although CDKs are directly and indirectly involved

the majority of tumors, CDK inhibitory drugs have yet to be fully approved by the FDA as anticancer therapeutics due to issues related to cross reactivity[33].

1.5 Cyclin dependent kinases

Cyclin dependent kinases (CDKs) are heterodimeric complexes of a CDK catalytic subunit and a cyclin acting as a positive regulatory subunit. The different CDK/cyclin complexes known to date have key roles in regulating both cell cycle check points and transcription events[33,34]. Most CDKs are activated by associating with a particular cyclin and further through phosphorylation of the catalytic subunit on a threonine residue adjacent to the active site. Prior to activation, the ATP binding site of CDKs is hidden by the T-loop. Binding of cyclin leads to a conformational change including movement of T-loop from the active site entrance. These structural changes also arrange the ATP binding residues in the correct confirmation to allow catalysis at the active site and which is completed through phosphorylation by CDK7 (CDK activating kinase, CAK) on the T-loop threonine. The fully activated CDK/cyclin complexes are then able to phosphorylate threonine and serine residues on CDK substrates[35,36]. For the cell cycle CDKs it is known that key substrates require recruitment prior to phosphorylation. This occurs through a shallow and mainly hydrophobic binding site known as the cyclin binding groove (CBG). The CBG is also involved in regulation of CDK catalytic activity by endogenous cell cycle inhibitory proteins which act as CDK inhibitors (CDKIs)[37]. The CDKIs are classified in two families known as the INK4 and Cip/Kip proteins that bind to catalytic sub unit or the whole CDK/cyclin complex respectively. Members of INK4 family include p15, p16, p18 and p19 which inhibit

CDK4 and CDK6 whereas the Cip/Kip includes p21, p27 and p57 that can inhibit each of the cell cycle CDK complexes[38,39].

There are at least 13 CDKs and 11 cyclins that have been identified so far [40,41]. CDKs are mainly classified into two groups based on their roles in the cell cycle as (i) check point regulators and (ii) transcriptional regulators. The complexes of CDK4/cyclin D1, CDK6/cyclin D1 and CDK2/cyclin E regulate G1/S transition by phosphorylating the retinoblastoma protein (Rb). Further action of CDK2/cyclin A modulates the progression of S phase and CDK1/cyclin B controls the G2/M transition and entry into mitosis. CDK7/cyclin H, CDK9/cyclin T and CDK8/cyclin C function in regulating transcription through phosphorylation of RNA polymerase II thereby facilitating initiation and elongation of RNA transcripts3[33,42]. A summary of the roles of CDK/cyclin complexes is depicted in figure 1.3.
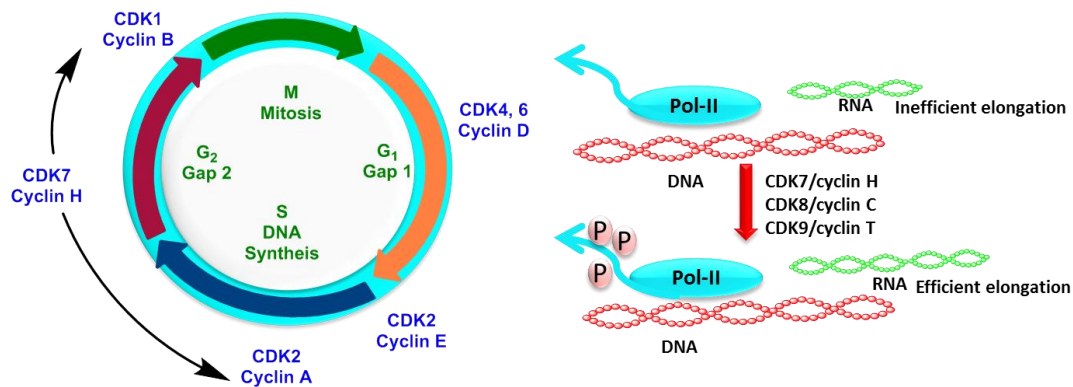
Figure 1.3 Role of CDK/cyclin complexes in cell cycle progression and transcription

1.6 Deregulation of cyclin D-CDK4/6-p16^{INK}4-Rb pathway in cancer

The retinoblastoma protein Rb is a key regulator of the G1 to S phase transition. Its function in transcriptional repression is inactivated by sequential phosphorylation by CDK4/cyclin D, CDK6/cyclin D and CDK2/cyclin E. CDK4/6/cyclin D assists in

progression through G1 by phosphorylation of the Rb-E2F complex. INK4 family protein p16[INK4] associates with CDK4/6 to regulate G1 progression by the release of cyclin D. CDK4/cyclin D and CDK6/cyclin D also binds to the CDK2 inhibitors p21[CIP1] or p27[KIP1], p57[KIP2] sequestering these from CDK2. Mitogenic signals stimulate the synthesis of the D cyclins and release of CDK4 and CDK6 from p16[INK4]. Cyclin D associates with CDK4/6 which subsequently forms an assembly with Cip/Kip proteins. CDK4/cyclin D relieves the assembly of Cip/Kip with CDK2/cyclin E, thus activating it and leading to further phosphorylation of the Rb-E2F1 complex. Full activation of E2F results in gene expression and production of proteins required for progression through S phase. During this process, cyclin E gene is produced, binds to CDK2 by antagonizing Cip/Kip inhibitory proteins and creating a positive feedback loop. Late in S phase, CDK2/cyclin A maintains Rb in its inactive state and also phosphorylates E2F, releasing it from the DNA after gene transcription for S-phase progression is complete (figure 1.4). The Rb and Cip/Kip proteins play significant roles in maintain cells in a quiescent state[33,34].

In general the cyclinD-CDK4/6-p16[INK4]/Rb pathway is disrupted in many forms of cancer. Cyclin D is particular is overexpressed in many tumors including breast cancer (due to gene rearrangement), multiple myeloma (due to translocation) and mutation of cyclin D is found in esophageal cancer. Gene amplification of cyclin D is observed in mantle cell lymphoma. Loss of the tumor suppressor p16[INK4] occurs in many cancers due to gene deletion, point mutation or transcriptional silencing ultimately resulting in increased activity of CDK4/cyclin D. Due to the overexpression of cyclin D or the loss of p16[INK4], excessive CDK4 kinase activity results, further leading to up-regulated

CDK2/cyclin E and in turn generating higher activity levels of the E2F transcription factor[43].
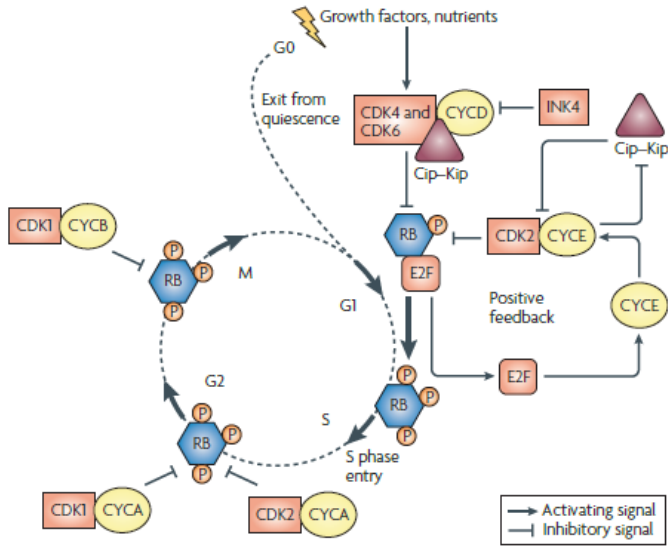
Figure 1.4 Role of cyclin D-CDK4/6-p16^{INK}4-Rb in cell cycle

1.7 Selective apoptosis of cancer cells by the inhibition of CDK2/cyclin A through E2F1 pathway

The Rb protein when in its hypo phosphorylated state acts as a transcriptional repressor (i.e. bound to E2F) and is converted to a transcriptional activator when phosphorylated resulting in its dissociation from E2F. E2F is then released to bind to the DP1 protein and form a dimeric complex. The E2F1-DP1 heterodimer initiates gene transcription through its DNA binding transcription factor activity. After replication is complete, the activity of E2F1 must be neutralized prior to exit from S phase. CDK2/cyclin A is responsible for this function through interaction with the N-terminus of E2F and ultimately phosphorylates both E2F and DP1 to release the complex from DNA. Since many tumors have high base line levels of E2F1 due to a deregulated Rb pathway, inhibition of CDK2/cyclin A activity can lead to accumulation of E2F1 and persistent

11

activity. The result of this is to surpass the threshold required for the induction of apoptosis in a p53 independent fashion. Inhibition of CDK2/cyclin A in the context of normal cells has a much lower effect due to the lower levels of E2F1 activity and the cells proceed with S phase (figure 1.5). Hence inhibition of CDK2/cyclin A should promote selective apoptosis of cancer cells and as a result should be considered as an important target for cancer[34].
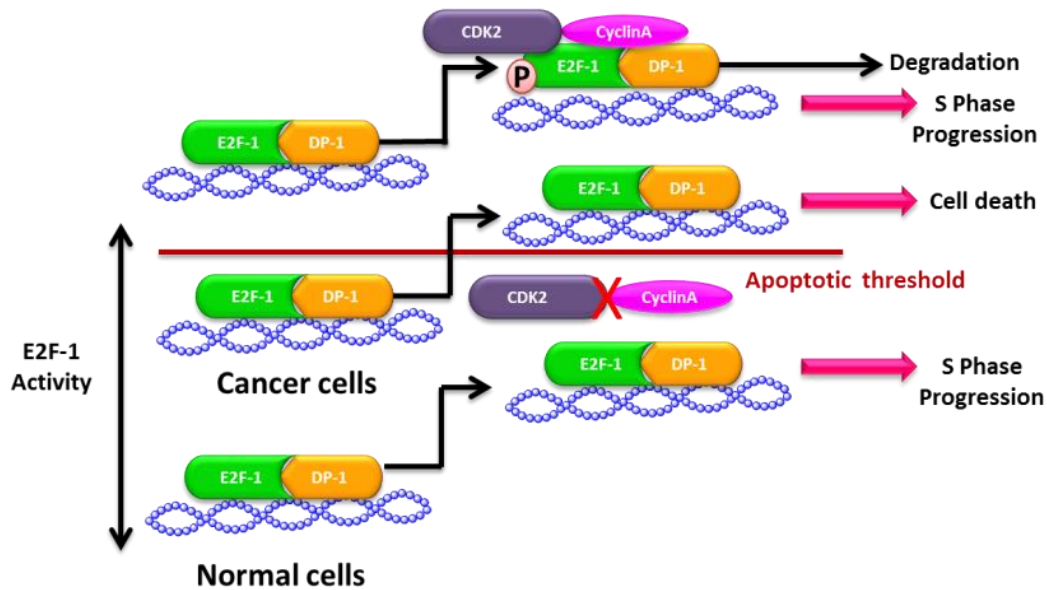
Figure 1.5 Role of CDK2/cyclin A in cancer cell apoptosis through E2F1 pathway

1.8 Strategies for the inhibition of CDK/Cyclin complex

The general strategies for the inhibition of CDK/Cyclin complexes include direct and indirect modulation such as (i) ATP competitive and (ii) non-ATP competitive inhibition respectively[44]. Direct modulators mainly antagonize ATP binding whereas indirect mechanisms act in other ways. These include blocking substrate recruitment through the cyclin binding groove, inhibition of kinase activation by interfering with formation of the complex with the cyclin, and also stabilizing an inactive conformation of

the complex[45]. The ATP binding pocket and cyclin binding groove are shown in figure 1.6.
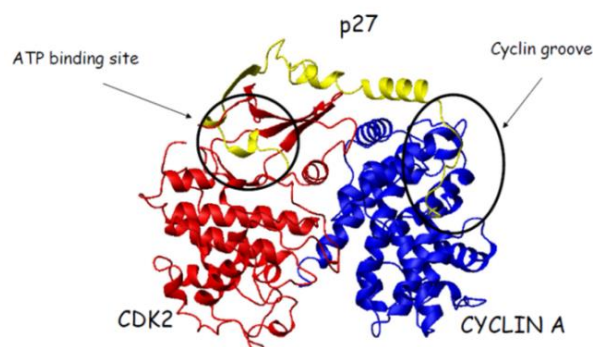
**Figure 1.6 CDK2/cyclin A complex showing CBG
and ATP binding site[46]**

The majority of identified protein kinase inhibitors and FDA approved drugs are based on these come under the category of direct modulators that block the binding of ATP binding. The ATP binding site is highly conserved among the family of 519 kinases and therefore limits the selectivity of these molecules. The non-specificity of ATP competitive inhibitors can lead to cross reactivity with other members of the kinome potentially resulting in off target side effects and toxicities[44]. The first generation of CDK inhibitors included flavopiridol and roscovotine and exhibited limited activity and unacceptable toxicities in clinical trials. These molecules were not specific for the desired CDK2 target and were found to be capable of inhibiting several CDK/cyclin complexes in addition to other kinome members. One side effect of Flavopiridol is hyperacute tumor lysis syndrome and damage to the photoreceptor layer in eyes. Roscovitine has been used in the treatment of NSCLC in phase I-II stage of clinical trials, where the reported side effects are nausea, vomiting, elevations in serum creatinine levels and hypokalemia. Other CDK inhibitors developed subsequent to these first generation inhibitors include

R547, AT7519, and AZD5438. Most of these compounds have good preclinical activity but also are non-specific and are pan CDK inhibitors. This results in effects through inhibition of transcription is a likely reason for the observed toxicities. A list of CDK inhibitors that have been clinically investigated are shown in figure 1.7. The drug PD-0322991(Palbociclib) has been given breakthrough status is in phase III clinical trials for post-menopausal estrogen receptor positive breast cancer. It is the most selective CDK inhibitor so far since it acts only on CDK4 and CDK6 thus inhibiting Rb [25,33,42,47].
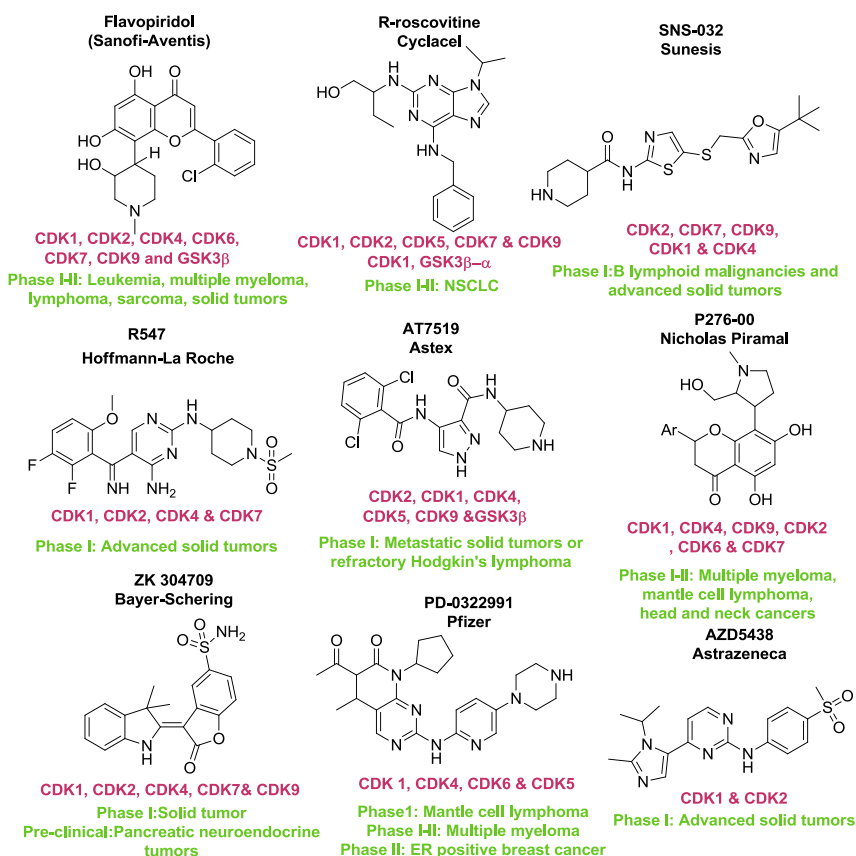
Figure 1.7 CDK inhibitors in clinical trials

Non-ATP competitive CDK inhibitors developed to date include substrate derived peptides (p53 and Rb derived peptides). The tumor suppressor p53 derived peptides target the docking site of p53 tetramerization domain on CDK2 surface. A 20 mer peptide

derived from this site is known as CIP and inhibits phosphorylation. A GEF-CIP fusion protein induces cell death in A375 melanoma cell lines by reducing p53 activity along with suppression of p21. As discussed in section 1.6 and 1.7, the Rb protein is very important for regulation of the G1/S transition and S phase. A 39 residue peptide in cell permeable form derived from Rb (Spa310) has been shown to induce apoptosis via G0/G1 arrest by the inhibition of CDK2 activity. Inhibitors of the interaction between CDK and the cyclin have been recently discovered. C4, an inhibitor of the CDK2 cyclin A interaction is a 22mer peptide derived from the α5 helix of cyclin A. This peptide adopts a α-helical structure and mimics hydrophobic interactions between CDK2 and cyclin A leading to an inactive conformation of CDK2/cyclin A complex. This peptide is specific for the inhibition of CDK2 activity when introduced into MDA-MB-231 breast cancer cell lines as a TAT fusion peptide. NBl1 is a hexapeptide which targets a cleft present in the monomeric cyclin A, affecting the interactions of CDK2/cyclin A and also the stability of the complex. This peptide inhibits most of the cell cycle CDK complexes including CDK2/cyclin A, CDK2/cyclin E, CDK6/cyclin D and CDK1/cyclin E. Cellular studies of an NBl1-TAT fusion peptide on cell lines including HCT116, HT29, T98G, and A2780 showed that it also inhibits CDK2/cyclin A. Fluorescence polarization studies showed that this peptide also inhibits CDK1/cyclin B1, CDK6/cyclin D3 however does not affect other serine/threonine kinases such as glycogen synthase kinase and mitogen-activates kinase[45]. As can be seen, the majority of molecules in the category of non-ATP competitive inhibitors is peptide based and are in the stage of early pre-clinical development.

In general, peptides are not suitable for drug development due to their non-drug like characteristics including lack of cell permeability and susceptibility to proteolytic degradation[48]. In this project an alternative approach for non-ATP competitive inhibition has been pursued by targeting the cyclin binding groove (CBG). The CBG is primarily a hydrophobic groove that is distant from ATP binding site and is present in cyclins A, D and E[46]. It has been shown that a consensus sequence derived from CDK substrates and inhibitory proteins interacts with the CBG and inhibits the cell cycle CDKs i.e. those that associate with cyclins A, D and E. The overall goal of this project is to convert an optimized CBM peptide to a non-peptidic inhibitor using the REPLACE drug design strategy[49].

1.9 Cyclin binding motif

Substrates of the cell cycle CDKs include the E2F and Rb proteins and these in addition to the tumor suppressor inhibitory proteins (e.g. p21, p27, p57 and p53) contain a conserved sequence (CBM) essential for the regulation of CDK activity and for substrate recruitment. This motif is comprised of the ZRXL sequence (figure 1.8) in which "Z" and "R" are basic residues. The residue "Z" is most frequently Lys and "X" is a strictly conserved Arg residue (figure 1.8). Previous studies have shown that CDK4/cyclin D and CDK2/cyclin E phosphorylation can be inhibited by the 20 mer peptide (residues 141-160) derived from the C-terminus of p21. The same sequence of peptides did not inhibit the phosphorylation of histone H1, hence has no effect on the activity of CDK1/cyclin B further illustrating that early cell cycle CDKs can be selectively blocked in this manner.

				Z	**R**	**X**	**L**	**Y**	**Y'**		
p21 WAF1 (N-terminal)	F	Y	H	S	K	R	R	L	I	F	S	K
p21 WAF1 (C-terminal)	G	S	K	A	C	R	R	L	F	G	P	V
p27 KIP1	K	P	S	A	C	R	N	L	F	G	P	V
p57 KIP2	R	T	S	A	C	R	S	L	F	G	P	V
p53			S	R	H	K	K	L	M	F		
E2F1	R	P	P	V	K	R	R	L	D	L	E	T
E2F2	R	L	P	A	K	R	R	L	D	L	E	G
E2F3	G	P	P	A	K	R	R	L	E	L	G	E
p107 pRBL1	A	G	S	A	K	R	R	L	F	G	E	D
p130 pRBL2	A	S	T	T	R	R	R	L	F	V	E	N
pRb	P	P	K	P	L	K	K	L	R	F	D	I
CDK7 c-terminal		G	G	L	P	K	K	L	I	F		

**Figure 1.8 CBM sequences present in tumor suppressors and substrates
that interact with CDK2/cyclin A, CDK2/cyclin E and CDK4/cyclin D**

The sequence of p21^{WAF} (DFYHSKRRLIF) determined to be the most active in cyclin binding and CDK inhibition was found to be from residues 149 to 160. A structure-activity relationship (SAR) study was carried out by exchanging each of the residues within this sequence for alanine and therefore probing the contribution of each side chain. It was found that the replacement of Ser153 resulted in potency gains in both CDK4/cyclin D (IC$_{50}$-10μM) and CDK2/cyclin E (IC$_{50}$-0.004±0.005μM) (figure 1.9)[50].

p21waf1 (149-160)												Kinase inhibition IC 50 (µM)	
												CDK4/D1	CDK2/E2
D	F	Y	H	S	K	R	R	L	I	F	S	20±2	4.5±0.5
A	F	Y	H	S	K	R	R	L	I	F	S	22±4	11±2
D	A	Y	H	S	K	R	R	L	I	F	S	37±6	5.9±0.4
D	F	A	H	S	K	R	R	L	I	F	S	121±31	5.3±0.6
D	F	Y	A	S	K	R	R	L	I	F	S	73±42	5.1±0.5
D	F	Y	H	A	K	R	R	L	I	F	S	10	0.04±0.005
D	F	Y	H	S	A	R	R	L	I	F	S	200	12.9±2.4
D	F	Y	H	S	K	A	R	L	I	F	S	-	-
D	F	Y	H	S	K	R	A	L	I	F	S	-	30±8
D	F	Y	H	S	K	R	R	A	I	F	S	-	-
D	F	Y	H	S	K	R	R	L	A	F	S	53±20	14±3
D	F	Y	H	S	K	R	R	L	I	A	S	-	-
D	F	Y	H	S	K	R	R	L	I	F	A	40	54±1.1

Figure 1.9 Alanine scan of p21^{WAF1} (149-160) sequence

Further studies on the consensus cyclin binding motif (ZRXL) indicated that the flanking residues (Ala on the N-teminus and Phe on C-terminus) make hydrophobic interactions shown to be important for binding. Octapeptides including those from p21 C-terminus (HAKRRLIF), E2F1(PVKRRLDL) and p107 (SAKRRLFG), were tested for kinase inhibition against CDK2/cyclin A, CDK2/cyclin E and CDK4/cyclin D and for competitive binding with cyclin A. Of the peptides tested, HAKRRLIF was found to be the most potent with an IC$_{50}$ value of 0.028µM which is comparable to full length human recombinant p21WAF1 (IC$_{50}$ = 0.011µM) in competitive binding assay of CDK2/cyclin A. Hence the CBM was optimized to the octapeptide, HAKRRLIF and which was further minimized to a pentapeptide RRLIF (IC$_{50}$-1.4µM in CDK2/cyclin A). The crystallographic structure of CDK2/cyclin A/p27^{KIP1} shows how the CBM (SACRNLFG) interacts with the CBG. Similarly the modeled structure of CDK2/cyclin A/p21^{WAF1} was

generated and in which HAKRRLIF interacts with the CBG[46,50]. It has been shown that CBM peptides derived from E2F linked to the transfection sequence of HIV-TAT induces a cytotoxic effect on tumor cells including U2OS and MDA-MB-435, cell types which possess deregulated cyclin D-CDK4/6-p16[INK4]-Rb. At the same time, CBM peptides exert little effect on non-transformed cells including HaCaT and rat 1A fibroblasts. A further study investigated a 20mer peptide from the C-terminus of p21[WAF1] conjugated to a 16 residue sequence from the homeodomain of Antennapedia protein (penetratin) and E2F derived peptides linked to Tat. These permeable peptides were tested in cancer lines and flow cytometry suggested that cell death was due to nuclear condensation and sub diploid DNA suggestive of apoptosis[51,52].

1.10 Cyclin binding groove

The CBG is primarily a hydrophobic groove, distinct and distant from ATP binding pocket, found only in cell cycle CDKs, through which cyclins recruit substrates and inhibitory proteins. Targeting CBG leads to selective inhibition of CDK2/cyclin A and CDK4/cyclin D over other members of the CDK family. The structure of the CBG is somewhat different between cyclin A and cyclin D however in general consists of three sub sites interacting with binding determinants from the octapeptide HAKRRLIF (figure 1.10). These sub sites include a primary hydrophobic pocket and a smaller secondary one separated by a ridge of negatively charged residues[49].
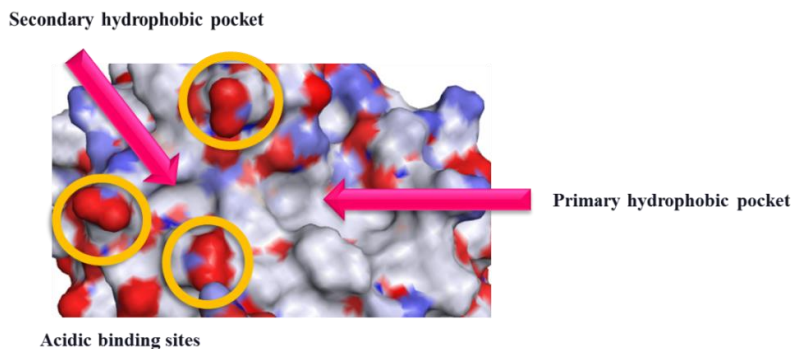
Figure 1.10 Structure of CBG

HAKRRLIF binds at the CBG in such a way that the N-terminal tetrapeptide interacts with the secondary pocket and acidic residues while the C-terminal region contacts the primary pocket (figure 1.11). The types of interactions occurring between HAKRRLIF and CBG include ion-pairing, hydrogen bonding and hydrophobic effects through van der Waals interactions. The basic residues of HAKRRLIF undergo ion-pairing interactions with the acidic residues of the CBG and include Glu220, Glu224 and Asp283. The backbone amides of His1, Ala2, Lys3 and Arg4, form hydrogen bond (H-bonds) with Glu224, Trp217, Gln254 and Ile 281 respectively. The methyl side chain of Ala2 fills the secondary pocket while the side chains of Leu6 and Phe8 occupy the primary lipophilic pocket. These interactions are listed in detail in figure 1.11 and table 1.1.
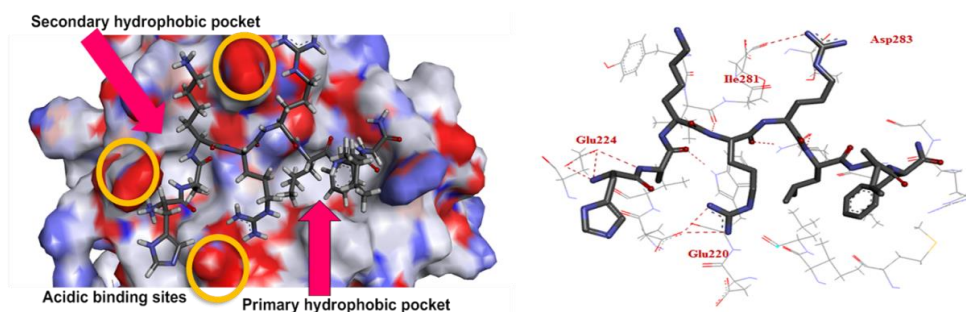
Figure 1.11 Binding and interactions of HAKRRLIF in CBG

20

Table 1.1 List of interactions of HAKRRLIF with CBG

Type of interaction	N-terminal and central region	C-terminal region
Ion-pairing	Basic amino acids (H,K,R,R) with acidic residues(Glu224, Glu220 and Asp283)	NA
H-bonding	Amide backbones of HAKRR (Glu224, Trp217, Ile281, Gln254)	NA
van der Waals hydrophobic effect	Ala methyl side chain with the secondary hydrophobic pocket	Leu, Phe side chain with the primary pocket

1.11 Comparison of CBG in cyclin A and cyclin D

Previous studies were conducted in the McInnes laboratory in order to investigate the structural differences between the CBG of cyclins A and D1. The major differences in the residues of the cyclin groove include the exchange of Ile132, Val60 and Thr62 for Tyr286, Leu214 and Asp216 in cyclin A respectively. The superposition of cyclin A and D1 structures reveals that these variations are accompanied by movement of a helix-loop segment from residues 119 to 136 resulting in conformational differences between the cyclins (figure 1.12). This conformational variation results in cyclin D having a shallower but extended primary pocket. Furthermore, a narrow secondary pocket and fewer acidic residues occur in cyclin D relative to cyclin A (figure 1.13). These variations could potentially be exploited in the design of selective inhibitors of CDK4/cyclin D if these were desired[53].
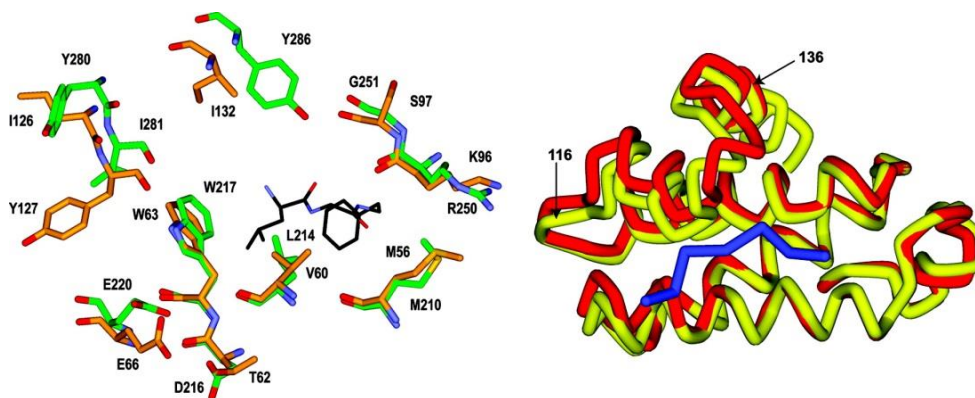
Figure 1.12 Comparison of CBG residues of cyclin A and cyclin D

Left- Overlay of crystal structures of cyclin D1 (orange carbon atoms; PDB code 2W96) and cyclin A2 (PDB code 1OKV) The Leu and Phe residues of the CBM interacting with the primary hydrophobic pocket are shown. E220 and D216 comprise the acidic region, and the secondary hydrophobic pocket is to the left of W217.
Right - Ribbon representation of the overlay highlighting the differences in the cyclin box helices. Cyclin D1 is shown in yellow and the CGI peptide in blue. The region displaying the largest structural differences after superimposing the backbone atoms is labeled (residues 116_136 of cyclin D1)
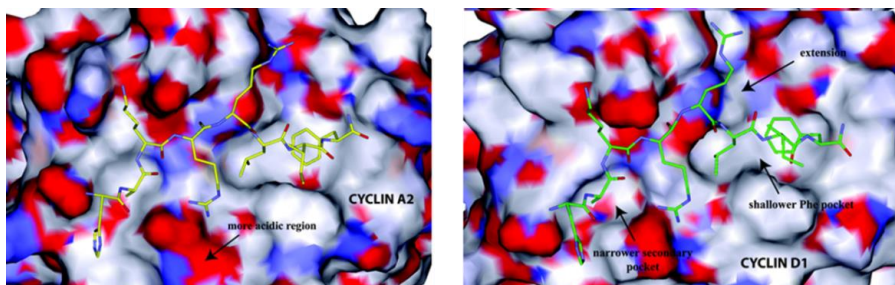
Figure1.13 Comparison of CBG of cyclin A and cyclin D

Comparison of the solvent accessible surface of the cyclin grooves of A2 (left) and D1 (right). The following regions displaying structural differences in cyclin binding determinants are labeled: (left) The more acidic region of cyclin A compared to cyclin D1, which results in differential interactions with Arg4 (peptide sequence HAKRRLIF).
Right-The primary hydrophobic extension of cyclin D1 (top right); the shallower cyclin D1 primary hydrophobic pocket (the Leu214_Val60 interchange, bottom right); and the narrower cyclin D1 secondary hydrophobic pocket (bottom left). Each of these structural features explains the differential requirements for cyclin groove inhibitor binding.

1.12 Rationale and hypothesis

Data supports the hypothesis that inhibition of cell cycle CDKs (CDK2 and CDK4) by CBM peptides will lead to selective apoptosis of cancer cells. The structure of the CBG in complex with CBM peptides (i.e. HAKRRLIF and RRLIF) have been utilized in the development of non-ATP competitive CDK inhibitors. Furthermore the REPLACE (REplacement with Partial Ligand Alternatives through Computational Enrichment) strategy has been applied in order to convert optimized peptides into non-peptidic and more pharmaceutically appropriate molecules. Truncation of key peptide determinants and substitution of these with PLAs (Partial Ligand Alternatives) in the context of the truncated p21WAF peptide, RRLIF has been undertaken in order to construct more drug-like FLIPs (Fragment ligated inhibitory peptides). The resulting FLIP molecules should retain the potency and interactions of the parent peptide however with improved physicochemical properties more akin to drug-likeness. Based on this rationale the following hypothesis and major goals of this project were proposed: "REPLACE is a viable strategy to generate more drug-like inhibitors that selectively inhibit cell cycle CDK/cyclin complexes and induce apoptosis in cancer cells"

In order to confirm the hypothesis and achieve the project goals, PLAs were identified by computational and synthetic methods. The N-terminus of the RRLIF was replaced fragment like small molecules to generate FLIPs based on derivatives of phenyl heterocyclic scaffolds (chapter 2), heterocyclic fragments substituted with basic groups (chapter 3), phenylacetic acid systems (chapter 3) and benzoic acid derived moieties (chapter 5) in order to mimic key interactions of the peptide. In addition to N-cap optimization, the hydrophobic C-terminal motif was replaced with residues designed to

impart enhanced proteolytic stability and cell permeability (chapter 4). The competitive binding efficiency of generated FLIPs was determined by a fluorescence polarization assay developed in the McInnes laboratory and lead compounds were tested for their anti-proliferative activity in U2OS and DU145 cell lines[52,54].

In summary, the REPLACE strategy has been successfully utilized in the development of FLIPs with improved drug like properties and results demonstrate significant progress towards the overall goal of generating next generation and cell cycle CDK inhibitors targeting the CBG and leading to selective apoptosis of cancer cells.

CHAPTER 2

OPTIMIZATION OF CDK/CYCLIN GROOVE INHIBITORS THROUGH REPLACE MEDIATED FRAGMENT ASSEMBLY

2.1 Introduction

REPLACE (REplacement with Partial Ligand Alternatives through Computational Enrichment) is a fragment based approach developed for the design of inhibitors targeting protein-protein interactions[49]. In simple terms REPLACE is an iterative strategy useful for the conversion of a peptide inhibitor into a more drug-like molecule in order to make protein-protein interaction targets more broadly accessible. REPLACE combines techniques at the interface of chemistry and biology including both computational and both solution and solid phase synthetic chemistry to generate non-peptidic compounds which are then evaluated in binding and cellular assays is shown in figure 2.1. Peptides in general do not make good drugs due to their lack of membrane permeability, and metabolic instability[48]. In this study the iterative conversion of a peptidic cyclin groove inhibitor has been undertaken by replacing key N and C-terminal binding determinants with more drug-like fragments. After a generation of FLIPs which are N and/or C-terminally capped, these will be much less susceptible to proteolysis. Reduction in polar surface area and molecular weight of an inhibitor should lead to greater cell permeability thereby improving drug likeness.
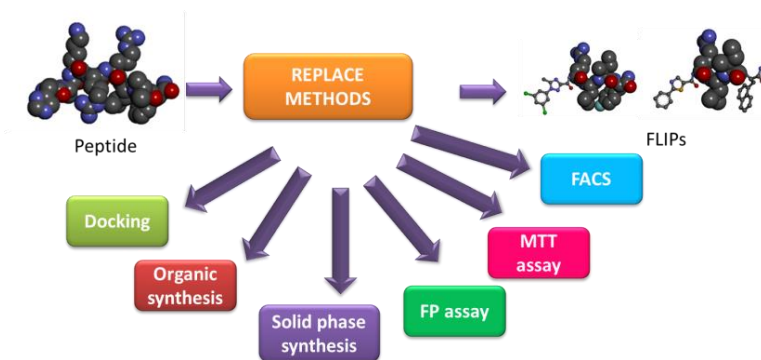
Figure 2.1 REPLACE methods

In REPLACE we utilize the structure activity relationship (SAR) combined with interactions of HAKRRLIF in its receptor in the Discovery studio 3.0 to design capping groups. The pentapeptide RRLIF is used as stating point to design FLIPs in which the N-terminal Arg is truncated. A library of commercially available molecules or molecules designed in our lab is used for docking in the hollow region created by truncation of Arg. Partial ligand alternatives (PLAs) or N-caps are selected such that these molecules would retain most of the interactions of truncated binding determinants. Such a library is docked (computationally placed in the binding site) using molecular modeling software (e.g. LigandFit[55] within Discovery studio 3.0) after which the docked poses are prioritized based on the scoring function which is an assessment of their ability to bind. Top scoring virtual hits are then obtained from commercial sources or synthesized so as to be evaluated as capping groups. To do this they are ligated to the truncated peptide sequence by solid phase synthesis in order to generate FLIP molecules[56]. These are tested in an in vitro assay (e.g. FP[57] assay to determine their competitive binding efficiency) to determine if the activity of the parent peptide has been recapitulated however in a more drug-like molecule. If so, FLIPs can be further evaluated in order to determine if any

cellular activity has been achieved. An overview of the REPLACE strategy is illustrated in scheme 2.1.
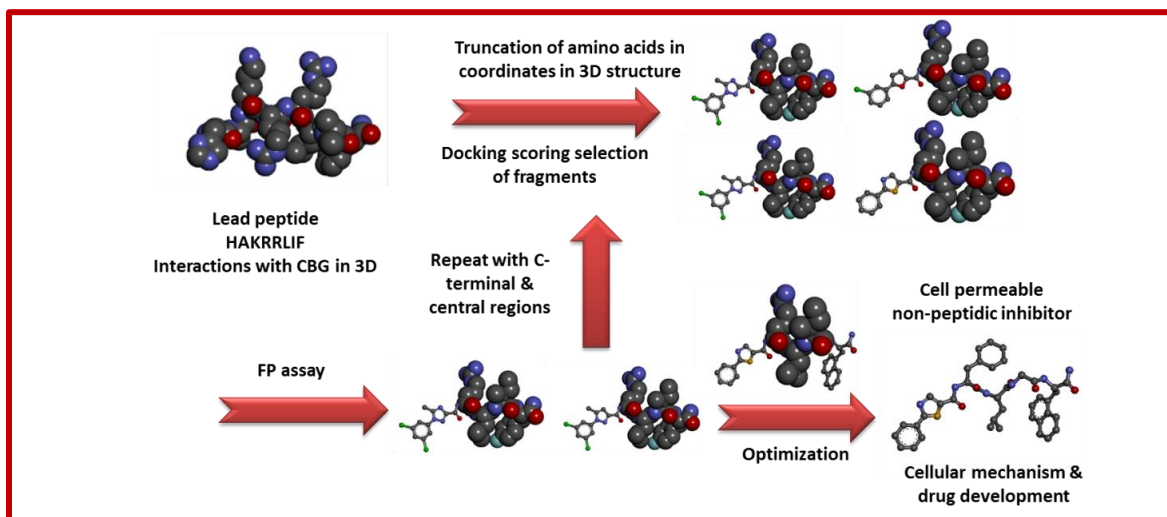
Scheme 2.1 Schematic representation of REPLACE strategy

The REPLACE strategy has been utilized to convert the peptidic inhibitor RRLIF into a more drug like non-ATP competitive CDK inhibitor acting through the cyclin groove. The initial objective of this project is to identify low molecular weight non-charged fragment alternatives for N-terminal arginine residue. Since arginine is the most basic amino acid, it makes strong electrostatic interactions with the acidic region of CBG but also potentially limits cell permeability. In order to improve drug likeness, several uncharged fragment molecules based on phenyl heterocyclic carboxylic acids were investigated. These were designed based on a previously reported N-capping group, 1-(3,5-dichlorophenyl)-5-methyl-1H-1,2,4-triazole-3-carboxamide (35DCPT) ligated to RLIF. The crystal structure of this N-cap confirmed that the 35DCPT takes up the same

position occupied by the N-terminal tetrapeptide of the p21 parent peptide (HAKRRLIF).
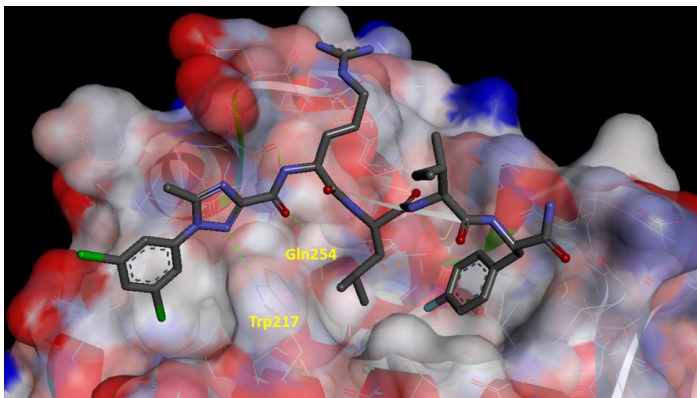
Figure 2.2 Binding mode of 3,5-DCPTRLIF in CBG

Binding of 3,5-DCPTRLIF is shown with hydrogen bonding interactions (depicted in green dotted lines) with N-atom of Trp217 and Gln254

The 3,5-dichlorophenyl ring makes hydrophobic contacts through van der Waals interactions with the secondary hydrophobic pocket replacing those of the peptide Ala2 methyl side chain. Further, the N-2 atom of the triazole ring and the amide carbonyl of the capping group accept hydrogen bonds with the side chains of Trp217 and amide bonds of Gln254 respectively (figure 2.2). The 35DCPT N-capped peptide (FLIP) successfully recapitulated the activity of the intact pentapeptide providing proof of concept for the REPLACE strategy[49]. In this study, the triazole core structure was substituted with other heterocyclic isosteres (including pyrazole, furan, pyrrole, imidazole and thiazole) to investigate the effect of alternate heteroatoms on binding. In addition to this the phenyl ring was derivatized with methyl, methoxy and halogen substituents to probe with the binding affinity of the secondary pocket. A structure activity relationship (SAR) was carried out for this diverse set of heterocyclic core structures with substitutions on phenyl ring was studied to establish the optimal requirement of functional groups for binding. Along with improving binding affinity, optimization of the

Ncapping group was investigated to improve the physicochemical properties (clogP, polar surface area) and metabolic stability that determine drug likeness of the inhibitors.

2.2 Results

2.2.1 Synthesis of N-caps

In order to probe the structure-activity relationship of the 35DCPT Ncap scaffold, a number of variants of this substructure were synthesized. These included 5-methyl-1-phenyl-1H-1,2,4-triazole-3-carboxylic acid (phenyltriazole), 5-methyl-1-phenyl-1H-pyrazole-3-carboxylic, acid (phenylpyrazole), 1-phenyl-1H-pyrrole-3-carboxylic acid (phenylpyrrole), 2-phenyl-2H-imidazole-4-carboxylic acid (phenylimidazole), 5-phenylfuran-2-carboxylic acid (phenylfuran), and 2-phenylthiazole-4-carboxylic acid (phenylthiazole). Each of these was modified by including a variety of substitutions on the phenyl ring as shown in table 3.1.

Scheme 2.2 Preparation of phenyltriazole N-capping groups
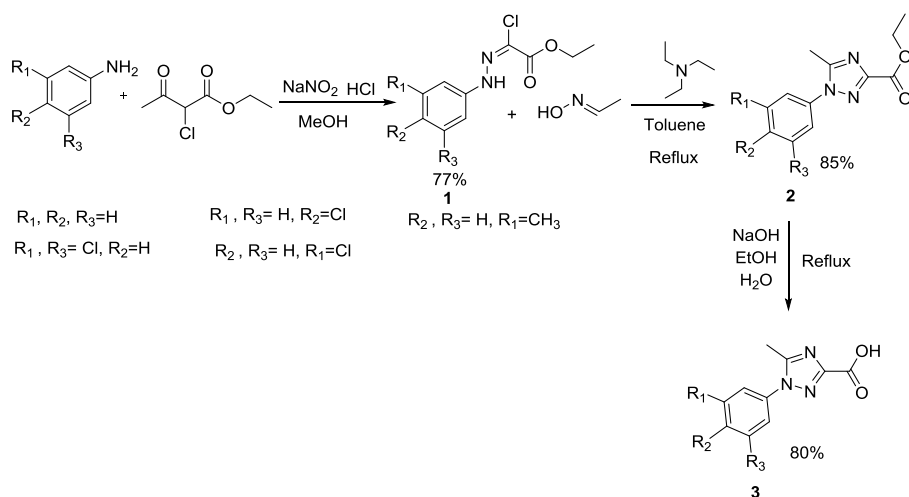
The phenyltriazole carboxylic acid derivatives were synthesized by reacting the diazonium salt of an appropriately substituted aniline with ethyl 2-chloroacetoacetate and subsequent cyclization to the 1,2,4-triazole using acetaldehyde oxime, triethylamine in

toluene. The resulting ester was subjected to base hydrolysis to generate the final capping group product of about 80% yield (scheme 2.2)[58,59]. The phenylpyrazole capping groups were prepared by the reaction of substituted phenyl hydrazines with ethylacetopyruvate in triethylamine/ acetonitrile to generate the cyclized product as an ester with a yield of 21%. Base hydrolysis was then employed to convert to the free carboxylate obtained in quantitative yield (scheme 2.3)[60]. Initial attempts at this reaction used base catalysis however led to the formation of two isomers (figure 2.3) in equal amounts (these could be separated by flash chromatography). The structure of the desired isomer was confirmed by one dimensional nuclear overhauser effect (1D-NOE) NMR experiments. In this experiment, irradiation of the methyl group in pyrazole ring lead to the enhancement of two ortho aromatic proton signals. Further variants of this reaction showed that acid catalysis of the cyclization reaction protonated the hydrazine leading to suppression of the formation of the undesired isomer. The phenyl ring of the pyrazole substructure was derivatized as 3,5-dichloro, 3 and 4-chloro, 3-fluoro, 3 and 4-methoxy derivatives in order to study the effect of these substitutions on the interactions with secondary pocket.

Scheme 2.3 Preparation of phenylpyrazole N-capping groups
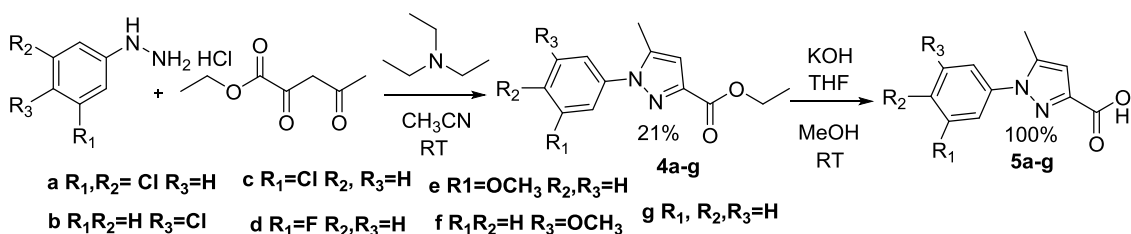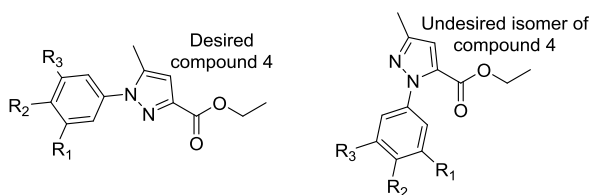
Figure 2.3 Ethyl 1-(substituted phenyl)-5-methyl-1H-pyrazole-3-carboxylate

To generate phenylfuran derivatives, appropriate aniline was diazotized with sodium nitrite and hydrochloric acid. The intermediate diazonium salt was then reacted with furoic acid through catalysis with copper chloride (scheme 2.4) [61]. The yield of the final product was about 28%. In this series the 3-chloro and 3,5-dichloro derivatives were successfully synthesized. Phenylpyrrole capping groups were prepared by reaction of a substituted aniline (4-chloro and 3,5-dichloro) with 3,5-dimethoxytetrahydrofurancarboxaldehyde through refluxing in acetic acid to generate the cyclized phenylpyrrole as an aldehyde precursor with 94% yield. To obtain the final capping group, this was oxidized to carboxylic acid (65% yield) using silver nitrate and sodium hydroxide (scheme 2.5) [12] . All the N-caps were ligated to RLIF by solid phase synthesis and tested in FP assay.

Scheme 2.4 Preparation of phenylfuran N-capping groups
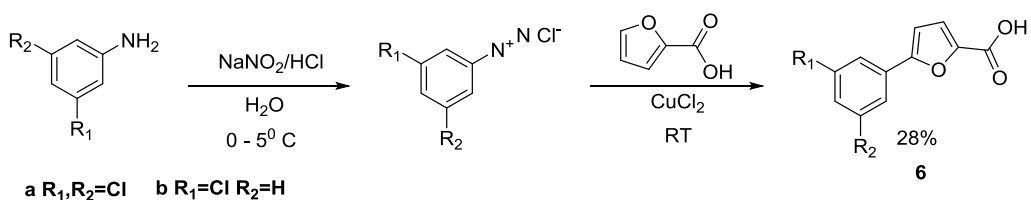
Scheme 2.5 Preparation of phenyl pyrrole N-capping groups

31
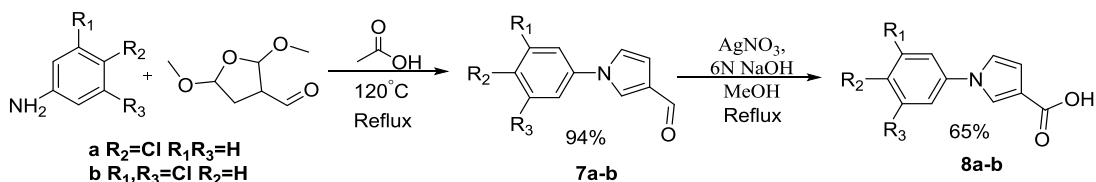
2.2.2 Structure activity relationship of phenyl heterocyclic isosteres as N-caps

As comparators for the Ncapped peptides that were generated through application of REPLACE, the potency of both the parent peptide (HAKRRLIF and RRLIF) were evaluated in the FP competitive binding assay. It was found the HAKRRLIF (IC_{50} values of 0.13 µM; CDK2/cyclin A, 0.22 µM; CDK4/cyclin D) shows better inhibitory potential compared to RRLIF (1.4 µM; CDK2/cyclin A and 16.1 µM; CDK4/cyclin D). HAKRRLIF is therefore about 10 fold more potent compared to RRLIF in the cyclin A and 70 fold in cyclin D context. RRLIF has a higher affinity for cyclin A compared to cyclin D. As mentioned above, the crystal structure of 35DCPT Ncapped peptides have been previously solved. These structures reveal that this capping group only partially mimics the interactions of N-terminal residues. The FP assay results of all heterocyclic core structures with different phenyl substituents were compared and the isosteres exhibited significant differences in potency as shown in table 3.1[63].

The SAR of FLIPs containing phenyl heterocyclic carboxylic acids was carried out for understanding the importance of heteroatoms (N and O) with binding at CBG and also the substituents on phenyl ring for van der Waals interactions with second pocket. In the SAR of phenyl heterocyclic scaffolds, the most potent core structure incorporated into a FLIP was found to be the starting phenyltriazole derivative followed by phenylpyrazole and phenylfuran containing FLIPS. FLIPs having the phenylpyrrole, phenylthiazole and phenylimidazole scaffolds displayed marginal or no activity. FLIPs **5773** (35DCPT-RLIF) and **5774** (1-(4-chlorophenyl)-5-methyl-1H-1,2,4-triazole-3-carboxamide-RLIF) were shown to be the most potent compounds with IC_{50} values for CDK2/cyclin A of 4 µM and 11.5 µM respectively and in cyclin D was 27.3 µM and 12.0 µM respectively.

Thus, **5773** has better activity in the CDK2/cyclin A assay whereas the potency of **5774** is reversed in that it has greater affinity towards CDK4/cyclin D. The activity of **5906** (1-(3-chlorophenyl)-5-methyl-1H-1,2,4-triazole-3-carboxamide containing FLIP, IC_{50} 5.7 µM) was comparable to **5773** and **5907** (3-methylphenyl)-5-methyl-1H-1,2,4-triazole-3-carboxamide-RLIF, IC_{50}-13.8 µM) was comparable to **5774** in the cyclin A context in the FP assay. The unsubstituted phenyltriazole FLIP, **5843** showed the lowest activity (cyclin A-16.2 µM, cyclin D-49.2 µM) among the phenyltriazole series.

Table 2.1 Structure activity of phenyl heterocyclic N-terminal Partial Ligand Alternatives
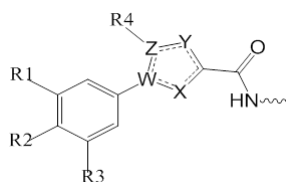
Core	SCCP ID	R1	R2	R3	R4	W	X	Y	Z	CDK2/cyclin A IC_{50} (µM)	CDK4/cyclin D1 IC_{50} (µM)
Triazole	5843	H	H	H	H	N	N	N	C	16.2±3	49.2±7.60
	5773	Cl	H	Cl	CH$_3$	N	N	N	C	4.0±0.6	27.3±3.40
	5774	H	Cl	H	CH$_3$	N	N	N	C	11.5±3.3	12.0±2.06
	5906	Cl	H	H	CH$_3$	N	N	N	C	5.7±0.99	26.5±7.49
	5907	CH$_3$	H	H	CH$_3$	N	N	N	C	13.8±1.13	51.05±16.05
Pyrazole	5762	H	H	H	CH$_3$	N	N	C	C	40.3±6.5	54.2±3.05
	5763	Cl	H	Cl	CH$_3$	N	N	C	C	21.8±13.7	>100
	5764	Cl	H	H	CH$_3$	N	N	C	C	11.9±2.0	70.3±12.79
	5771	F	H	H	CH$_3$	N	N	C	C	29.6±12.2	65.9±6.60
	5765	H	Cl	H	CH$_3$	N	N	C	C	33.7±8.1	54.7±20.43
	5766	OCH$_3$	H	H	CH$_3$	N	N	C	C	64.1±4.2	>100
	5767	H	OCH$_3$	H	CH$_3$	N	N	C	C	>180	>180
Pyrrole	5776	H	Cl	H	H	N	C	C	C	>180	>180
	5775	Cl	H	Cl	H	N	C	C	C	>180	>180
Furan	5768	Cl	H	Cl	H	C	O	C	C	>180	>180
	5769	Cl	H	H	H	C	O	C	C	>180	>180
Imidazole	5760	H	H	H	CH$_3$	C	N	C	N	>180	>180
	5852	F	H	H	H	C	N	C	N	34.3±0.6	68.5±14.84
Thiazole	5583	H	Cl	H	H	C	N	C	S	>180	>180

For the pyrazole isosteric FLIP series which have one less nitrogen heteroatom in

the five membered ring, comparison of the 3,5-dichloro (**5763**, IC_{50}-21.8 μM) and 4-chloro (**5765**, IC_{50}-21.8 μM) substituted derivatives with **5773** shows a relative loss of activity by about 3-5 fold against CDK2/cyclin A. Similar to results obtained for the phenyltriazole series, the 3,5-dichloro substituted analog (**5763**, IC_{50}>100 μM) shows lower potency compared to 4-chloro substituent (**5765**, IC_{50} -54.7μM) of pyrazole in the CDK4/cyclin D assay. Although the size of a methyl group is similar to that of a chlorine atom, the 3-substituted methylphenyltriazole derivative (**5907**) is about 3.5 fold less potent compared to **5773** and **5906**. The same trend was observed in the phenylpyrazole series in that the 3,5-dichloro, 3-chloro and 3-fluoro derivatives show greater affinity for CDK2/cyclin A2. The other FLIP showing detectable activity in this series is 3-fluorophenylimidazole-RLIF (**5852**), the activity of which is comparable to corresponding phenylpyrazole (**5771**) in both CDK2/cyclin A2 and CDK4/cyclin D1. From these results it is evident that the presence of nitrogen atom in the heterocycle (for H-bonding with Trp217) is required for good activity.

The inhibitory activity of a FLIP molecule capped with 3-fluorophenylpyrazole (**5771**) was determined to be 29.6 μM for CDK2/cyclinA and 65.9 μM in CDK4/cyclin D. Substitution of the 4-position on the phenyl ring provides improved binding relative to the 3-position for CDK4/cyclin D as evidenced by the results for the phenyltriazole and phenylpyrazole capped peptides. Binding of the unsubstituted phenylpyrazole containing FLIP (**5762**, 40.3 μM for CDK2/cyclin A2; 54.2 μM for CDK4/cyclin D1) was similar to the 4-chloro derivative. The increased steric bulk of the methoxy groups relative to chorine and fluorine contributes to the potency drop for both 3- (**5766**) and 4-methoxy (**5767**) phenylpyrazole derivatives.

2.2.3 **Docking of phenyl heterocyclic isosteres as N-capping groups**

A docking analysis was carried out for all the isosteric phenyl heterocyclic series to correlate with the binding potencies of FLIPs obtained from the FP assay. Computational studies of these Ncaps were performed using the parameters obtained in the validation of the use of the LigandFit program (docking validation and parameters are explained in chapter 4) for high- throughput docking of ligands into the cyclin groove of cyclin A (2UUE). The potential Ncapping groups shown in table 3.2 were docked and subsequently analyzed and prioritized based on superimposability with the crystal structure of 35DCPT, hydrogen bonding (with the side chains of Trp217 and Gln254), and also PLP1 and consensus scoring. Consensus scoring is a combination of all the seven scoring functions in LigandFit and it gives more accurate estimate of the various interactions between the receptor and ligand.

Table 2.2 Docking results of phenyl heterocyclic N-terminal Partial Ligand Alternatives

Core structure	Highest PLP1 score	Consensus score	H-bond length with Trp217(Å)
Triazole	57.29	5-7	1.38 to 2.34
Pyrazole	55.28	5-7	1.24 to 2.43
Furan	53.04	4-7	>2.5
Imidazole	50.20	3-6	>2.5
Thiazole	47.3	1-4	>2.5
Pyrrole	47.1	0-3	NA

Phenyltriazole (PLP1-57.29) derivatives were found to have the highest PLP1 score and this was followed by phenylpyrazoles (PLP1-55.28), phenylfurans (PLP1-

53.04), phenylimidazoles (PLP1-50.20), phenylthiazoles (47.3) and phenylpyrroles (PLP1-47.1). For the most part, the consensus score was predictive for capping groups with substitutions at 3-position and 3,5-position. High consensus score values (between 5 and 7) were obtained for poses that have 3-chloro or 3,5-dichloro substituents on the phenyltriazole and phenylpyrazole and which were the most potent in the CDK2/cyclin A context. The exception to this was methoxy derivatives of the phenylpyrazole FLIP series where both high PLP1 score (>58) and consensus score (7) values were obtained for incorrect poses and which did not interact well with the secondary pocket. Despite the high scores, the incorrect binding mode is consistent with lack of activity of 5966 and 5967.

2.3 Discussion and conclusion

In this study protein-protein interactions at CBG are being targeted through application of the REPLACE strategy[49]. REPLACE is a novel strategy for converting peptidic molecules into more drug like molecules by sequential replacement of residues of peptidic inhibitors with small molecule capping groups. FLIPs are peptidic molecules where key determinants have been substituted with fragments that potentially have increased drug likeness compared to the parent peptides and retain important interactions of the truncated residues. Hence the goal in this section was to focus on the structure activity relationship through optimizing interactions with the secondary pocket and mimicking hydrogen bonding contacts observed with the peptide and in a previous study where preliminary heterocyclic N-caps were identified.

A library of phenyl heterocyclic N-capping group derivatives was designed in order to replace the N-terminal arginine residue of RRLIF and to potentially exploit

additional interactions of the N-terminal tetrapeptide of HAKRRLIF. These include ion-pairing interactions with acidic residues of the cyclin groove, hydrophobic interactions of Ala2 with secondary pocket and backbone hydrogen bonds with various side chains of the CBG. The N-caps were based on phenyltriazolecarboxylic acid derivatives identified using REPLACE which were then used to construct FLIP molecules. X-ray crystallographic analysis of 35DCPT ligated to RLIpfF-NH$_2$ and in complex with CDK2/cyclin A(PDB ID 2UUE) revealed that the 1,2,4-triazole core occupies the position of Arg4 backbone on the ridge that separates both the hydrophobic pockets while the dichlorophenyl group occupies the hydrophobic secondary pocket and provides affinity through van der Waals interactions. The N-2 atom of the 1,2,4,-triazole ring and the amide carbonyl oxygen act as hydrogen bond acceptors for the indole N-atom of Trp217 and amide N-atom of Gln254 respectively.

For the library design, information from another recent study examining the structural differences of the cyclin groove between cyclin A and cyclin D was exploited (explained in more detail in chapter 1, section 1.11)[53]. Peptide analog SAR was used to delineate the key variations in the major and minor hydrophobic pockets and in the acidic regions between the two cyclins. Using the SAR revealed in these studies, a library of isosteric heterocyclic N-caps were designed in order to retain similar interaction of 3,5-DCPT and also to probe the contributions of this fragment replacement to cyclin groove binding. An extensive SAR study was carried out by generating isosteres in which the triazole core was replaced with other heterocyclic systems including pyrazole, furan, pyrrole, imidazole and thiazole rings. Furthermore the SAR of the phenyl ring attached at N1 of the triazole was explored through introduction of a variety of substitutions at

positions 3, 4 and 5. The SAR of heterocyclic isosteres was carried out to provide insight into the contributions of H bonding with indole N-atom of Trp217. The incorporation of different heteroatoms in the appropriate position where an H bond is contributed by the N2 of the triazole ring was undertaken through synthesis of the corresponding isostere (nitrogen: pyrazole, thiazole and imidazole also oxygen: furan). Substitution of the phenyl ring of the phenyl heterocycle with halogens (Cl, F), methyl or methoxy groups was undertaken to identify groups that provide better interactions and complementarity with the secondary pocket.

A common feature of all the molecules in the synthesized library is the presence of carboxylate group which when ligated to the truncated peptide forms an amide bond mimicking the H- bonding to the side chain amide N-atom of Gln254 as observed in the peptide crystal structures. A docking study was carried out to determine if the N-caps in this library were capable of making H bonding with Gln254 (figure 2.4) and with Trp217 as proposed. The results showed that this indeed was the case however variable lengths and strengths of H-bonds would be expected.
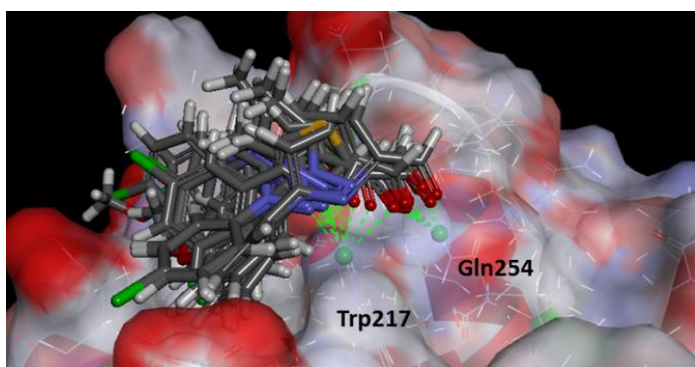
Figure 2.4 Overlay of docked structures of N-caps

The interaction filters (Trp217 & Gln243) are indicated as green spheres and hydrogen bonding are indicated in green dotted lines on the surface of cyclin A (PBD ID2UUE)

The results obtained from binding of the FLIPs to CDK2/cyclin A revealed that the heterocyclic core is a critical determinant for potency. Since both the two ring structures expected to have the strongest H-bond (triazole and pyrazole) were the most potent, the conclusion was drawn that the H-bond is essential for the activity of this isosteric FLIP series. Comparison of the N-caps having a 3,5 dichloro substitution strongly indicated the importance of having an atom capable of acting as an H-bond acceptor to the NH group of indole ring in Trp217. In the phenylfuran containing FLIPs, the N-atom is replaced with an oxygen atom. Since oxygen is more electronegative (3.44, Pauling's scale) than the nitrogen (3.04, Pauling's scale) [64] and the oxygen lone pairs of electrons participates in the furan aromatic system, a much weaker H-bond interaction would be expected compared to the triazole and pyrazole. Although the five membered ring of triazole and pyrazole is also aromatic and the lone pairs participate in the aromaticity there are however three and two lone pairs present respectively and at least any one pair of electrons are more available for H bonding. These factors provide a strong reasoning for the inactivity of the phenylfuran analogs and increased relative activity of the phenyltriazole and phenylpyrazole containing FLIPs. Since only one phenyl imidazole FLIP was generated, this could not be directly compared with the phenyltriazole series. The 3-fluoro derivative was available however and could be compared with 3-fluorophenylpyrazole. The comparable activity of these two FLIPs indicates that similar H-bonding contributions are made to the phenylpyrazole FLIP. The phenylpyrrole isosteres do not exhibit good activity because the pyrrole ring does not have H-bond acceptor to interact with the indole group of Trp217 and that the two H atoms may even clash with each other. The docking results obtained support these results in terms of

39

PLP1 score and hydrogen bond length. In case of phenyltriazole and phenylpyrazole derivatives the hydrogen bond length between N-2 nitrogen atom and Trp217 varies between 1.24 to 2.43Å whereas the hydrogen bond length between the weak hydrogen bond acceptors in the phenylfuran and Trp217 is greater than 2.7Å.

Comparison of the binding activity results suggests that the phenyltriazole containing FLIPs are considerably more potent that the phenylpyrazole containing ones by 3 to 5 fold. These results suggest that the N-2 nitrogen atom is not the only binding determinant in the heterocyclic ring and that the triazole N-4 atom plays an additional role in binding. This observation was initially difficult to explain in structural terms since no interactions between N-4 and the cyclin groove are observed in the crystal structures. A modeling study was carried out in which a water molecule was placed between N-4 atom of the triazole (**5773**) and carboxylate side chain of Asp283 (cyclin A) or Asp129 (cyclin D). This water molecule can thus form a bridging hydrogen bond between N-4 atom of triazole and carboxylate group of the acidic residue (figure 3.3) thereby suggesting a reason for the potency increase of the phenyltriazole series. Since the phenylpyrazole derivatives cannot make such an interaction this potentially explains the lower activity potential of this series. As a whole the SAR of phenyl heterocyclic Ncaps demonstrates the importance of hydrogen bonding with the cyclin groove and furthermore highlights the structural differences contributing to diversity in activity profile.

The contributions of the substitutions on the phenyl ring to their interaction with the secondary hydrophobic pocket were studied from the SAR of the phenyltriazole and phenylpyrazole containing FLIPs. The activity profile of appropriate phenyl substituents

could be correlated in both triazole and pyrazole based FLIPs. The phenyl group makes hydrophobic contacts through van der Waals interaction with the secondary pocket and appropriate substitution in phenyl ring provides better interaction. As mentioned earlier 3,5-dichloro derivative was the most potent compound (comparable potency with 3-chloro derivative) followed by 4-chloro and 3-methyl derivatives in CDK2/cyclin A. Substitution at the 3-position offers better activity for inhibition of CDK2/cyclin A. Of all the substituents incorporated into the phenyl ring in these two isosteric series, chlorine was found to be the most effective in binding to cyclin A and cyclin D in their respective CDK complexes. The FP results also showed that the position of the substituents on the phenyl ring determines specificity towards a particular cyclin. A 3-chloro substituted phenyl ring (**5906, 5907, 5764** and **5771**) and 3, 5-dichloro substitution (**5773, 5763**) in both the triazole and pyrazole context have better activity in binding to cyclin A compared to cyclin D. The 4-chloro substituted analogs however (**5774** and **5765**) have a reverse potency order with respect to binding to the two cyclins. This observation can be explained by the structural differences of secondary hydrophobic pocket between cyclin A and cyclin D. In cyclin A this pocket in shallower and larger whereas it is smaller and deeper in cyclin D. Hence larger volume of this sub site in cyclin A can accommodate 3 and 3,5 dichloro substituents with a better complementarity. As a result of the smaller hydrophobic sub site in cyclin D, the 3 and 3,5-disubstituted phenyl group is displaced relative to cyclin A and is further out of the secondary pocket. The 4-chloro substituent binds deeper in the secondary pocket of cyclin D, allowing better van der Waals interactions of the phenyl and furthermore allowing interaction with Glu66 and Glu70. An overlay of modeled structure of **5773** in complex with CDK4/cyclin D1 and

41

CDK2/cyclin A2 shown in figure 2.5 explains the binding modes of 3,5-disubstuted phenyl ring in the second pocket of cyclin A and cyclin D[63].
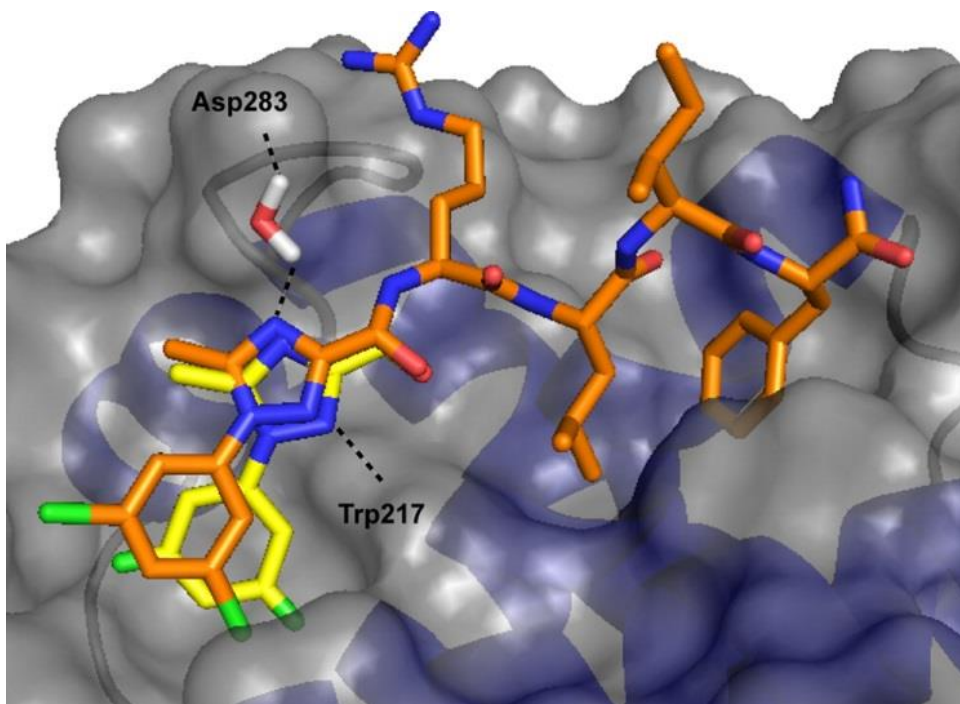
Figure 2.5 Modeled structure of 5773 in cyclin A & cyclin D

Showing bridging hydrogen bond between the ligand and the receptor
Modeled structure of SCCP 5773 in complex with CDK4/cyclin D1 (tan carbon atoms) overlaid with the crystal structure of the same N-cap bound to CDK2/cyclin A2 (yellow carbon atoms). A Connolly surface representation of cyclin A is shown along with the putative water molecule contributing bridging hydrogen bonds.

The difference in the potency between 3-chloro and 3-fluoro substituents could be observed with the phenylpyrzaole containing FLIP series is indicated by increased complementarity of the larger chloro substituent with the secondary pocket. In comparison with the fluoro substituent, the chloro also allows closer contact of the phenyl ring in the pocket (figure 2.6). Decreased potency of the 3-methyl substitution could be due to less favorable interactions of the slightly larger group with the secondary pocket in comparison with 3-chloro substituent. The methoxy groups in turn are too large due to

42

the extra connecting atom (oxygen) and it is displaced outside of the minor hydrophobic pocket due to the resulting steric clash also leading to loss of hydrogen bonding with Trp217 in 4-methoxyphenylpyrazole derivative (figure 2.7).
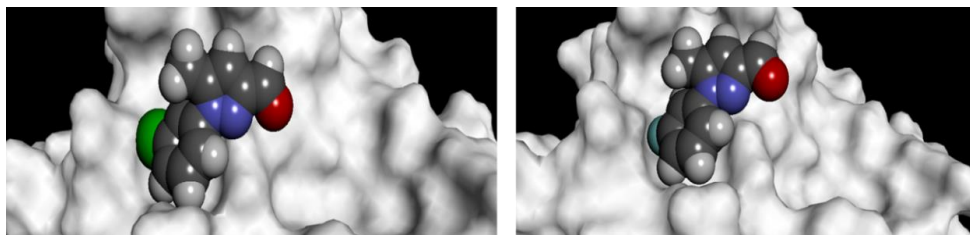
Figure 2.6 Comparison of complementarity of 3-Chloro and

3-Fluoro substituents on phenyl ring of pyrazole
Complementarity of 3-chlorophenyl pyrazole (left) and 3-fluorophenyl pyrazole (right) derivatives in the second pocket are shown as CPK structures on the surface of cyclin A
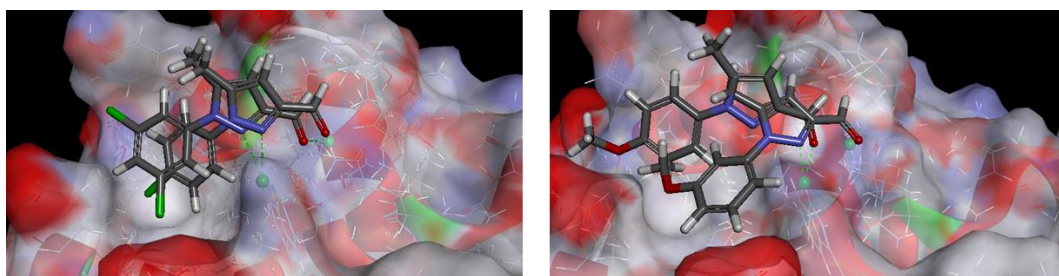
Figure 2.7 Comparison of binding modes of chloro substituents and methoxy substituents on the phenyl ring of pyrazole

Binding mode and complementarity of 3-chlorophenyl pyrazole, 3,5-dichlorophenyl pyrazole (left) and 3-methoxy phenyl pyrazole and 4-methoxy phenyl pyrazole (right) derivatives in the second pocket are shown on the surface of cyclin A.

In conclusion, the phenyltriazole Ncapping series was found to be the best heterocyclic isostere and substitution at the 3 and 5 positions resulted in the most potent FLIP molecule (**5773**) through the most favorable interactions and providing the best complementarity with the secondary pocket. The position of chloro substituent of the

43

phenyl ring determined specificity towards a particular cyclin with the 3-chloro and the 3,5-dichloro binding better to CDK2/cyclin A and the 4-chloro substitution resulting in high affinity for CDK4/cyclin D. In this study one of the most important N-terminal residues Arg of RRLIF was successfully replaced with phenyl heterocyclic based small molecules. Through this SAR studies on phenyl heterocyclic capping groups, the important interactions of N-capping groups that are key for binding have been explored. H bonding with Trp217 and Gln254 are crucial for binding and the size of substituents in the phenyl ring also contributes to complementarity and proper positioning of N-capping groups on top of secondary pocket. In addition, the drug likeness of the most potent molecule **5773** has been considerably improved compared to RRLIF. Physical properties such as clogP and total polar surface area (tPSA) helps in determining drug likeness and efficiency of the molecules to cross cell membranes. The clogP and polar surface area of 5773 is (+2.42 and 243) is better than RRLIF (-2.86, 303.52). The standard values for clog P are between -0.4 to 5.6 and tPSA is less than 140 Å based on Lipinski's rule of 5 for orally available drugs[65,66]. The FLIP molecule **5773** could be further improved for drug likeness with modifications on C-terminus with non-natural amino acids such as (β-Leu for Leu and Ile, NMePhe or 3thienylAla for Phe), as is discussed in detail in chapter 5. These observations related to the optimization of functional groups for binding and physicochemical properties of **5773** were utilized in the design of improved N-capping groups and converting the peptide RRLIF into more drug like molecule.

2.4 Experimental section

2.4.1 Synthesis

2.4.1.1 Materials and method

All solvents and reagents were used as obtained. ^{1}H NMR and ^{13}C NMR spectra were recorded with a Varian Mercury 300 and 400 Spectrometer, respectively. Mass spectra were measured with Micromass QTOF: Tandem quadruple-time of flight mass spectrometer electrospray ionization (ESI) and VG 70S: Double-focusing magnetic sector mass spectrometer (EI). Analytical purities of evaluated compounds were >95% unless stated otherwise. The following analytic method (unless stated otherwise) was used on a Waters Alliance 2695 HPLC with a 2996 diode-array detector and equipped a C18 (2) 100 A, 250 x 4.6mm, 5µ column (Phenomenox Luna). A gradient from 100% water (0.1% trifluoroacetic acid) to 60% acetonitrile (0.1% trifluoroacetic acid) was run over 30 mins and held for 4 mins. The chromatograms were extracted at 226 and 254 nm.

2.4.1.2 Synthesis of N-caps

The N-caps 1-(4-chlorophenyl)-5-methyl-1H-1,2,4-triazole-3-carboxylic acid, 1-(4-methylphenyl)-5-methyl-1H-1,2,4-triazole-3-carboxylic acid, 2-(3,5-dichlorophenyl)-1H-imidazole-5-carboxylic acid, 2-(3-chlorophenyl)-1H-imidazole-5-carboxylic acid were obtained commercially and the compound 2-(4-chlorophenyl)thiazole-5-carboxylic acid was synthesized in our lab. The NMR and MS spectra chromatograms for representative N-capping groups are shown in appendix. The analytical characterization data for all the FLIPs are shown in appendix table 1.

Preparation of phenyltriazole N-capping groups[57,58] **(5843, 5773, 5774, 5906, 5907)**

Ethyl 2-chloro-2-(2-(3,5-dichlorophenyl)hydrazono)acetate (**1a**)

To a solution of 3,5-Dichloroaniline (1.62g, 10mmol) in 10 ml methanol, 10 ml of 6 N Hydrochloric acid was added while maintaining the temperature at 0°C. Sodium nitrate (1.38g, 20mmol) was then slowly added as a solid. The reaction mixture was stirred for 15 mins at 0°C after which sodium acetate was added as a solid to adjust the reaction to pH 5. Subsequent to this, a solution of ethyl 2-chloroacetoacetate (1.64, 10mmol) in methanol was slowly added while maintaining the temperature at 0°C, after which the reaction mixture was allowed to warm to ambient temperature and stirred for 12 h. The reaction was monitored by TLC using 25% ethyl acetate in hexanes, for completion. Methanol was then removed under reduced pressure, diethyl ether was added and the organic layer was separated and washed with saturated sodium bicarbonate and water prior to drying over sodium sulfate. The organic layer was concentrated and the product crystalized from ethanol to give an orange solid 2.29g (77.7%).

^{1}H NMR (methanol-d4, 300 MHz) δ (ppm) 7.2 (s, 3H), 7.0 (s, 1H), 4.32-4.39 (q, J=3.52, 3H) 1.35-1.4 (t, J=3.41Hz, 3H). EI+ 294

Ethyl 2-chloro-2-(2-(3,5-dichlorophenyl)hydrazono)acetate (**1b**)

^{1}H NMR (chloroform-D, 300 MHz) δ (ppm) 7.27-7.25(m, 1H), 7.22(d, J-8.28Hz, 1H), 7.05(s, 1H), 7.02(d, J=10.56Hz, 1H), 6.99(d, J=7.92Hz, 1H), 4.39(q, 21.54Hz, 2H), 1.40(t, J=6.99Hz, 3H) EI+260

Ethyl 1-(3,5-dichlorophenyl)-5-methyl-1H-1,2,4-triazole-3-carboxylate (**2a**)

The step 1 product, Ethyl 2-chloro-2-(2-(3,5-dichlorophenyl)hydrazono)acetate (**1**) (2.29g, 7.7mmol), and acetaldehyde oxime (0.473g, 7.7mmol) were dissolved in

toluene and heated to reflux for 2h after which triethylamine (0.81g, 7.7mmol) was added. The reaction was monitored by TLC using 25% ethyl acetate in hexanes. After completion, the reaction mixture was then concentrated and partitioned between ethyl acetate and water. The layers were separated and the aqueous layer was washed with ethyl acetate. The combined organic layers were washed with water and brine, dried with sodium sulfate, filtered, and then concentrated. The residue was crystallized from diethylether/hexanes to give the product as fine, tan needles weighing 1.97g (84.5%).

^{1}H NMR (chloroform-D, 300 MHz) δ (ppm) 7.45 (s, 2H), 7.49 (s, 2H) 4.46-4.53 (q, J=3.36Hz, 2H) 2.62 (s, 3H), 1.41-1.46 (t, J=3.35Hz, 3H) ES+ 300

Ethyl 1-(3-chlorophenyl)-5-methyl-1H-1,2,4-triazole-3-carboxylate (**2b**)

^{1}H NMR (chloroform-D, 300 MHz) δ (ppm) 7.54(s,1H), 7.48-7.42(m, 3H), 4.50(q J=6.93Hz, 2H), 2.58(s, 3H), 1.44(t, J=7.14Hz, 3H) EI+265

1-(3,5-dichlorophenyl)-5-methyl-1H-1,2,4-triazole-3-carboxylic acid (**3a**)

The step 2 product, Ethyl 1-(3,5-dichlorophenyl)-5-methyl-1H-1,2,4-triazole-3-carboxylate (**2**) (1.9g, 6.33mmol) was refluxed in sodium hydroxide (2.02g, 50.64mmol), 19ml of ethanol and 19ml of water for 2h and the reaction was monitored by TLC (35% ethyl acetate in hexanes). After the completion of reaction, the reaction mixture was cooled, the alcohol was evaporated and diluted with water. The reaction mixture was acidified with 1N hydrochloric acid and stirred to precipitate the product.

^{1}H NMR (chloroform-D, 400 MHz) δ (ppm) 7.86 (t, J=1.04Hz) 7.8 (d, J= 1.12Hz3H) 2.54 (s, 3H)

^{13}C NMR (Dimethyl sulfoxide-D6, 400 MHz) δ (ppm) 160.6, 154.5, 154.11, 138.5, 135.1, 134.7, 129.0, 123.8

HRMS EI+ observed 270.9914, calculated 270.9915, 0.4ppm

1-(3-chlorophenyl)-5-methyl-1H-1,2,4-triazole-3-carboxylic acid (3b)

1H NMR (Dimethylsulfoxide, 400 MHz) δ (ppm) 7.80(s,1H), 7.64 (s, 2H), 2.51(s, 3H)

^{13}C NMR (Dimethyl sulfoxide, 400 MHz) δ (ppm) 160.80, 154.21, 154.00, 137.87, 133.69, 131.20, 129.29, 124.73, 123.55, 12.81

EI+237

Preparation of phenylpyrazole N-capping groups[59] (5762-5767, 5771)

Ethyl 1-(3,5-dichlorophenyl)-5-methyl-1H-pyrazole-3-carboxylate (**4a**)

1 g (4.68mmol) of 3,5-dichlorophenyl hydrazine was dissolved in 25 ml of acetonitrile in a 100 ml round bottom flask, triethylamine (0.47g, 6.9mmol) and ethyl aceto pyruvate (0.74g, 4.68mmol) were added to the reaction mixture under stirring and left to continue overnight. The reaction was monitored by TLC (25% ethyl acetate in hexanes) for completion. After the reaction was complete, the reaction mixture was diluted with dichloromethane and washed with water. The organic layer was separated, dried over sodium sulfate and concentrated. The crude mixture was then purified by flash chromatography (Biotage SP4) using a SNAP 100g column with a gradient run starting from 6% ethylacetate: 94% hexanes to 50% ethyl acetate and 50% hexanes over 15 column volumes to yield a white solid 0.39g (21% yield).

^{1}H NMR (chloroform-D3, 300MHz) δ (ppm) 7.431 (s, 3H), 6.744 (s, 1H), 4.49-4.44 (t, J=7.0Hz, 2H), 2.39 (s, 3H), 1.39-1.42 (t, J=2.54Hz, 3H), EI+298

Ethyl 1-(4-chlorophenyl)-5-methyl-1H-pyrazole-3-carboxylate (**4b**)

^{1}H NMR (chloroform-D3, 300MHz) δ (ppm) 7.37(q, J=8.61Hz, 4H), 6.81(s,1H), 4.23(q, J=7.14Hz, 2H), 2.34(s,3H), 1.26(t, J=7.29Hz, 3H) EI+265

Ethyl 1-(3-chlorophenyl)-5-methyl-1H-pyrazole-3-carboxylate (**4c**)

^{1}H NMR (chloroform-D3, 300MHz) δ (ppm) 7.52(t, J=8.48Hz, 1H), 7.22(t, J=7.08, 3H), 6.88(s,1H), 4.42(q, J=7.02Hz, 2H), 3.86(s,3H), 1.40(t, J=7.29Hz, 3H) ES-263

Ethyl 1-(3-fluorophenyl)-5-methyl-1H-pyrazole-3-carboxylate (**4d**)

^{1}H NMR (chloroform-D3, 300MHz) δ (ppm) 7.49(t, J=8.40Hz, 1H), 7.21(t, J=7.01, 3H), 6.78(s,1H), 4.38(q, J=7.02Hz, 2H), 3.76(s,3H), 1.34(t, J=7.18Hz, 3H) EI+249

Ethyl 1-(3-methoxyphenyl)-5-methyl-1H-pyrazole-3-carboxylate (**4e**)

^{1}H NMR (chloroform-D3, 300MHz) δ (ppm) 7.36(t, J=7.92Hz, 1H), 6.99(t, J=4.32, 3H), 6.95(s,1H), 4.41(q, J=6.96Hz, 2H), 3.86(s,3H), 2.32(s, 3H), 1.39(t, J=7.17Hz, 3H) EI+261

Ethyl 1-(4-methoxyphenyl)-5-methyl-1H-pyrazole-3-carboxylate (**4f**)

^{1}H NMR (chloroform-D3, 300MHz) δ (ppm) 7.45(d, J=8.79Hz, 2H), 7.07(d, J=8.79, 2H), 4.26(q, J=7.19Hz, 2H), 3.81(s,3H), 2.49(s, 3H), 1.27(t, J=7.19Hz, 3H) EI+ 261

ethyl 5-methyl-1-phenyl-1H-pyrazole-3-carboxylate (4g)

^{1}H NMR (chloroform-D3, 300MHz) δ (ppm)7.41(s, 5H), 6.79(s, 1H), 4.19(s, 2H), 2.35(s, 3H), 1.22(s, 3H) EI+231

1-(3,5-dichlorophenyl)-5-methyl-1H-pyrazole-3-carboxylic acid (**5a**)

The ester obtained from step1, ethyl 1-(3,5-dichlorophenyl)-5-methyl-1H-pyrazole-3-carboxylate (**4**) (0.39g, 1.3mmol) was dissolved in 10 ml methanol. The ester solution was treated with a 10 ml solvent mixture of tetrahydrofuran, 20% potassium hydroxide and methanol (1:1:1). The solution was stirred at room temperature overnight and after completion, as evidenced by TLC (25% ethylacetate in hexanes), methanol was evaporated and the reaction solution was partitioned between ethylacetate and water.

After washing with ethyl acetate, the aqueous layer was collected and acidified to pH 2 using 1N hydrochloric acid. The acidified aqueous layer was then partitioned between dichloromethane and additional water. The organic layer was dried over sodium sulfate and concentrated to get solid product 0.23g (100%).

^{1}H NMR (dimethyl sulfoxide-D6, 400MHz) δ (ppm) 7.78-7.79 (t, J=0.937Hz,) 7.8 (d, J=1.14, 1H), 6.74 (s, 1H), 2.50 (s, 3H)

^{13}C NMR (dimethyl sulfoxide-D6, 400MHz) δ (ppm) 162.9, 144.5, 141.4, 140.8, 134.5, 128.0, 123.5, 11.9

HRMS EI+ Observed 269.9959, calculated 269.9963, 1.5ppm

1-(4-chlorophenyl)-5-methyl-1H-pyrazole-3-carboxylic acid (**5b**)

^{1}H NMR (chloroform-D3, 300MHz) δ (ppm) 7.45(q, J=9.30Hz, 4H), 6.79(s, 1H), 2.36(s,3H) ES- 235

1-(3-chlorophenyl)-5-methyl-1H-pyrazole-3-carboxylic acid (**5c**)

^{1}H NMR (chloroform-D3, 300MHz) δ (ppm) 7.42(t, J=8.52Hz, 1H), 6.98(t, J=7.19Hz, 3H), 6.54(s,1H), 3.81(s, 3H), 2.32(s,3H) EI+ 237

1-(3-fluorophenyl)-5-methyl-1H-pyrazole-3-carboxylic acid (**5d**)

^{1}H NMR (chloroform-D3, 300MHz) δ (ppm) 7.48(t, J=8.71Hz, 1H), 7.02(t, J=7.45Hz, 3H), 6.74(s,1H), 3.92(s, 3H), 2.46(s,3H) EI+ 221

1-(3-methoxyphenyl)-5-methyl-1H-pyrazole-3-carboxylic acid (**5e**)

^{1}H NMR (chloroform-D3, 300MHz) δ (ppm) 7.38(t, J=8.55Hz, 1H), 7.00(t, J=7.17Hz, 3H), 6.77(s, 1H), 3.84(s, 3H), 2.36(s,3H) EI+ 233

1-(4-methoxyphenyl)-5-methyl-1H-pyrazole-3-carboxylic acid (**5f**)

^{1}H NMR (chloroform-D3, 300MHz) δ (ppm) 7.43(d, J=8.76Hz, 2H), 7.04(d, J=8.76Hz, 2H), 3.86(s, 3H), 2.38(s, 3H) EI+ 233

5-methyl-1-phenyl-1H-pyrazole-3-carboxylic acid (5g)

^{1}H NMR (chloroform-D3, 300MHz) δ (ppm) 7.57 (s,1H), 7.44(s, 2H), 7.38(s, 1H), 6.80(s, 1H), 2.38(s,3H) ES- 201

Preparation of phenylfuran N-capping groups [60] (5768, 5769)

Synthesis of 5-(3,5-dichlorophenyl)furan-2-carboxylic acid (6a)

A mixture of 3,5-dichloro aniline (0.84g, 5mmol), hydrochloric acid (15%, 3ml) and water (4.5ml), was heated until a clear solution was obtained. This solution was then cooled to 0°C, diazotized with aqueous sodium nitrite (30%, 1.2ml) and filtered. To the filtered solution, water (2.5ml) and furoic acid (0.56g, 5mmol) were added. An aqueous solution of cupric chloride (0.125g in 10 ml water) was added dropwise and stirred for 4h at room temperature and kept aside for 16h. The resulting solid was filtered off, suspended in water and purified by flash chromatography (Biotage SP4) using a SNAP 100g column with a gradient 0% to 40% ethylacetate for 5 column volumes, the concentration of ethyl acetate at 40% was kept constant for 2 column volumes and then increased to 100% in 5 column volume. The purified product obtained weighed 0.36g (28%)

^{1}H NMR (dimethyl sulfoxide-D6, 400MHz) δ (ppm) 7.85 (d, 2H), 7.65 (t, 2H), 7.36 (d, J=3.88Hz, 1H), 7.40 (d, 3.96, 1H)

^{13}C NMR (dimethyl sulfoxide-D6, 400MHz) δ (ppm) 159.0, 152.9, 145.0, 134.9, 132.2, 128.0, 122.7, 119.7, 110.5

HRMS EI+ Observed 255.9698, calculated 255.9694, 1.6ppm

Synthesis of 5-(3,5-dichlorophenyl)furan-2-carboxylic acid (**6b**)

^{1}H NMR (dimethyl sulfoxide-D6, 300MHz) δ (ppm) 7.80(d, J=8.64Hz, 2H), 7.53(d, J=12.36Hz, 2H), 7.30(d, J=4.53Hz, 1H), 7.17(d, J=3.69Hz, 1H) ES-221

Preparation of phenylpyrrole N-capping groups [61] (5775, 5776)

1-(4-chlorophenyl)-1H-pyrrole-3-carbaldehyde (7a)

4-chloroaniline (0.51g, 4 mmol), 2,5-dimethoxytetrahydrofuran-3-carbaldehyde (0.76g, 4.8 mmol), acetic acid (16ml) were stirred in a round bottom flask until a red colored solution was observed. The reaction mixture was then refluxed at 120°C for 15 mins and a dark reddish brown solution was obtained. The reaction was monitored by TLC (25% ethyl acetate: 75% hexanes) and worked up when complete. The reaction mixture was cooled, extracted with ethyl acetate and the organic layer was washed with saturated sodium bicarbonate, dried over sodium sulfate and concentrated to get 0.77g (94%)

^{1}H NMR (chloroform-D3, 300MHz) δ (ppm) 9.85 (s, 1H), 7.62-7.63 (t, J=1.8Hz, 1H), 7.44-7.47 (d, J=9Hz, 2H), 7.34-7.37 (d,J=9.3Hz, 2H) 7.05 (t, J=0.9Hz, 1H), 6.57-6.58 (q, J=1.5Hz, 1H) EI+204

1-(3,5-dichlorophenyl)-1H-pyrrole-3-carbaldehyde (7b)

^{1}H NMR (chloroform-D3, 300MHz) δ (ppm) 9.86(s,1H), 7.64(s, 3H), 7.34(s, 1H), 7.06(s,1H), 6.82(s,1H) ES+ 240

1-(4-chlorophenyl)-1H-pyrrole-3-carboxylic acid (8a)

1-(4-chlorophenyl)-1H-pyrrole-3-carbaldehyde(7) (0.76g, 3.58mmol) obtained from step 1, silver nitrate (1216.26mg, 7.16mmol), 6 N sodiumhydroxide (15ml) and methanol (5.8ml) were refluxed for 5h and the reaction was monitored by TLC for completion. The reaction mixture was filtered through celite and the aqueous layer was acidified to get a white precipitate. The precipitate was filtered off, dissolved in ethyl acetate, and dried over sodium sulfate to get the product 0.6g (65%)

^{1}H NMR (dimethyl sulfoxide-d6, 400 MHz) δ (ppm) 7.95 (t, J=0.93, 1H), 7.71-7.73 (d, J=4.6Hz, 2H), 7.53-7.56 (d, J= 4.7Hz, 2H), 7.43-7.44 (t, J= 1.33Hz1H), 6.61-6.62 (q, J=0.88Hz, 1H)

^{13}C NMR (dimethyl sulfoxide-d6, 400 MHz) δ (ppm) 165.0, 137.9, 130.5, 129.5, 123.9, 121.7, 120.7, 118.6, 111.5 HRMS

EI+ observed 221.0242, calculated 221.0244, 0.9ppm

1-(4-chlorophenyl)-1H-pyrrole-3-carboxylic acid (8b)

^{1}H NMR (chloroform-D3, 300MHz) δ (ppm) 7.64(s,1H), 7.34(s,3H), 7.06(s,1H), 6.82(s,1H) ES+ 256

2.4.2 Fluorescence Polarization Binding Assay

CDK4D1 FP assay: This assay was performed using black 384-well plates using a previously described procedure[2] with the following modifications. To each well were added: 5 µl CDK4D1 (0.3 µg/well purified recombinant human kinase complex from Invitrogen), 5 µl compound solution, 5 µl 30 nM fluoresceinyl-Ahx-Pro-Val-Lys-Arg-Arg-Leu-(3ClPhe)-Gly tracer peptide. Compounds and kinase complexes were diluted

using assay buffer (25 nM HEPES pH 7, 10 nM NaCl, 0.01% Nonidet P-40, 1mM dithiothretiol (DTT). Plate was centrifuged for 1 min at 500 rpm and then incubated with shaking for 45 mins at room temperature. Fluorescence polarization was read on DTX880 multimode detector (Beckman Coulter, Brea, CA) fitted with 485 nm/535 nm excitation/emission filters and a dichroic mirror suitable for fluorescein. Relative mp was calculated for each concentration tested using the equation showing below. IC_{50} values were determined by logarithmic regression by correlating relative mps and testing concentrations.

$$\text{Relative mp} = \frac{\text{mP(compound)-mP(DMSO, protein, tracer)}}{\text{mP(DMSO, protein)-mP(DMSO, protein, tracer)}}$$

CDK2A2 FP assay: This assay was performed using black 384-well plates. To each well were added: 5 µl CDK2A2 (0.3 µg/well purified recombinant human kinase complex), 5 µl compound solution, 5 µl 30 nM fluoresceinyl-Ahx-Pro-Val-Lys-Arg-Arg-Leu-Phe-Gly tracer peptide. Compounds and kinase complexes were diluted using assay buffer (25 nM HEPES pH 7, 10 nM NaCl, 0.01% Nonidet P-40, 1mM dithiothretiol (DTT). Plate was centrifuged for 1 min at 500 rpm and then incubated with shaking for 45 mins at room temperature. Fluorescence polarization was read on DTX880 multimode detector (Beckman Coulter, Brea, CA) fitted with 485 nm/535 nm excitation/emission filters and a dichroic mirror suitable for fluorescein. Relative mp was calculated for each concentration tested using the equation showing below. IC_{50} values were determined by logarithmic regression by correlating relative mps and testing concentrations.

2.4.3 Docking[55]

All the N-capping groups were docked in the cyclin A/CDK2 crystal structure (PDB ID 2UUE) using 1-(3,5- dichlorophenyl)-5-methyl-1H-1,2,4-triazole-3-carbaldehyde as control ligand. The parameters of the LigandFit (Discovery Studio 3.0, Accelrys) were PLP1 energy grid, minimization sphere "on", number of poses 10. All the docked poses analyzed with PLP1 scoring function, hydrogen bonding and were subjected to visual analysis for complementarity with second pocket.

2.5 Acknowledgement

This chapter is written based on the following article with permission from the publisher **Shu Liu, Padmavathy Premnath (joint first author),** Joshua Bolger and Campbell McInnes, Optimization of CDK/cyclin groove Inhibitors through REPLACE mediated Fragment Assembly, *Journal of Medicinal Chemistry*, 2013, 56 (4), 1573–1582

CHAPTER 3

FRAGMENT BASED DISCOVERY OF ARGININE ISOSTERES THROUGH REPLACE: TOWARDS NON-ATP COMPETITIVE CDK INHIBITORS

3.1 Introduction

In the chapter 2, the design, SAR and optimization of fragment alternatives based on phenyl heterocyclic carboxylic acids was described. These were designed from a phenyltriazole Ncap that was discovered during proof of concept for the REPLACE strategy[49]. Despite the search for replacements for the critical Arg4 residue, this capping group only retained the interactions of the Ala2 methyl side chain and hydrogen bonding interactions with Trp217 and Gln254[49]. The ion-pairing contacts of Arg4 were not observed in this for any of the subsequent phenyl heterocyclic isosteres. As next step, the design of N-capping groups retaining hydrophobic contacts with the secondary pocket and H-bonding interactions observed in the previous series but adding basic functionality were explored to identify surrogates for arginine and more completely mimic the contacts of the native peptide. The REPLACE strategy was used to identify FLIPs synthesized from derivatives of phenyl acetic, furoic and picolinic acids as N-capping groups. These fragment alternatives were identified through molecular docking studies. The LigandFit[55] method was used after validation that it was predictive for similar known fragment ligands that were docked into the binding site for Arg4 after its deletion from the structural complex. Virtual fragment hits were obtained and used to generate Fragment

Ligated Inhibitory Peptides (FLIPs)[56] and tested in the previously mentioned assay to study their competitive binding efficiency[57].

3.2 Results

3.2.1 Validation of LigandFit docking method

The first step for any in silico screening method is to assess its predictive capability. LigandFit[55] is an accurate, fast and shape based method which can identify and generate poses of ligands that are complementary to the active site of the protein of interest. The procedure involves two main steps: (i) cavity detection for the identification of active site and (ii) docking of ligands at the active site. In the case of an unknown binding site, LigandFit utilizes a cavity detection algorithm for detecting a potential ligand interacting site and in case of a known active site through the crystal structure of a protein-ligand complex, the ligand structure is used to define the active site points. A shape based comparison filter combined with a Monte Carlo conformational search is employed for generating ligand poses that have shape complementarity to the active site. Furthermore, a grid based method is employed to generate more realistic protein-ligand interactions for poses minimized based on the active site[55].

As mentioned above, parameters used in any docking protocol should be optimized prior to docking of unknown ligands to ensure that these will be predictive. To do this a ligand with known orientation in the cyclin groove is redocked to assess if correct binding modes are reproduced by the algorithm. To accomplish this, docking was carried out in CBG of CDK2/cyclin A (PBD ID:2UUE) by varying the parameters of the docking protocol using the ligands (1-(3,5-dichlorophenyl)-5-methyl-1H-1,2,4-triazole-3-carbonyl (35DCPT) and 1-(4-chlorophenyl)-5-methyl-1H-1,2,4-triazole-3-carbonyl)

(4CPT) as positive controls and 5-chloro-2-phenyl-1,8a-dihydroimidazo[1,2-a]pyridine-3-carbaldehyde as a negative control. These molecules were used as controls based on previous studies in which 35DCPT and 4CPT were shown to occupy the position of Arg4 at CBG in their respective crystal structures (PBD ID: 2UUE, 2V22). FLIPs N-capped with 35DCPT and 4CPT bind to CBG and inhibit CDK2/cyclin A whereas the negative control containing FLIP had very poor inhibitory activity[49]. The structures of positive and negative control are shown in figure 3.1. Important parameters of the LigandFit protocol affecting the generated binding mode were optimized and include the type of energy grid and minimization algorithm and also the number of poses generated and scoring function used to differentiate good from bad poses.
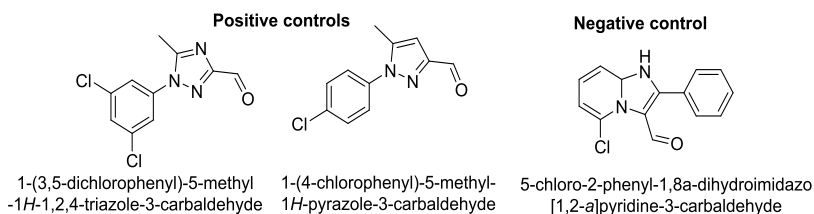

Positive controls   Negative control

1-(3,5-dichlorophenyl)-5-methyl
-1*H*-1,2,4-triazole-3-carbaldehyde

1-(4-chlorophenyl)-5-methyl-
1*H*-pyrazole-3-carbaldehyde

5-chloro-2-phenyl-1,8a-dihydroimidazo
[1,2-*a*]pyridine-3-carbaldehyde

Figure 3.1 Structures of positive and negative controls

The energy grid is the force field for calculating ligand-receptor interaction and three types are available within LigandFit: the Dreiding force field with Gasteiger charges, the CFF (Consistent Force Field) and PLP1 (Piecewise linear potential). The first step in the validation study was to evaluate each of these energy grids and then select the one that generates the highest number of accurate poses. After finding a suitable energy grid, the use of a minimization algorithm was studied by turning it on or off during LigandFit docking. It can be used to generate poses with relaxed conformations and also to remove steric overlap that occurs during docking and results in bad poses. The next step in the validation exercise is to determine which overall force field is optimal.

58

CHARM and CFF are two examples of those available to generate atom types and to assign partial charges to the atoms of the simulation and ultimately to estimate the binding affinity as sum of the strength of intermolecular van der Waals and electrostatic interaction between atoms of the ligand and receptor. Docking time is a concern when evaluating thousands of compounds and thus it is very important to set an optimal value for the number of poses generated for each ligand docked determines length of the calculation. For this validation, the number of poses generated was varied between 5, 10 and 20 to determine the optimal number required in order to reduce the docking time. The last step in the docking validation is to determine which scoring function is able to correctly assess experimental binding modes for a known ligand. Scoring functions are used to rapidly estimate the binding affinity of a docked ligand pose based on the geometry of the conformation and its non-covalent interaction with the target receptor. Ligscore1_Dreiding, Ligscore2_Dreiding, PLP1, PLP2, PMF, DOCKSCORE and Jain scoring functions were evaluated.

The LigandFit parameters were optimized based on the number and accuracy of poses for the known ligands docked into the cyclin groove i.e., maximum number of correct poses of the positive control ligands and minimum or no poses of negative control ligand in top scoring poses. A correct pose is one that binds in the receptor in a very similar orientation to the true ligand and thus superimposes well with true ligand binding mode and interactions with the defined interaction filters. A close pose is one where the positive control ligand binds in similar orientation to the correct pose and has RMSD (root mean square distance) of less than 2.0 Å compared to the true ligand binding mode. Optimized parameters obtained in the validation exercise will then be selected for

59

docking of the library of unknown fragments.

The binding modes of the 35DCPT Ncap have been previously characterized by X-ray crystallography and were used for the generation of site points. The volume occupied by the ligand at the binding site determines the site points. In this study, site points cover the interaction of the phenyl ring (attached to N-1 atom of triazole) in the secondary hydrophobic cleft of the CBG and those of the H-bonds of the triazole N-2 atom with indole nitrogen of Trp217 and carbonyl oxyen with the amide side chain of Gln254. Along with these interactions, the correct orientation of the carbonyl group was studied because this is required for the formation of an amide bond to the peptide in FLIP synthesis. As the crystal structure is a tetrameric complex of two CDK2/cyclin A heterodimers, both cyclin subunits were evaluated in the validation by docking the positive and negative control ligands into the CBG (PBD ID 2UUE).

Table 3.1 Determination of the optimal cyclin subunit (2UUE)

Energy Grid	Dreiding		CFF		PLP1	
Sub units	Subunit B	Subunit D	Subunit B	Subunit D	Subunit B	Subunit D
No. of correct poses of 3,5-DCPT	2	-	4	-	6	-
No. of correct poses 4-DCPT	-	-	-	-	8	-
No. of closer poses (<2.0Å) of 3,5-DCPT	3	-	4	-	4	-
No. of closer poses (<2.0Å) of 4-DCPT	15	-	8	-	6	11
-ve controls in top 25	18	-	15	-	-	-
Best scoring functions	LigScore2_Dreiding	-	PLP1, PLP2	-	PLP1, PLP2	Ligscore1_dreiding, Ligscore2_dreiding, PLP1

Docking results for B subunit showed that 10 and 14 correct/close poses respectively were obtained for 35DCPT and 4CPT respectively whereas for the D

subunit, 11 close poses of 4-CPT and no correct poses for 3,5-DCPT resulted from the calculations. There were no poses of the negative control ligand in the top 25 poses for either subunit. As a result, the B subunit was considered for further parameter optimization (Table 3.1). For each energy grid evaluated, the number of correct/close poses in top 25 based on ranking of the scoring function (Ligscore1_Dreiding, Ligscore2_Dreiding, PLP1, PLP2, Jain, PMF and DOCKSCORE) was determined. The energy grids, Dreiding, CFF and PLP1 generated 2, 4 and 6 correct poses respectively for 35DCPT. In top 25 scoring poses, there were 18 and 15 poses of negative ligands observed for Dreiding and CFF respectively but there were no negative ligand poses found for PLP1. After confirming that the PLP1 energy grid was the most effective, it was used for further validation runs where scoring functions were analyzed individually. The best scoring function was found to be PLP1 which generated 6 correct and/or close poses of 35DCPT and 4CPT in the top 25 ranked poses. Results for the docking parameter optimization are shown in Table 3.2.

Table 3.2 Optimization of LigandFit docking parameters for the cyclin A groove

Energy Grid	Dreiding	CFF	PLP1
No. of correct poses 3,5-DCPT	2	4	6
No. of correct poses 4-DCPT	-	-	8
No. of -negative controls in top 25	-PLP1(4), -PLP2(4), Jain (4), PMF(4), DOCK SCORE(6)	-PMF (7), DOCK SCORE (6)	No -ve control poses in all the scoring functions
Best scoring functions	LigScore2_Dreiding	PLP1, PLP2	PLP1, PLP2
3,5-DCPT(rank of top 25 correct/closer poses for the best scoring function)	4,5 (for all the scoring functions)	PLP1(9-12,25), PLP2(13-16,25)	PLP1(7-14,25), PLP2(11-18)
4-DCPT (rank of top 25 correct/closer poses for the best scoring function)	-	PLP1(1-8), PLP2(17-24)	PLP1(1-6) PLP2(20-25)

Having minimization sphere "on" minimizes the ligands to their lowest energy conformations after docking. Hence 10 was considered an optimal number for number of poses generated because it generated sufficient number of poses for interpreting the results while saving the docking time. The conclusion of this docking validation study is that the optimized parameters were found involve the use of the PLP1 energy grid the minimization sphere, and the generation of 10 poses. The docking carried out for the known ligands showed that the experimental binding modes of ligands can successfully be reproduced and therefore the method should be predictive.

3.2.2. Docking of the virtual capping group library.

To more completely exploit the interactions of high affinity peptidic cyclin groove inhibitors, a library of compounds based on the crystal structure ligand (1-(3,5-dichlorophenyl)-5-methyl-1H-1,2,4-triazole-3-carboxaldehyde 35DCPT) and using SAR of the parent peptide (HAKRRLIF) was designed. The criteria used in the library design included (i) molecular weight less than 400, (ii) presence of a carboxylic acid group for the formation of amide bond with the peptide sequence, (iii) incorporation of alkyl/aryl substitutions for van der Waals interactions with the secondary pocket, (iv) basic functionality for ion-pairing interaction with acidic residues and (iv) synthetic feasibility/ commercial availability. This library was built using the following cores strucures: 5-membered heterocyclic ring substituted with a carboxylate, phenyl acetic acids and 6-membered heterocyclic ring substituted with a carboxylate.

1. 5-membered heterocyclic rings: These include 1,2,4- triazole, pyrazole, furan, pyrrole, and thiophene rings. The latter were linked to another 5-membered heterocyclic structure (imidazole, pyrazole and thiophene). In addition to these, the

62

furoic acids were substituted with diethylaminomethyl and piperazinylmethyl groups. Some examples are shown in figure 3.2. These basic groups were included to exploit ion-pairing interactions with the acidic residues (Glu220, Glu224 and Asp283; cyclin A numbering) made by Lys3 and Arg4 (HAKRRLIF). The heteroatoms in the 5-membered ring were included to interact with H bond donors in the cyclin groove (e.g. the indole nitrogen of Trp217).
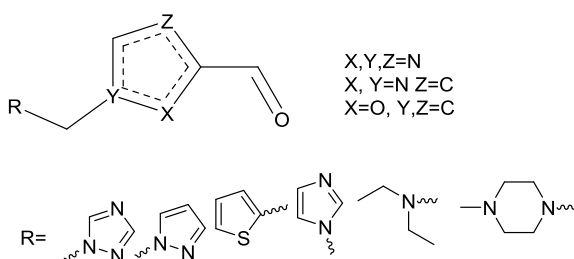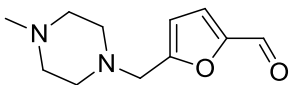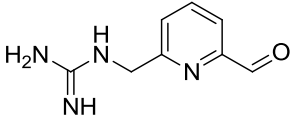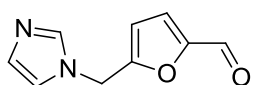

X,Y,Z=N
X, Y=N Z=C
X=O, Y,Z=C
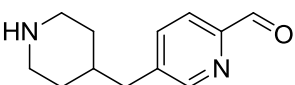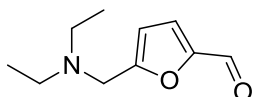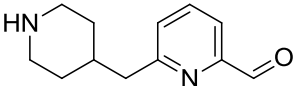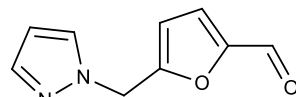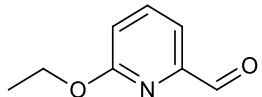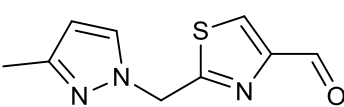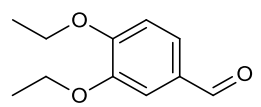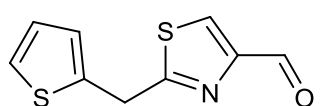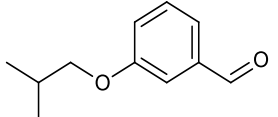
Figure 3.2 Examples of structures 5-membered heterocyclic structures docked

2. Phenyl acetic acids: These were substituted with alkoxy groups at the 3 position and were expected to interact with the secondary pocket occupied by the Ala2 methyl side chain in the peptide.

3. Picolinic acids: These were substituted with alkyl groups at the 3 position for interacting with the secondary pocket and with basic groups at the 4 position for ion-pairing interactions (piperazinylmethyl, guanidomethyl and dimethylaminomethyl groups).

Each potential Ncap was docked as an aldehyde into the cyclin groove of CDK2/Cyclin A (PBD ID 2UUE) using the validated LigandFit docking method in order to predict the correct orientation. Presence of carboxylic acid group would be hindrance and interfere with interaction filter. Hence the molecules were docked as aldehydes. Docked molecules were prioritized based on high PLP1 score, shape complementarity

and consensus scoring. Consensus scoring is a way of assessing poses that score well in multiple scoring functions (in this case, the seven scoring functions used) with the aim of obtaining a more accurate estimate of the various interactions between the receptor and the ligand. The PLP1 scoring and the shape complementarity of top scoring poses were comparable with the true ligands 3,5-DCPT and 4-CPT. The structures and PLP1 scoring values of virtual hits are shown in table 3.3.

Table 3.3 Hit molecules with their PLP1 scoring

Structure	PLP 1	Structure	PLP 1
	54.28		48.83
	42.61		53.12
	52.1		49.18
	48.4		45.32
	45.35		46.7
	43.84		45.92
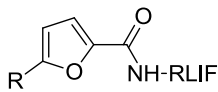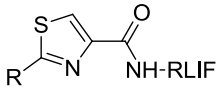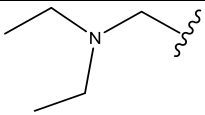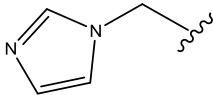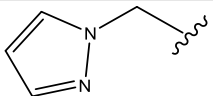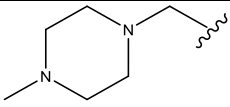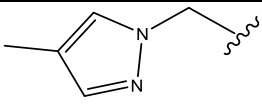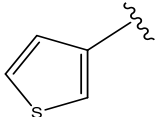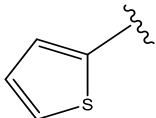
3.2.3. Structure activity relationship of N-capping groups

In Chapter 3, phenylheterocyclic carboxamido FLIPs, were described and the structure-activity was explored for interactions with the secondary pocket and H-bonding residues of the cyclin groove (e.g. Trp217 and Gln254)[63]. Residues of the N-terminal

tetrapeptide of HAKRRLIF make ion-pairing interactions with acidic side chains surrounding the secondary pocket. Arg4 of HAKRRLIF occupies the ridge of the cyclin groove that separates both the major and minor lipophilic pockets and makes ion-pairing interactions with Glu220 and Glu224 thus providing a significant portion of the affinity for the peptide. Here, groups capable of ion-pairing interactions were incorporated onto various scaffolds. Some of these scaffolds were designed to be capable of H-bonding and hydrophobic interactions. The heterocyclic carboxylic acids substituted with basic functionality were designed to make ion-pairing interactions with the acidic residues (Glu220 and Glu224) and H-bonding contacts with cyclin groove side chain atoms (Trp217 and Gln254). 5 and 6 membered nitrogen and oxygen heterocycles were hypothesized to facilitate H-bonding interactions observed in the 35DCPT capping group (to the indole nitrogen of Trp217). The amide group present in all the compounds makes hydrogen bonding with Gln254. Phenylacetic and picolinic acid derivatives were substituted with alkyl/alkoxy groups to further explore SAR of the minor hydrophobic pocket.

After scoring the docked ligands, potential capping groups were further prioritized based on commercial availability and/or ease of synthesis and subsequent to this incorporated into FLIPs (appended onto the RLIF sequence). Of all of the FLIPs synthesized and derived from furoic acids (table 4.4), only **5581** (CDK2/cyclin A- 43.4 μM, CDK4/cyclin D-41.9μM) and **5589** (CDK2/cyclin A- 50.3 μM, CDK4/cyclin D-43.2 μM) possessed significant activity and exhibited similar potency in binding to both CDK2/cyclin A and CDK4/cyclin D. All the other FLIPS from this series and those derived from thiophene carboxylic acids showed weak activity (table 3.4).
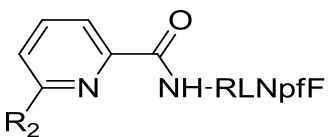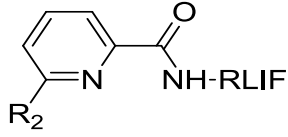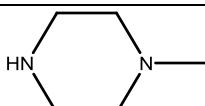
Table 3.4 SAR of 2-Furoic acid and Thiazole-4 carboxylic acid based FLIPs

SCCP ID	R	Core		CDK2/cyclin A IC$_{50}$ (mM)	CDK4/cyclin D1 IC$_{50}$ (mM)
5581		1	-	43.5±1.2	41.9±3.1
5585		1	-	>100	>100
5586		1	-	>100	>100
5589		1	-	50.3±1.3	43.2±5.0
5761		1	-	>100	>180
5582		-	2	56.2±1.2	>180
5584		-	2	>180	>180

An additional scaffold which was explored and verified computationally was the picolinic acid based fragment. The 6 position was substituted with alkyl, alkyloxy and piperazinylmethyl groups and these were incorporated as Ncaps into either the RLIF or RLNpfF peptide. Thus, unsubstituted, 6-methoxy, 6-ethoxy derivatives were ligated to RLNpFF while 6-methyl and 5-piperazinylmethyl analogs (**5856**) were appended to the RLIF sequence. The compound having a piperazinyl methyl substitution at the 5 position, **5856** shows moderate activity in binding to CDK2/cyclin A (>100μM) and greater

potency for inhibition of the cyclin groove of CDK4/cyclin D (21.9 µM) with roughly equal activity compared to RRLIF (CDK4/cyclin D- 16.4 µM). The results are shown in table 3.5.

Table 3.5 SAR of Picolinic acids based FLIPs

SCCP ID	R2	Core		CDK2/cyclin A IC$_{50}$ (mM)	CDK4/cyclin D1 IC$_{50}$ (mM)
525	H	1	-	29.2±1.3	48.4±1.2
5845	Me	-	2	>100	85.7±1.9
524	OMe	1	-	36.4±1.2	>100
523	OEt	1	-	39.7±1.2	>100
5856	HN—(piperazine)—N—	-	2	>100	21.9±1.1

Phenylacetic acid derivatives were a third scaffold that was studied and analogs were designed to explore the effect of the incorporation of methylene bridge between the phenyl ring and the carboxyl group, on the lipophilic interactions with the secondary pocket. Three analogs 3-ethoxy (**5854**), 3-propoxy (**5853**) and 3-isobutyloxy (**5855**) phenylacetic acid were synthesized by alkylation of 3-hydroxyphenylacetic acid using the appropriate alkyl bromide followed by base hydrolysis of the ester which occurs due to concomitant alkylation of the carboxylate (scheme 4.1)[67]. These N-capping groups were then ligated to RLIF with the exception of **530** where 3,4- diethoxyphenyl acetic acid was

obtained commercially and appended to RLNpfF. This bis-substituted analog showed the

best activity in this phenylacetic acid derived series with IC_{50} values of 5.2 µM and 3 µM

in CDK2/cyclin A and CDK4/cyclin D respectively. All other compounds were

marginally or completely inactive. The activity of the phenylacetic acid based FLIPs are

shown in table 3.6.

Scheme 3.1 Synthesis of phenyl acetic acid derivatives

.
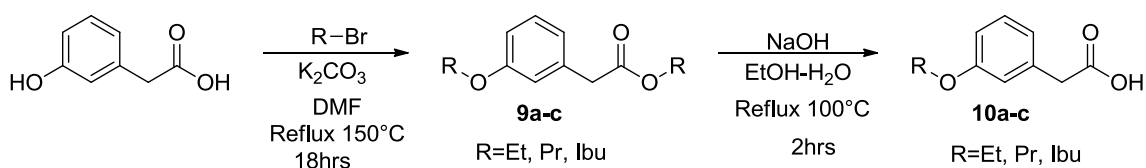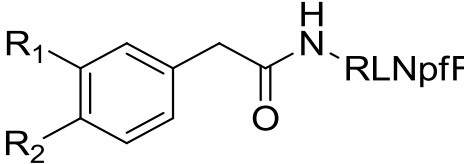
Table 3.6 SAR of Phenylacetic acid based FLIPs

SCCP ID	R1	R2	CDK2/cyclin A IC_{50} (mM)	CDK4/cyclin D1 IC_{50} (mM)
5854	H	OEt	>100	>100
5853	H	n-OPr	>100	>50
5855	H	t-OBu	>100	>100
530	OEt	OEt	5.2±1.3	3.0±2.12

3.3 Discussion and conclusion

Optimizing docking parameters is a mandatory step for every receptor-ligand complex as interactions vary considerably with each target. For every target we need to find the optimal set of parameters that will reproduce experimental binding modes and thus will be customized to that particular target. Validation of the LigandFit method was carried out to ensure that the method is able to reproduce experimental binding modes for known ligands of the cyclin groove and therefore show that the docking results of unknown compounds will be predictive. The PLP1 energy grid and scoring function were selected as optimal parameters that were effective in reproducing the binding modes of native ligands (35DCPT, 4CPT). Energy grid PLP1 was able to reproduce maximum number of correct or closer poses compared to Dreiding and CFF. Scoring functions in general are calculated based on assessment of a combination of electrostatic, van der Waals and hydrogen bonding energies. Of all the seven scoring functions (Jain, Ligscore1, Ligscore2, PLP1, PLP2, DOCKSCORE and PMF) studied PLP1 was found to be the most successful as this includes hydrogen bonding terms and hydrophobic interactions. In this study the binding efficiency at the cyclin groove – substrate protein-protein interaction interface is being evaluated and thus is comprised of a variety of interactions with H-bonding being a major contributor to affinity of CGI ligands. A library of small molecules based on 5-furoic acid, thiazole-4-carboxylic acid, 5 and 6 substituted picolinic acids, and also 3 and 4 substituted phenylacetic acids were docked to evaluate for their ability to completely interact with cyclin groove. Among the docked molecules, 16 molecules were synthesized as FLIPs and tested in FP assay.

Among the Ncap series based on furoic acids, FLIPs having furoic acid with basic

substituents (5-((diethylamino)methyl)furan-2-carboxylic acid - **5581** and 5-((4-methylpiperazin-1-yl)methyl)furan-2-carboxylic acid - **5589**) showed greater activity towards both cyclin complexes than 5-((1H-imidazol-1-yl)methyl)furan-2-carboxylic acid - **5585** and 5-((1H-pyrazol-1-yl)methyl)furan-2-carboxylic acid - **5586**. The basic groups in the Ncaps will be protonated and thus positively charged at physiological pH. This activity observed for **5581** and **5589** is most likely because of the ion-pairing interaction of the charged basic groups with acidic residues in the cyclin groove (Glu220 and Glu224; cyclin A and Glu66; cyclin D). In addition to their ion-pairing interactions, docked poses indicate that the ethyl groups of **5581** and the piperazine ring carbons of **5589** interact with the secondary pocket occupied by the Ala side chain of the parent peptide and also mimicking the van der Waals interactions of the phenyl ring of the 35DCPT capping group. Among the thienyl FLIP analogs (5-(thiophen-2-yl)furan-2-carboxylic acid - **5584**) and (5-(thiophen-3-yl)furan-2-carboxylic acid -**5582**), **5582** possessed the greatest affinity for cyclin A in complex with CDK2 most likely because it has a larger secondary pocket to accommodate the thiophene ring.

As previously discussed in chapter 3, the oxygen atom in the furan ring is a poor hydrogen bond acceptor compared to nitrogen containing heterocycles (i.e. 1,2,4-triazoles and pyrazoles) resulting in weak binding affinity of FLIPs containing this ring system[63]. This is a likely reason for the overall weak affinity of this series relative to the phenyltriazole capping groups discussed in chapter 3. But **5581** and **5589** exhibit better binding affinity towards CBG compared to other phenylfuroic acid derivatives as a result to the presence of basic groups. Therefore, it is likely that appending the basic substituents evaluated in furoic acid series onto the 1,2-4 triazole should result in

significant improvements in binding. The interactions of selected results are shown in figure 3.3. In addition, benzoic acid derived capping groups incorporating basic groups were evaluated and are discussed in chapter 5.

Picolinic acids derivatives were designed to incorporate a heteroatom capable of mimicking H- bonding interactions (Trp217, Gln254) observed in the 35DCPT capping group and in the peptide context. This was confirmed by the respectable activity of the unsubstituted picolinamide capped peptide (**525**). In addition to H-bonding, the methyl or alkoxy group at the 6 position was hypothesized to provide hydrophobic complementarity with the second pocket while the piperazinylmethyl group should offer both ion-pairing and van der Waals interactions (**5856**). This did not prove to the case since the designed FLIP was inactive in binding to the CDK2/cyclin A complex. The considerable binding activity of 5856 for cyclin D/CDK4 is likely the result of closer positioning of the free piperazine N-atom for ion-pairing with Glu66. Minimal activity of the 6-methoxy (**524**) and 6-ethoxy (**523**) derivatives relative to the unsubstituted compound (**525**) indicate that these substitutions are not appropriately positioned to interact with the pocket. Since the picolinamide capping group is a six membered ring system, placing larger substituents in the 6-position may lead to a steric clash leading to weaker interaction with Trp217.

5581 (PLP1- 52.1)
IC_{50} (CDK2/cyclin A- 43.5±1.2µM
CDK4/cyclin D-41.9±3.1µM)

5585 (PLP1- 42.61)
IC_{50} (CDK2/cyclin A> 100µM
CDK4/cyclin D>100µM

5589 (PLP1-54.28)
IC_{50} (CDK2/cyclin A- 50.3±1.3µM,
CDK4/cyclin D-43.2±5.0µM)

5856 (PLP1-35.03)
IC_{50} (CDK2/cyclin A- >100 µM
CDK4/cyclin D – 21.9 ±1.1 µM)
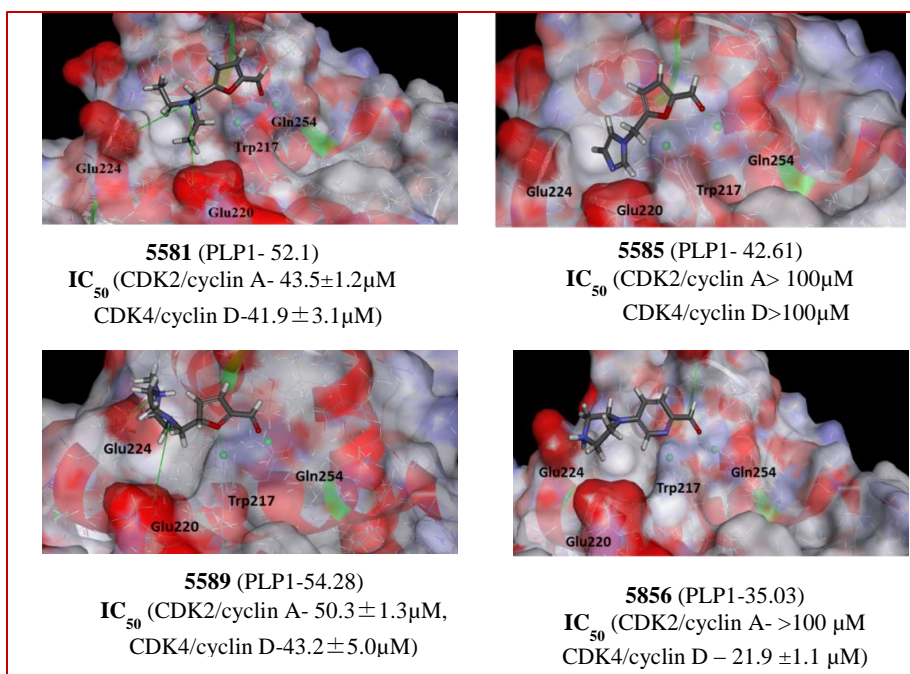
Figure 3.3 Interactions of 5581, 5585, 5589 and 5856 at the Arg binding site of CBG

The binding of hit molecules at the Arg binding site of CBG is shown. The interaction filters NH-atom of Trp217 and Gln254 are shown as green spheres; hydrogen bonds with the interaction filters are shown as green dotted lines. The closer acidic residues and interaction filters are shown in three letter codes. Ion-pairing interactions with GLu220 and Glu224 are depicted in green lines

The loss of activity for the mono substituted phenylacetic acid derivatives could be a result of the absence of the potential hydrogen bonding interaction with Trp217. The increased potency of the diethoxy analog (**530**) is likely due to the presence of the additional substituent at 4 position enabling better placement of the 3-ethoxy group in the secondary pocket[68]. The activity of this type of substitution was explored in the context of benzoic acid derivatives which do not have the methylene bridge and these results are discussed in chapter 5.

Validation of the LigandFit docking method was useful for predicting binding interactions of unknown compounds at the protein-protein interface. The results obtained

from FLIP CGI compounds derived from furoic, thiazole, picolinic and phenylacetic acid derivatives as N-capping groups suggests that these groups are good substituents for N-terminal Arg. The results correlated from docking analysis and binding assay of FLIPs confirms validation of docking parameters. In addition to hydrogen bonding interactions, basic groups substituted in furoic acid and picolinic acid provided insights on ion-pairing interactions. Overall these FLIP molecules developed in this series contribute to validation of REPLACE strategy for the development of drug like molecules and also provides a platform for further investigation of ion-pairing interactions with acidic region of CBG through the use of more optimal scaffolds.

3.4 Experimental section

3.4.1 Validation of LigandFit

The parameters of the LigandFit (Discovery Studio 3.0, Accelrys) docking method were validated using ligands from cyclin A/CDK2 crystal structures. The crystallographic ligands 1-(3,5- dichlorophenyl)-5-methyl-1H-1,2,4-triazole-3-carbaldehyde (3,5-DCPT) (PDB ID:2UUE) and 1-(4- chlorophenyl)-5-methyl-1H-1,2,4-triazole-3-carbaldehyde (4-CPT) (PDB ID:2V22) were used as positive controls and 5-chloro-2-phenyl-1,8a-dihydroimidazo[1,2-a]pyridine-3-carbaldehyde was evaluated as a negative control. The three ligands were docked successively into the cyclin grooves of two structures (2V22, 2UUE) and 20 poses were generated for each. This was repeated by variation of the LigandFit parameters including the forcefield used for the energy grid (Dreiding, CFF and PLP1), use of minimization sphere (on or off) and different scoring functions (Ligscore1_Dreiding, Ligscore2_Dreiding, PLP1, PLP2, PMF, DOCKSCORE)

to determine which generated a calculated binding energy most predictive of the experimental binding mode. For each parameter and scoring function, the number of correct poses of the positive controls in the top 25 ranked binding modes (out 25 of 60 possible, 20 for each of the three ligands) was determined. A library of 20 potential fragment alternatives was manually built using ChemDraw for Excel (Perkin Elmer) and subsequently imported into DiscoveryStudio 3.0 (Accelrys). For docking of unknown compounds, 10 poses were generated since this was sufficient to generate correct poses for the control ligands**.**

3.4.2. Synthesis

3.4.2.1 Material and methods

All the starting materials, solvents and reagents were used as obtained without further purification. Analytical thin layer chromatography was performed on silica gel (GF-254 plates). 1H NMR and 13 C NMR spectra were recorded with a Varian Mercury 300 and 400 Spectrometer, respectively. Mass spectra were measured with a Micromass QTOF (Tandem quadruple-1 time of flight mass spectrometer), electrospray ionization (ESI) and VG 70S (Double-focusing magnetic sector mass spectrometer, EI). Analytical purities of evaluated compounds were >95% unless stated otherwise. The following analytical method (unless stated otherwise) was used on a Waters Alliance 2695 HPLC with a 2996 diode-array detector and equipped with a C18 (2) 100 A, 250 x 4.6mm, 5μm column (Phenomenox Luna). A gradient from 100% water (0.1% trifluoroacetic acid) to 60% acetonitrile (0.1% trifluoroacetic acid) was run over 30 mins and held for 4 mins. The chromatograms were extracted at 226 and 254 nm.

3.4.2.2 Synthesis of capping groups

Furoic acid, picolinic acid and 2-(3,4-dihydroxyphenyl)acetic acid N-terminal capping groups were all obtained commercially (Chembridge, Matrix Scientific and UKROrgSyth). 3-alkoxy phenyl acetic acid derivatives were synthesized using the following procedure:

Step 1: Synthesis of ethyl 2-(3-ethoxyphenyl) acetate (9a) [67]

3-hydroxyphenylacetic acid (0.76 g, 5 mmol), ethyl bromide (0.25 g, 23 mmol) and potassiumcarbonate (0.13 g, 16.5 mmol) were refluxed in 5 ml of DMF for 12-18 hrs. The reaction was monitored by TLC (Ethylacetate: Hexanes= 35:65), after the reaction was complete, the reaction mixture was cooled to room temperature; water was added to dissolve potassium carbonate. The aqueous layer was extracted with ethyl acetate and the combined organic layers were washed with saturated sodium bicarbonate, brine, dried over sodium sulfate and evaporated to yield reddish oil (0.31 g, yield-30.0%).

^{1}H NMR (Chloroform-D, 300MHz) δ (ppm) 7.13(t, J=7.32Hz, 1H), 6.75(t, J=8.73Hz, 3H), 4.06(q,24 J=7.80Hz, 2H), 3.93(q, J=6.75Hz, 2H), 3.50(d, J=7.26Hz, 2H), 1.31(t, J=6.87Hz, 3H), 1.16(t,25 J=7.02Hz, 3H)

EI 208

propyl 2-(3-propoxyphenyl)acetate (9b)

Reddish oil (yield-28.2%) ^{1}H NMR (Chloroform-D, 300MHz) δ (ppm) 7.25-7.19(m, 1H), 6.83(t,29 J=8.07Hz, 3H), 4.05(t, J=6.78Hz, 2H), 3.91(t, J=6.39Hz, 2H), 3.59(d,

J=6.96Hz, 2H), 1.80(q, 30 J=7.35Hz, 2H), 1.64(q, J=6.00Hz, 2H), 1.03(t, J=7.32Hz, 3H), 0.91(t=7.33Hz, 3H)

EI 224

isobutyl 2-(3-isobutoxyphenyl)acetate (9c)

Reddish oil (yield-24.2%) ^{1}H NMR (Chloroform-D, 300MHz) δ (ppm) 7.22(t, J=8.34Hz, 1H), 6.85-4 6.79(m, 3H), 3.89(d, J=6.48Hz, 2H), 3.71(d, J=6.93Hz, 2H), 3.60(s, 2H), 2.12-2.03(m, 1H), 1.97-5 1.88(m, 1H), 1.03(d, J=6.18Hz, 6H), 0.92(d, J=6.60Hz, 6H)

EI 264

Step 2: 2-(3-ethoxyphenyl) acetic acid (10a)[3]

The ethyl 2-(3-ethoxyphenyl) acetate (1.41g, 5mmol) obtained from step 1 was treated with sodium hydroxide (2.8 g, 70 mmol) and a solution of 15 ml ethanol and 15 ml water. The reaction mixture was refluxed for two hours and the reaction was monitored by TLC (Ethylacetate: Hexanes= 35:65). After the completion of reaction, the reaction mixture was cooled; the alcohol was evaporated and diluted with water. The reaction mixture was acidified with 1N hydrochloric acid and stirred to precipitate the product as white solid (0.73 g, Yield-81.2%).

^{1}H NMR (chloroform-D, 500MHz) δ (ppm) 7.28-7.24(m, 1H), 6.88-6.83(m, 3H), 4.05(q, J=6.80Hz, 2H), 3.63 (s, 2H), 1.42 (t, J=7.25Hz, 3H)

^{13}C NMR (chloroform-D, 125MHz) δ (ppm) 177.15, 159.14, 134.61, 129.60, 121.55, 115.65, 113.41, 63.41, 41.01, 14.80

EI 180

2-(3-propoxyphenyl)acetic acid (10b)

White solid (yield-85.2%) ^{1}H NMR (chloroform-D, 300MHz) δ (ppm) 7.21(d, J=7.44Hz, 2H), 6.83(t,22 J=7.86Hz, 2H), 3.90(t, J=6.03Hz, 2H), 3.61(s, 2H), 1.79(q, J=6.42Hz, 2H), 1.02(t, J=7.05Hz, 3H)

EI 194

2-(3-isobutoxyphenyl)acetic acid (10c)

White solid (yield-82.8%) ^{1}H NMR (chloroform-D, 300MHz) δ (ppm) 7.22(d, J=8.19Hz, 1H), 6.83(t, 26 J=8.70Hz, 3H), 3.70(d, J=7.26Hz, 2H), 3.62(s, 2H), 2.11-2.00(m, 1H), 1.01(d, J=6.69Hz, 6H)

EI 208

Analytical data (NMR and MS) of representative N-caps are shown in appendix. Characterization data for FLIPs are shown in appendix table 2.

3.4.3 Fluorescence polarization assay[57]

CDK4D1 FP assay: This assay was performed using black 384-well plates using a previously described procedure with the following modifications. To each well were added: 5 µl CDK4D1 (0.3 µg/well purified recombinant human kinase complex from Invitrogen), 5 µl compound solution, 5 µl 30 nM fluoresceinyl-Ahx-Pro-Val-Lys-Arg-Arg-Leu-(3ClPhe)-Gly tracer peptide. Compounds and kinase complexes were diluted using assay buffer (25 nM HEPES pH 7, 10 nM NaCl, 0.01% Nonidet P-40, 1mM

dithiothretiol (DTT). Plate was centrifuged for 1 min at 500 rpm and then incubated with shaking for 45 mins at room temperature. Fluorescence polarization was read on DTX880 multimode detector (Beckman Coulter, Brea, CA) fitted with 485 nm/535 nm excitation/emission filters and a dichroic mirror suitable for fluorescein. Relative mp was calculated for each concentration tested using the equation showing below. IC_{50} values were determined by logarithmic regression by correlating relative mps and testing concentrations.

$$\text{Relative mp} = \frac{\text{mP(compound)-mP(DMSO, protein, tracer)}}{\text{mP(DMSO, protein)-mP(DMSO, protein, tracer)}}$$

CDK2A2 FP: assay This assay was performed using black 384-well plates. To each well were added: 5 μl CDK2A2 (0.3 μg/well purified recombinant human kinase complex), 5 μl compound solution, 5 μl 30 nM fluoresceinyl-Ahx-Pro-Val-Lys-Arg-Arg-Leu-Phe-Gly tracer peptide. Compounds and kinase complexes were diluted using assay buffer (25 nM HEPES pH 7, 10 nM NaCl, 0.01% Nonidet P-40, 1mM dithiothretiol (DTT). Plate was centrifuged for 1 min at 500 rpm and then incubated with shaking for 45 minutes at room temperature. Fluorescence polarization was read on DTX880 multimode detector (Beckman Coulter, Brea, CA) fitted with 485 nm/535 nm excitation/emission filters and a dichroic mirror suitable for fluorescein. Relative mp was calculated for each concentration tested using the equation showing below. IC_{50} values were determined by logarithmic regression by correlating relative mps and testing concentrations.

3.5 Acknowledgement

This chapter is written based on the below article with permission of publisher

Padmavathy Premnath, Shu Liu, Tracy Perkins, Erin Anderson and Campbell McInnes, Furoic and picolinic acid derived isosteres for arginine: towards non-ATP competitive CDK inhibitors. *Bioorganic and medicinal chemistry*

CHAPTER 4

STRUCTURE ACTIVITY RELATIONSHIP LEADING TO CONVERSION OF CYCLIN BINDING GROOVE PEPTIDES TO DRUG LIKE CDK INHIBITORS THROUGH REPLACE

4.1 Introduction

In this chapter, structure-activity relationships of peptidic cyclin groove inhibitors derived from the p21^{WAF} CDK inhibitory protein and the Rb like substrate, p107 are described. This was carried out towards the overall aim of targeting substrate recruitment through the cyclin binding groove (CBG) present in cell cycle CDK/cyclin complexes. The Cyclin Binding Motif (CBM) has been studied in detail and shown to be comprised of the consensus sequence, ZXRLYY' where Z, X are basic residues (Lys, Arg), L is leucine and Y, Y' are non-polar residues with a requirement for Phe at one of these two positions. Ala scanning of the p21^{WAF} sequence from residues 149 to160 has been carried out showing that the sequence, DFYHAKRRLIFS was a potent inhibitor of CDK4/cyclin D and CDK2/cyclin E in kinase assays. Minimization studies showed that the peptide octamer, HAKRRLIF was a highly potent inhibitor of CDK2/cyclin A when tested in competitive binding assay and also that the activity was comparable to the intact human recombinant p21^{WAF}(IC$_{50}$ = 0.028μM vs. 0.011μM). This octamer was further truncated to RRLIF (IC$_{50}$-1.4μM in CDK2/cyclin A) showing that respectable levels of potency could be retained with a MW more akin to drug-likeness. Overall these results show that potent and selective inhibition of cell cycle CDKs can be obtained in p21 derived

peptides that are non-ATP competitive compounds. Similarly another octapeptide derived from the retinoblastoma like protein p107, SAKRRLFG binds to the CBG and results in potent inhibition of cell cycle CDKs (IC_{50} - 0.035μM in CDK2/cyclin A) [46]. Because of their lack of cell permeability and metabolic instability, peptides in general do not make good drugs[48]. The first aim of this study is to investigate the SAR of the CBM in greater depth in order to replace peptide residues that prevent it from crossing the cell membrane and to incorporate substitutions to improve metabolic stability. The liabilities of the CBM peptides include the basic residues (Lys, Arg) that limit cell permeability and the susceptibility of the amide backbone to proteolytic degradation. Furthermore, the goal was to iteratively convert the peptide RRLIF into drug like FLIP molecules utilizing REPLACE strategy. Based on the SAR data, a variety of modifications were included to replace Arg5 and to stabilize the C-terminal motif against degradation. These were then then converted into more pharmaceutically appropriate compounds through addition of the 35DCPT as the most effective Ncap identified to date.

4.2 Results

A detailed structure activity relationship was carried out for peptides derived from p21[WAF] and p107 with several modifications of the key residues to determine how the key determinants of binding could be replaced and based on the results allow conversion to more drug like molecules. Three series of CGI peptides were selected for a detailed study of their structure activity relationships. Two of these include the p21WAF derived peptides HAKRRLIF and its truncated variant RRLIF. The third series is from the Rb like protein substrate, p107 and has the sequence SAKRRLFG. Previous SAR information revealed that the residues His1, Lys3, Arg4 and Arg5 make ion-pairing

interactions with the acidic regions and are therefore important or critical for activity[44].
Furthermore Ala3, Leu6 and Phe8 contact the two hydrophobic pocket regions through
van der Waals interactions and these are essential determinants for binding to the CBG.
Inclusion of the Ile spacer residue between Leu and Phe in the p21^{WAF} peptide
(HAKRRLIF) improves potency relative to the p107 peptide (SAKRRLFG) [69]. An
extensive SAR investigation was therefore carried out so as to find residue alternatives
that might reduce peptide length and consequently improve the drug likeness.
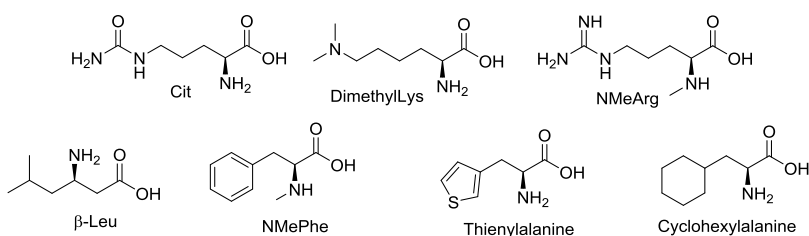
Figure 4.1 Structure of non-natural amino acids

For the octapeptides, HAKRRLIF and SAKRRLFG, modifications of the C-
terminus were attempted. For RRLIF, Arg 4 was substituted with non-natural amino acids
or fragment capping groups designed to further probe its contributions and Arg5 was
replaced with isosteric residues. These modifications were carried out to study SAR
which then would help in investigating the effect of substituted residues in retaining the
inhibitory activity but with improved stability and drug likeness. The isosteric residues
incorporated are shown in figure 4.1. Modified peptides were synthesized by standard
solid phase chemistry[56], and then tested for their ability to bind to the cyclin groove of
CDK2/cyclin A and CDK4/cyclin D1. Furthermore the experimental binding affinity was
correlated with the calculated interaction energies for peptides modeled in complex with
CDK2/cyclin A.

4.2.1 Structure activity relationship of SAKRRLFG (p107) and HAKRRLIF (p21^{WAF}) based peptide analogs

Peptides derived from p107 and p21^{WAF} have been shown to exhibit potent non-ATP competitive inhibitory activities against CDK2/cyclin A and CDK4/cyclin D. The key residues that contribute to binding and inhibitory activity need to be investigated to extend the structure-activity relationships. As discussed, the CBG has three major subsites including an acidic region and a major (primary) and a minor (secondary) hydrophobic pocket. Lys3 and Arg4 in the N-terminal tetrapeptide of the octapeptides interact with acidic residues (Glu220, Glu224 and Asp284) and whereas Ala2 interacts with the secondary hydrophobic pocket. Leu6 and Phe (7 or 8) in the C-terminal region of the octomer bind to the primary lipophilic pocket[49,70] . In this first instance, these C-terminal determinants were exchanged to determine their contributions with the major hydrophobic pocket and also the consequences of the structural differences of cyclin A and cyclin D on affinity of these inhibitors. The competitive binding efficiency determined by FP assay of a number of octapeptide variants based on SAKRRLFG and HAKRRLIF are shown in table 4.1.

C-terminal modifications of SAKRRLFG were designed to examine (i) effect of C-terminal functional group (CONH$_2$ or COOH), (ii) extension of the C-terminus to probe interaction with the major hydrophobic pocket (iii) replacement of Arg5 and (iv) modification of the motif interacting with the major hydrophobic pocket by deletion and substitution of key residues. Modification of the C-terminal functional group was assessed by synthesizing SAKRRLFG as its C-terminal amide (SAKRRLFG-NH$_2$, **457**). Compared to the corresponding C-terminal acid peptide (**5815**), 457 showed similar

binding to both CDK2/cyclin A (0.05 µM, 0.07 µM) and CDK4/cyclin D (0.66 µM, 0.88 µM). Extension of the peptide with methionine (SAKRRLFGM, **5564**) shows comparable results with **5815** (CDK2/cyclin A- 0.07 µM, CDK4/cyclin D-0.70 µM). **5814** with the 3TA Phe replacement shows a 3 fold decrease in potency in CDK2/cyclin A (0.18 µM) and 2 fold decrease in CDK4/cyclin D (1.67 µM) compared to **5815**. Replacement of Leu with betahomoleucine (β-Leu) leads to 2-3 fold potency improvement (**5820**, CDK2/cyclin A- 0.02 µM, CDK4/cyclin D- 0.29 µM) compared to **5815**. CBM peptides of p21 with LIF sequence on C-terminus are more potent than p107 peptides that have LFG sequence. The isoleucine of HAKRRLIF (**5816**) acts as spacer residue and thus adding the extra carbon in the β-Leu (compared to leucine) provides for more optimal spacing to allow adaptation of the Phe to the pocket. In order to determine the effect of the β-Leu residue in the 3TA context, both Leu and Phe were replaced with these residues respectively (**5813**). These substitutions were found to be the most effective in this series with a 20 fold enhancement in potency compared to **5814** in both cyclin A and cyclin D context (CDK2/cyclin A- 0.01 µM, CDK4/cyclin D- 0.04 µM). Previous studies have indicated that Arg5 is less important for activity than Arg4 and which makes critical contributions to binding. . When Arg5 was substituted with Asn (**5557, 5558**) the activity decreased 3-4 fold for binding to both cyclins (CDK2/cyclin A- 0.19 µM, CDK4/cyclin D- 4.15 µM). Similarly replacement of Arg5 with Ala (**5559**) resulted in reduced potency. HAKRRLIF (**444**) exhibited comparable binding activity (CDK2/cyclin A-0.02 µM) with a peptide in which Phe was replaced with cyclohexylalanine(HAKRRLI(CHA), **5816**).

Table 4.1 Structure activity relationship of p21 and p107 derived peptide analogs

SCCP ID	Structure	CDK2/cyclin A IC50 (μM)	CDK4/cyclin D1 IC50 (μM)
457	SAKRRLFG-NH2	0.07±0.02	0.88±0.34
5815	SAKRRLFG-OH	0.05±0.02	0.66±0.21
5814	SAKRRL3TA G-OH	0.18±0.07	1.67±0.53
5564	SAKRRLFGM	0.07±0.04	0.70±0.30
5820	SAKRR{βLeu}FG-OH	0.02±0.00	0.29±0.07
5813	SAKRR{βLeu}3TAG-OH	0.01±0.00	0.04±0.07
5557	SAKRNLFGM	0.19±0.06	4.15±1.36
5558	SAKRNLFG-NH2	0.24±0.11	3.09±2.00
5559	SAKRALFGM	0.81±0.10	4.92±0.34
5816	HAKRRLI{CHA}	0.02±0.00	0.18±0.04
444	HAKRRLIF	0.02±0.01	0.12±0.05

4.2.2 Structure activity relationship of RRLIF (p21[WAF]) based peptide analogs

Previous SAR studies resulted in the identification of RRLIF as the minimal cyclin groove binding sequence with CDK inhibitory activity. Hence RRLIF was used as a starting point to convert the peptide to a more drug like molecule. A variety of peptide analogs derived from RRLIF (IC_{50} = 1.01 μM and IC_{50} = 25.12 μM for CDK2/cyclin A and CDK4/cyclin D respectively) were designed to introduce replacements for each of these residues and to probe their contributions and potential for replacement with more drug-like moieties. Results obtained from the SAR studies of RRLIF modifications are shown in tables 5.2, 5.4 and 5.5 and discussed in the following sections.

4.2.2.1 **Arg replacements**

Substitutions of both the N-terminal arginines were carried out to examine the sensitivity and binding requirement for each one. Previous studies have indicated that Arg4 critical for activity while Arg5 is less so. Both arginine residues were replaced with

citrulline as shown in **5812** (Cit-RLIF) and **5831**(RCitLIF) to study the effect of non-charged isostere urea in place of highly basic group guanidine. Activity data shows IC_{50} values of **5812** in CDK2/cyclin A as 43.17 μM and CDK4/cyclin D as 40.46 μM indicating a potency drop of 42 and 1.6 fold respectively. For **5831,** the IC_{50} values were found to be 5.19 μM and 15.76 μM in CDK2/cyclin A and CDK4/cyclin respectively which showed 5 fold less activity in CDK2/cyclin A and slightly improved potency in CDK4/cyclin D. Substitution of Arg5 with isosteric residues including N,N-dimethyllysine (Figure 4.1, **5925**- R(dimethyllys)LIF, IC_{50} 1.70 μM) and Nα−methylarginine (Figure 4.1, **5918** R(NMeArg)LIF, 20.62 μM) results in potency decreases in binding to CDK2/cyclin A. **5925** retains similar activity while **5918** undergoes a 20 fold decrease in binding activity. **5918** shows slight decrease in the activity for CDK4/cyclin D (IC_{50} 33.76 μM) while **5925** is about 2.7 fold more potent than RRLIF (IC_{50} 9.19μM) in this context.

Further subsitutions for Arg5 included the neutral residues Gly, Ala and Pro to study the loss of ion-pairing interactions with the acidic region. Peptides incorporating these replacements resulted in very weak or no binding to both CDK/Cyclin complexes evaluated. Proline substitution (RPLIF **5832**) was proven to be detrimental to the activity with IC_{50} values of greater than 180 μM for both CDK2/cyclin A and CDK4/cyclin D. Glycine substitution for this residue (RGLIF-**5873**- >180 μM for CDK2/cyclin A and CDK4/cyclin D) resulted in a similar loss of binding. The activity of the alanine surrogate (RALIF **5833**) significantly decreased with respect to the native residue by 20 fold with respect to CDK2/cyclin A (IC_{50} of 20.36 μM) but had no dramatic loss of binding to RRLIF in CDK4/cyclin D (IC_{50} > 28.76 μM). A molecular modeling study was carried

out in order to examine the structural basis for the potency loss of these Arg replacement analogs. After formation of the peptide cyclin complex by mutation of RRLIF (from the crystal structure 1OKV) and subsequent energy minimization, interaction energies were calculated for all of the Arg5 alternatives of RRLIF. The competitive binding efficiency of each peptide was compared with the interaction energy for its complex modeled with CDK2/cyclin A. A trend in the relationship between the interaction energy and the competitive binding data was observed with R^2 correlation coefficients of 0.85 and 0.87 for potential and electrostatic energy respectively (table 4.3, figure 4.2).

Table 4.2 N-terminal modifications with R substitutions

	SCCP ID	Structure	CDK2/cyclin A IC$_{50}$ (μM)	CDK4/cyclin D1 IC$_{50}$ (μM)
	5811	RRLIF	1.01±0.17	25.12±2.97
Non-natural amino acids	5812	Cit-RLIF	43.17±8.77	40.46±1.07
	5831	RCitLIF	5.19±1.56	15.76±1.94
	5918	R(dimethyllys)LIF	20.62±2.57	33.76±10.72
	5925	R(NMeArg)LIF	1.70±0.76	9.19±2.18
Natural amino acids	5832	RPLIF	>180	>100
	5833	RALIF	20.36±7.57	28.76±12.86
	5873	RGLIF	>180	>100
Peptoid	5877	R-X1-LIF	>180	>100
	5879	R-X2-LIF	>180	>100
	5878	NCAP1-X1-LIF	>180	>100
	5895	NCAP2-X1-LIF	>180	>100

X1- DMAM peptoid, X2-DMAMAla, NCAP1-2-(3-methoxyphenyl)acetic acid, NCAP2- 4-(piperidin-4-yloxy)benzoic acid

Table 4.3 Interaction energy calculated for the peptide analogs

Peptide sequence	$LogIC_{50}$	Potential Energy (kcal/mol)	Van der Waals Energy(kcal/mol)	Electrostatic Energy(kcal/mol)
RRLIF	0.004	-195.25	-47.03	-148.21
CitRLIF	1.635	-162.61	-47.97	-114.64
RCitLIF	0.715	-169.05	-48.02	-121.02
RALIF	1.309	-155.52	-43.6	-111.92
RGLIF	2.255	-155.03	-43.49	-111.54
R(NMeArg)LIF	0.23	-191.38	-47.15	-144.23
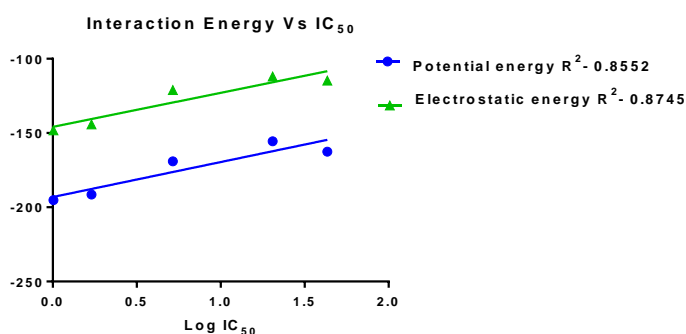
Figure 4.2 Correlation of interaction energy with binding affinity

Further to these exchanges for the second arginine, peptoid substitutions were utilized to attempt Arg5 replacement (Figure 4.3). Peptoids are peptidomimetics that have side chains attached to the amide N-atom and these are resistant to proteolysis. Two different peptoid residues were generated and incorporated. These included dimethylaminomethyl glycine and dimethylaminomethyl alanine which were included as Arg5 replacements in the RRLIF context (**5877, 5879**). **5878** and **5895** incorporated 3-methoxyphenylacetamide and 4-piperidiyloxybenzamide as Ncapping group replacements respectively for Arg4. Peptoid incorporation was not successful as shown by the inactivity for CDK2/cyclin A (**Table 4.2**). The loss of activity for these analogs suggests that shift of the side chains to the α-nitrogen from the α-carbon may not provide
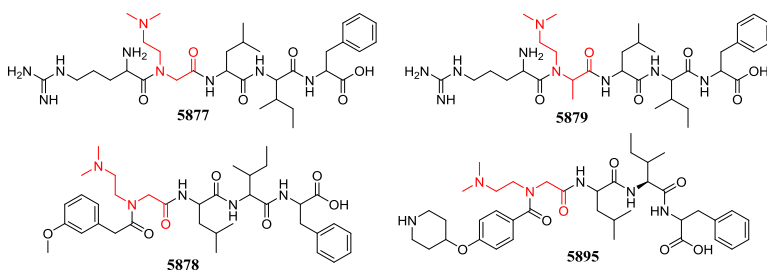
favorable contacts with CBGs.

Figure 4.3 Structure of FLIPs containing peptoids

4.2.2.2 **C-terminal modifications of RRLIF**

As previously described, Leu6 and Phe8 of the RRLIF sequence are critical residues for binding through the hydrophobic effect and van der Waals interactions with the primary pocket. Previously SAR modifications have not been extensively probed in the pentapeptide context for binding to both CDK/cyclin complexes, were further investigated. The C-terminus was modified by deletion of the isoleucine (RRLIF sequence) or glycine (RRLFG sequence) residues and also through substitution with rationally selected non-natural amino acids (table 5.4). Ile7 (RRLIF) is a spacer residue that enables proper positioning of both Leu and Phe for optimal hydrophobic contacts. Deletion of this residue (RRLF, **5874**) leads to a 35 fold decrease in potency for CDK2/cyclin A (IC$_{50}$ 35.651µM) and almost complete loss of activity for CDK4/cyclin D. Adding glycine to this sequence generates the p107 pentapeptide (**5871**- RRLFG) and results in a 2 fold improvement in binding to CDK2/cyclin A. Its IC$_{50}$ of 18.88 µM is still almost 20 fold higher compared to RRLIF however. Incorporation of the non-natural residues, β-Leu and N-MePhe previously investigated in the octapeptide context showed promising results with respect to activity improvements. Substitution of Leu with βLeu resulted in recovery of binding activity that was lost with the removal of Ile spacer

residue. RRβLF (**5875**) is only 2 fold less potent than RRLIF in the CDK2/cyclin A context (**5811**, 2.81 μM) and has similar binding in the CDK4/cyclin D context (21.17 μM). Extension of this sequence with Gly resulted in improved activity only in binding to CDK2/cyclin A (RRβLeuFG – **5876**, 1.73 μM, CDK2/cyclin A; 20.24 μM CDK4/cyclin D). Replacement of Phe with N-MePhe in both C-terminal acid and amide contexts shows drop in the activity CDK4/cyclin D compared to RRLIF however has comparable binding activity to CDK2/cyclin A. **5941,** RR{βLeu}NMeF-NH2 and **5930,** RR{βLeu}NMeF had IC_{50} values of 1.74 μM and 5.82 μM in CDK2/cyclin A and 45.58 μM and 81.13 μM in CDK4/cyclin D respectively. βLeu and N-MePhe were incorporated in the same peptide for the purpose of improving drug-likeness by enhancing metabolic stability. In addition, the C-terminal amide functionality of 5941 helps in reducing the total polar surface area (to 271.42 vs. 303.52 (RRLIF)).

Table 4.4 C-terminal modifications with LIF substitutions

ID	Sequence	CDK2A IC_{50} (μM)	CDK4D IC_{50} (μM)
5811	RRLIF	1.01 ± 0.17	25.12±2.97
5871	RRLFG	18.88±4.45	>100
5874	RRLF	35.65±10.51	>100
540	RRLNpfFG	0.70±0.19	9.26±2.07
5875	RR{βLeu}F	2.81±0.76	21.17±2.99
5876	RR{βLeu}FG	1.73±0.46	20.24±5.37
5930	RR{βLeu}{NMeF)	1.35±1.38	45.58±5.63
5941	RR{βLeu}{NMePhe}-NH$_2$	5.82±3.12	81.13±3.78

5.2.2.3 Combination of optimal Ncapping groups with SAR information to improve drug likeness of RRLIF derivatives.

In previous chapters, N-capping groups designed to exploit H-bonding (with Trp217, Gln254), van der Waals (secondary pocket) and ion-pairing interactions (acidic region) of CBG were described. An extensive SAR study of phenyl heterocyclic

carboxylic acids and Arg alternatives based on furoic, picolinic, thiazole and phenylacetic acid derivatives was undertaken/ These results indicated that 1-(3,5-dichlorophenyl)-5-methyl-1H-1,2,4-triazole-3-carboxylic acid (35DCPT) was among the most effective and drug-like N-caps. As a result, this fragment was combined with the substitutions described above that removed some of the metabolic liabilities of RRLIF while retaining its potency. Synthesized derivatives included 35DCPTCit {βLeu}NMeF (**5962**), 35DCPT Arg{βLeu}NMeF(**5963**), 35DCPT Arg{βLeu}3TA (**5964**) whose structures and activitites are shown in figure 4.5 and table 4.4 respectively. As a result of the citrulline substitution, FLIP **5962** has no activity in CDK2/cyclin A and CDK2/cyclin D. The other 35DCPT capped peptides containing arginine, **5963** and **5964** have respectable activity for CDK2/cyclin A with IC_{50}s of 8.95 μM and 5.70 μM respectively. Although these FLIPs have decreased compared to RRLIF, they possess greater drug likeness as evidenced by calculation of their physicochemical properties including of clog P (partition coefficient) and pTSA (total polar surface area).
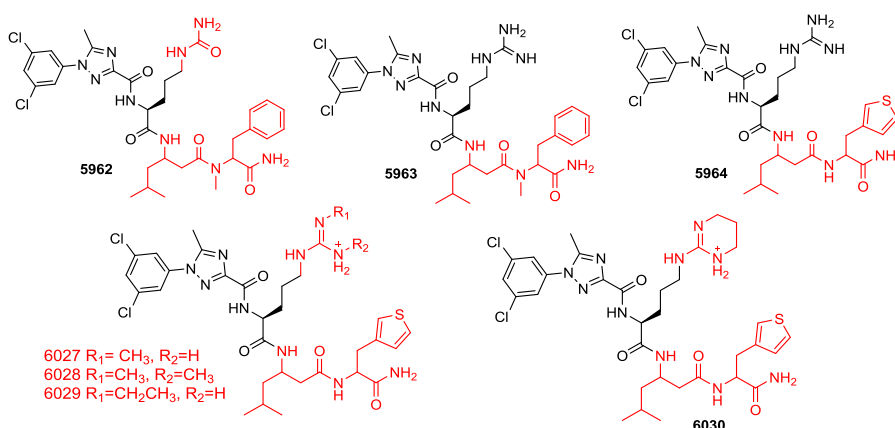

**Figure 4.4 FLIPs with modification on N-terminus and C-terminus**

As a further step to improve drug likeness, Arg5 was substituted with alkylated guanidine derivatives shown in a previous context to improve ion-pairing interactions

while potentially imporving cell permeability properties. Arg5 was replaced in the **5964** scaffold with alkylated arginine isosteres including monomethyl (**6030**); monoethyl (**6028)** and dimethyl (**6029**) derivatives and also the cyclic guanidine variant (**6027**) (figure 5.4). The IC_{50} values are 4.50 µM (**6030**), 16.39 µM (**6029**), 3.69 µM (**6028**) and 46.75 µM (**6027**). Testing of this set revealed that monalkyl derivatives had decreased binding compared to **5964** whereas the dimethyl and cyclic guanidine derivatives displayed similar affinity.

Based on the calculation of key properties (clog P and tPSA), it was concluded that these 35DCPT capped peptides had improved pharmaceutical like properties relative to RRLIF while potentially increasing permeability and stabilization against proteolytic degradation. These FLIPs were therefore evaluated for their ability induce anti-proliferative effects in U2OS (osteosarcoma) and DU145 (prostate cancer) cell lines as evidence for cell permeability and anti-tumor activity. In line with its decreased activity in the binding assay, **5962** did not show any growth inhibitory activity when evaluated in the MTT assay whereas the cyclin groove inhibitory FLIPS, **5963** and **5964** had respectable cellular activity on U2OS cells (IC_{50} 30.7 µM, 18.3 µM respectively) and DU145 (IC_{50} 36.5 µM, 21.8 µM respectively). Comparison of the anti-proliferative activities of **5963 and 5964** was suggestive of consistency between the binding affinity on CDK2/cyclin A and the cellular activity since a roughly 2 fold difference was observed in both. The modified guanidine derivatives all exhibit weaker cellular activities compared to 5964. Inhibition of cell cycle CDKs should lead to G1 arrest and therefore to determine if these FLIPs act by this mechanism, cell cycle distribution analysis was carried out by fluorescence activated cell sorting. The FLIP 5964 causes cell cycle arrest

at G1 compared to DMSO control and it is mechanistically distinct from Flavopiridol which leads to accumulation of cells in the G2/M phase (figure 4.5).

Table 4.5. FLIP Modifications to the N and C-terminii

G_{10} R_1= CH_3, R_2=H
G_{11} R_1=CH_3, R_2=CH_3
G_{12} R_1=CH_2CH_3, R_2=H

G_{19}
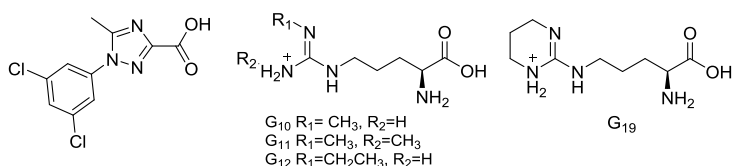
SCCP ID	Structure	FP assay IC$_{50}$ (μM)		Physical properties		**MTT assay** IC$_{50}$ (μM)	
		CDK2/cyclin A	CDK4/cyclin D1	clogP	tPSA*	**U2OS**	**DU145**
5811	RRLIF	1.4 ± 0.42	16.1±1.73	-1.64	303.52	NA	NA
5962	35DCPT-Cit{βLeu}{NMeF}-NH$_2$	>100	>100	5.142	242.57	>100	>100
5963	35DCPT-R{βLeu}{NMeF}-NH$_2$	8.95±4.15	78.25±11.09	4.947	249.35	30.7±2.7	36.5±2.6
5964	35DCPT-R{βLeu}{3TA}-NH$_2$	5.70±3.55	>100	2.573	220.25	18.3±1.5	21.8±0.32
6027	35DCPT-G10-{βLeu}{3TA}-NH$_2$	46.75±10.68	>100	3.32	208.76	>100	>100
6028	35DCPT-G11-{βLeu}{3TA}-NH$_2$	3.69±0.23	>100	3.8	194.77	75.6±1.2	102±14
6029	35DCPT-G12-{βLeu}{3TA}-NH$_2$	16.39±3.72	>100	3.85	208.76	108±4	130±27
6030	35DCPT-G19-{βLeu}{3TA}-NH$_2$	4.50±0.74	>100	2.34	194.77	60.5±3.3	81.0±8

Figure 4.5 Cell cycle analysis by FACS
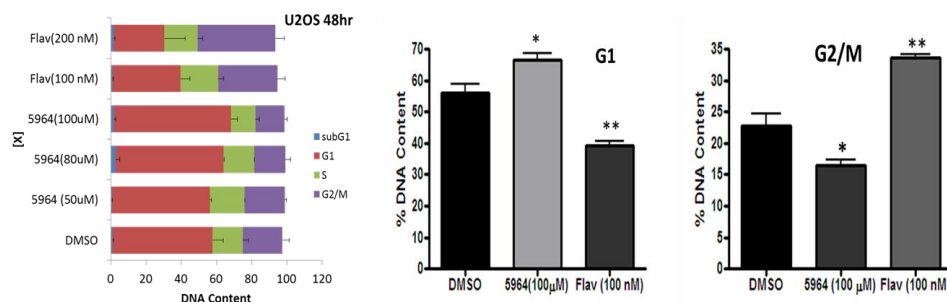
4. 3 Discussion and conclusion

As indicated previously, the CBG is comprised of two hydrophobic pockets and an acidic region. Key interactions of CBM peptides include ion-pairing interactions with acidic region, hydrogen bonding with backbone amides of the cyclin and van der Waals interactions with hydrophobic regions. The critical residues of the CBM include Arg4,

93

Arg5, Leu7 and Phe8 are conserved in the three parent peptides in this SAR study. The main objective in this chapter was to further investigate critical residues of the CBM and then determine ways to convert the CBM pentapeptides RRLIF to more drug like molecule through further application of REPLACE.

Contacts between species containing opposite formal charges are the strongest among non-bonded interactions. Since Arg4 and 5 of the CBM involve ion pairing interactions with negatively charged residues in the cyclin groove, both are important for binding of HAKRRLIF and its minimized counterpart. The decrease in potency observed when these were substituted with isosteric residues can be therefore attributed to decreased ion-pairing interactions in these analogs. Results obtained for citrulline substitution indicated that ion pairing contacts of Arg4 are more significant than those of Arg5, an observation consistent with the number of negatively charged residues of the cyclin contacting them. Citrulline which has an uncharged urea group in place of guanidine in Arg that leads to loss of ion-pairing interactions. Arg 4 makes multiple ion-pairing interactions at CBG unlike Arg5 hence replacing Arg4 with its uncharged isostere causes major activity loss. The difference in activity between cyclin A and cyclin D most likely arises from the structural differences between the cyclins and the variation in the CBM contacting residues in these two proteins. When bound to cyclin A, the Arg4 residue interacts with Asp283 through ion pairing. This residue occurs as Thr62 in cyclin D and results in fewer ion-pairing interactions[53]. Replacement of Arg with citrulline therefore is tolerated better in the cyclin D context. This is consistent with the results obtained for replacement of Arg5 with N,N-dimethyllysine (5918) which undergoes a 20 fold reduction in potency for binding to CDK /cyclin A and a decrease of 1.3 fold for

CDK4/cyclin D. Although 5918 has a basic residue available for ion paring interaction, the hindered methylated tertiary amine may prevent interaction with the Asp283 side chain. Methylation of the amide backbone nitrogen is a common strategy to stabilize peptides and make them resistant to proteolysis[71,72]. Incorporation of N-Me Arg in place of Arg5 lowers the potency less than 2 fold suggesting that N-methylation would be beneficial to increase proteolytic stability while preserving binding activity. Uncharged alternatives for the Arg5 were incorporated (Gly, Ala and Pro) and for the most part led to poor binding due to loss of ion-pairing and H-bond interactions. The peptide containing proline would undergo perturbation of its conformation (as observed in the modeled structure of RPLIF) along with the loss of H-bonding interactions from the backbone amide. Similarly RGLIF and RALIF suffer from loss of ion pairing. As a whole calculated interaction energies from the modeled complexes correlate very well with the IC_{50} values determined in FP assay. Consistent with the results obtained for pentapeptides, potency levels observed for the octapeptide Arg5 replacements decreased significantly.

Peptoids are peptide replacements based on N-substituted glycine residues i.e. where the side chain is attached to the α-N atom instead of α C-atom. Since these compounds are tertiary amides and non-natural, they are resistant to proteolysis[73]. In the peptoid series, Arg5 was substituted with dimethylaminomethyl glycine (DMAM) and dimethylaminomethyl alanine (DMAMAla) peptoid residues. Loss of activity for the peptoid series can be explained by these compounds adopting a different conformation leading to loss of hydrogen bonding and van der Waals interactions.

In order to explore substitutions for the key residues (Leu, Phe) contacting the

95

primary hydrophobic pocket and to imbue cyclin groove inhibitors with greater metabolic stability and cell permeability while further minimizing the size, β-Leu and non-natural residues were incorporated. Deletion of the Ile spacer residue (RRLF) leads a dramatic loss of binding to CDK2/cyclin A. The majority of the potency loss could be recovered by the addition of a methylene spacer in Leu of RRLF i.e, substituting β-Leu for Leu as seen in RR β-LeuPhe-NH$_2$ (**5941**) Incorporation of β-Leu has the advantage of improving stability of the peptide and also reducing the peptide length. Along with this, β-Leu provides similar van der Waals interaction from its side chain while the extra methylene also acts as a spacer offering flexibility to the Phe sidechain for improved complementarity with the primary hydrophobic pocket[69,70]. This was confirmed by testing of the octapeptides **5920** and **5813,** both were among the most potent in competitive inhibition of CDK2/cyclin A and CDK4/cyclin D and further corroborated by the binding potency for **5975** (RR{βLeu}F) and **5976** (RR{βLeu}FG) with CDK2/cyclin A. Results from both penta and octapeptide analogs suggest that 3TA is an effective replacement for Phe while also potentially improving drug likeness. N-methylation of the Phe residue did not lead to potency loss and therefore suggests that its inclusion into the peptide or FLIP would result in stabilization against proteolysis. Incorporation of β-Leu and N-MePhe/3TA (in place of LIF) results in a smaller peptide while retaining the majority of interactions. Apart from this, presence of the amide group on the C-terminus improves the tPSA compared to RRLIF. The tPSA and clog P are parameters that determine the exposed hydrophilic surface and overall hydrophobicity of a molecule. These should be in a balance if used in a predictive sense for estimating if a molecule will be useful as for drug development. According to Lipinski's rule of 5 and

other guidelines for drug likeness, the tPSA is typically less than 140 Å and clog P is between -0.4 to 5.6 for orally available drugs[65,66].

In previous chapters, the REPLACE strategy was described in the identification and optimization of N-capping groups as suitable ligand alternatives for Arg4. The molecule 1-(3,5-dichlorophenyl)-5-methyl-1H-1,2,4-triazole-3-carboxamide was found to be most potent N-capping group. As a result, FLIPs were synthesized combining this capping group with the C-terminal modifications in an attempt to improve drug likeness while retaining affinity of the original peptide. In order to provide insights into the cell permeability and anti-tumor effects of these FLIPs, cellular viability studies were undertaken. The results indicated that both cyclin groove inhibitors have antiproliferative effects on DU145 and U2OS cancer cell lines[52,54]. As these cell lines have deregulated Rb pathways, it is probable that the growth inhibitory effects of 5963 and 5964 are through inhibition of cell cycle CDKs and specifically through E2F1. In the MTT cell viability assay [74], the 3TA analog (**5964**) was observed to be 2 fold more potent compared to N-MePhe analog (**5963**) which is in accordance with the binding assay. Modifications to the guanidine side chain were attempted by addition of linear or cyclic alkyl groups. Although some of these have similar cyclin groove binding ability, their weaker cellular suggests that the modified guanidine group interferes with cellular permeability. This could result from steric hindrance of the modified guanidine group precluding interaction with negative charges of the lipid bilayer and therefore preventing permeability. Results from the binding assay and cell cycle analysis strongly indicate that **5964** is a lead compound in that it binds to and inhibits CDK2/cyclin A thereby inducing G1 cell cycle arrest and anti-proliferative effects in tumor cells. These results are consistent with on

target inhibition of the cell cycle CDKs and pave the way for more in depth studies with these FLIPs. Development of FLIPs with cellular activity is an important milestone in this project and contributes overall to the development of anti-tumor therapeutics using REPLACE strategy. Future studies will focus on the mechanism of action of the lead FLIP molecule **5964** in cancer cell lines and will be further optimized to improve its cellular activity.

4.4 Materials and methods

4.4.1. Peptide & FLIP Synthesis[56]

All N-terminally capped FLIPs were synthesized and purified using standard Fmoc chemistry by GenScript (Piscataway, NJ). HPLC and MS were used to confirm the purity and structure of each peptide. Peptides were assembled by using standard solid-phase synthesis methods. A sample procedure is given as follows: 5 equivalents of the C-terminal amino acid were coupled to Rink resin at the first place using 1 DIEA (0.082 mL) and HBTU (189.6 mg) in 2 mL of DMF for 1 h. The Fmoc of the C-terminal amino acid was removed using 20% piperidine in 3 mL of DMF for 10 min before addition of 5 equiv of the next amino acid using DIEA (0.082 mL) and HBTU (189.6 mg) in 5 mL of DMF. Wash cycles (5 x 10 mL of DMF + 5 x 10 mL of DCM) were applied to each step in between coupling and deprotection of Fmoc. Upon completion of assembly, side chain protecting groups were removed, and peptides were cleaved from Rink resin using 90:5:5 mixtures of TFA/H2O/TIPS. Crude peptides were purified using reverse-phase flash chromatography and semi preparative reverse-phase HPLC methods. Pure compounds were lyophilized and characterized using mass spectrometry and analytical HPLC (see Supplementary Table 3).

4.4.2 Energy minimization and Interaction energy calculation

Energy minimization was performed in Discovery studio 3.0 in the Cylin A (PBD ID: 1OKV) at the cyclin binding groove. Prior to minimization, the heavy atoms of the protein were set as constraints, CHARMm force field was applied to the receptor ligand-complex. The minimization protocol was used for calculating the energy minimization. The parameters used were Smart minimizer Algorithm with 2000 steps and 0.1 as RMS gradient, GBSW (Generalized Born with a Simple Switching) implicit solvent model using Dielectric constant as 1 and implicit solvent dielectric constant as 80. The other parameters non-bonded radius and electrostatics were set as default.

The interaction energy between the protein and each ligand was calculated with interaction energy protocol in Discovery studio 3.0. Default parameters were used for (i) In-Situ Ligand Minimization, (ii) Ligand Conformational Entropy (iii) Non-bonded radius (iv) Electrostatics (v) Advanced and (vi) Parallel processing. The implicit solvent model was set to GBSW (Generalized Born with a Simple Switching) along with dielectric constant as 1 and implicit solvent dielectric constant as 80.

4.4.3 Cell culture[74]

U2OS osteosarcoma cells and DU145 human prostate cancer cells were obtained from ATCC (Manassas, VA). All cells were grown in Dulbecco's modified Eagle's medium (DMEM , Fisher Scientific) supplemented with 10% Fetal Bovine Serum (FBS, USA Scientific) and 100μg/ml of Streptomycin (strep)/ 100 U/ml of Penicillin (pen). Cells were incubated at 37ºC with 5% CO_2.

4.4.4 Viability assay

Cells were seeded in 96-well plates at (2×10^3 cells/ml) and allowed to adhere overnight in DMEM growth media containing 10% NU serum and 1% Pen/Strep. The compounds **5962**, **5963,** and **5964** were dissolved in DMSO and added in a dose dependent manner (1 μM to 100 μM). The diluted compounds were added to the cells in triplicate and incubated for 72 hours at 37°C with 5% CO_2. The cell viability was determined using MTT (3-(4,5-Dimethylthiazol-2YI)-2,5-Diphenyl tetrazolium Bromide) assay[4]. Absorbance readings were obtained using a DTX880 multimode detector fitted with 595nm filter. Cell viability results were represented as the ratio of the absorbance reading in treated vs. untreated cells. IC_{50} values were obtained using a nonlinear regression line with 5.0 Graghpad Prism. Experiments performed in triplicates.

4.4.5 Cell Cycle Analysis

Cells were plated at 150,000/ml overnight in six well plates. CDK2 inhibitors were added in a dose dependent fashion for 48 hrs. The cells were then fixed with 70% Ethanol overnight at -20 degrees. The cells were centrifuged and ethanol was removed. The cells were washed twice with 1X PBS following staining with DAPI(4',6' diamino-2-phenylindole) and analyzed using BD LSR II (Becton Dickenson) with a blue filter. Experiments were performed in triplicates.

4.4.6 Fluorescence Polarization Binding Assay

CDK4D1 FP assay: This assay was performed using black 384-well plates using a previously described procedure[57] with the following modifications. To each well were added: 5 μl CDK4D1 (37 μg/ml purified recombinant human kinase complex from Invitrogen), 5 μl compound solution, 5 μl 12 nM fluoresceinyl-Ahx-Pro-Val-Lys-Arg-

Arg-Leu-(3ClPhe)-Gly tracer peptide. Compounds and kinase complexes were diluted using assay buffer (25 nM HEPES pH 7, 10 nM NaCl, 0.01% Nonidet P-40, BSA 1mg/ml, 20mM dithiothretiol (DTT). Plate was centrifuged for 1 min at 500 rpm and then incubated with shaking for 45 mins at room temperature. Fluorescence polarization was read on DTX880 multimode detector (Beckman Coulter, Brea, CA) fitted with 485 nm/535 nm excitation/emission filters and a dichroic mirror suitable for fluorescein. Relative mp was calculated for each concentration tested using the equation showing below. IC_{50} values were determined by logarithmic regression by correlating relative mps and testing concentrations.

$$\text{Relative mp} = \frac{\text{mP(compound)-mP(DMSO, protein, tracer)}}{\text{mP(DMSO, protein)-mP(DMSO, protein, tracer)}}$$

CDK2A2 FP assay :This assay was performed using black 384-well plates. To each well were added: 5 µl CDK2A2 (18 µg/ml purified recombinant human kinase complex), 5 µl compound solution, 5 µl 12 nM fluoresceinyl-Ahx-Pro-Val-Lys-Arg-Arg-Leu-(3ClPhe)-Gly tracer peptide. Compounds and kinase complexes were diluted using assay buffer (25 nM HEPES pH 7, 10 nM NaCl, 0.01% Nonidet P-40, BSA 1mg/ml, 20mM dithiothretiol (DTT). Plate was centrifuged for 1 min at 500 rpm and then incubated with shaking for 45 mins at room temperature. Fluorescence polarization was read on DTX880 multimode detector (Beckman Coulter, Brea, CA) fitted with 485 nm/535 nm excitation/emission filters and a dichroic mirror suitable for fluorescein. Relative mp was calculated for each concentration tested using the equation showing below. IC_{50} values were determined by logarithmic regression by correlating relative mps and testing concentrations.

4.5 **Acknowledgement**

CHAPTER 5

OPTIMIZATION OF BENZOIC ACID DERIVED INHIBITORS OF THE CYCLIN GROOVE OF CDK2 USING THE REPLACE STRATEGY

5.1 Introduction

As described, the pentamer RRLIF was found to be the minimal CBM sequence with sufficient potency to inhibit CDK2/cyclin A and CDK4/cyclin D. Chapters 3 and 4 describe the identification and optimization of arginine isosteres as N-terminal capping groups[63,68] and further peptide SAR. Extensive information was obtained for these Ncaps based mainly on substituted 5 membered heterocyclic rings. These fragment alternatives were designed to mimic peptide interactions with the secondary pocket and with cyclin residues interacting with the peptide backbone. The heteroatoms in these fragments provided H-bond acceptors observed in the peptide context with Trp 217 of the cyclin groove[63]. Interactions with the negatively charged residues (Glu220, Glu224, and Asp 283) observed in the peptide/cyclin complex were largely absent in the phenyltriazole Ncaps. Further series of Ncaps incorporating basic functionality in furoic and picolinic acid derivatives resulted in FLIPs with moderate activity therefore leaving considerable scope for improvement[68]. A literature precedent for CBG inhibitors provided insight an additional scaffold based on benzoic acids and which is capable of mimicking peptide interactions with the acidic region. These benzoic acid capped peptides were substituted on the Ncap with basic functionality and were found to possess potent activity against CDK2/cyclin A[75]. Based on SAR results and preliminary activities described in chapters

3 and 4 and the resulting scope for potency improvement, the benzoic acid derivative precedent was further investigated. Potential N-capping groups based on this scaffold were therefore designed to present groups with the capability of retaining interactions with the secondary pocket while including functionality to make ion-pairing interactions with acidic region. The REPLACE strategy therefore was further utilized in the design of FLIPs which have increased potency through more complete interactions with the cyclin groove[49]. In this series design, synthesis and optimization of benzoic acid derivative N-caps (ligated to RLIF) was undertaken through application of REPLACE. As before, their potential anti-cancer activity was assessed through use of the FP assay to measure competitive binding to CDK2/cyclin A and CDK4/cyclin D[57]. Optimization studies of N-capping groups were conducted based on SAR results and docking analysis. Promising compounds were then further tested for anti-proliferative activity on cancer cells through cell culture experiments[74].

5.2 Results

5.2.1 Synthesis of N-caps

The synthesis of benzoic acid derivatives with substitutions at 3-position and/or 4-position was undertaken (figure 5.1). Based on computational studies, it was hypothesized that substituents at the 3-position would make complementary interactions with the secondary hydrophobic pocket. In addition, functional groups incorporated at the 4-position were designed based on their predicted ion-pairing thus mimicking the contacts of the critical arginine. To examine SAR of the 3 position in the benzoic acid capping group, a number of alkoxy derivatives were generated by reaction of 3-hydroxy benzoic acid with the appropriate alkyl halide. Alkylation of the hydroxyl also results in

concomitant alkylation of the acid and therefore the corresponding ester was base hydrolyzed to generate the 3-ethoxy and 3-propoxy benzoic acids as desired products (21 a-b) (scheme 5.1)[76].
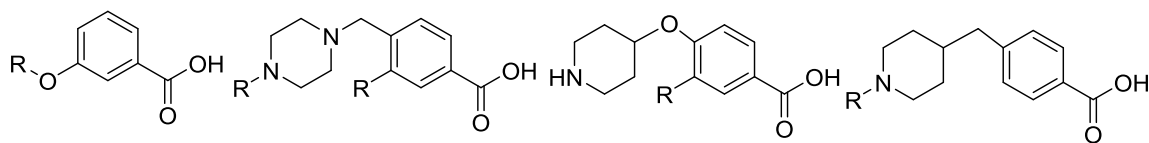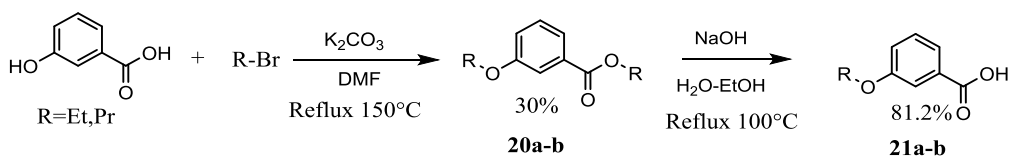

Figure 5.1 Core structures of benzoic acid derivatives

Scheme 5.1 Synthesis of 3-alkoxy benzoic acid derivatives[76]

Two commercially available N-caps included 4-(piperazin-1-yl) and 3-(piperidin-4-yloxy)benzoic acids were obtained as their free amines. In order to append these to the peptide as capping groups, the amino groups were first Boc protected using a standard method. The desired protected N caps were obtained in approximately 50% yield (22)[77]. The Boc protection reaction is shown in scheme 5.2.
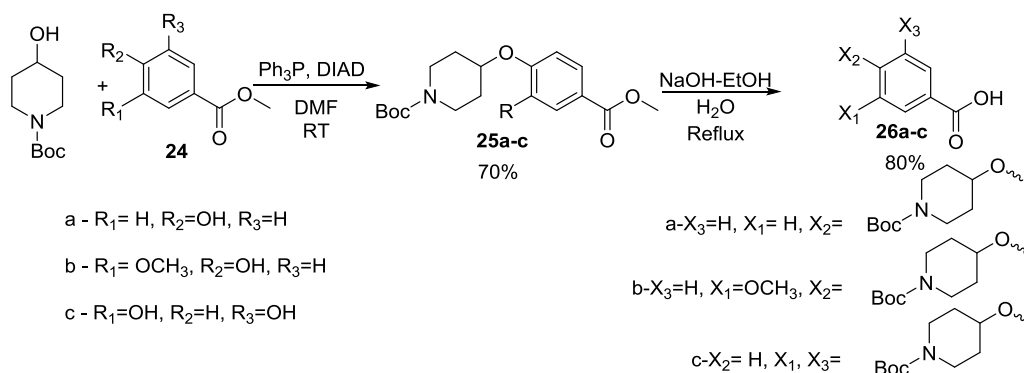
Scheme 5.2 Synthesis of Boc protected 4-piperazinyl benzoic acid[77]
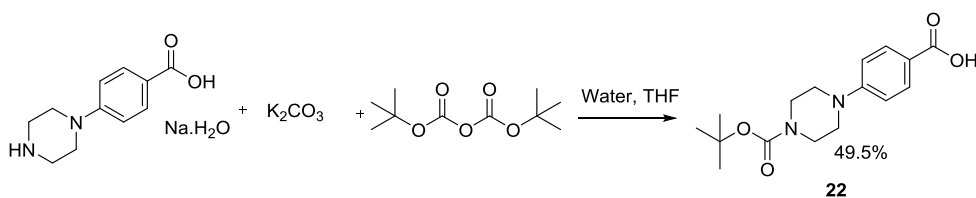
Further analogs in the piperidinyloxybenzoic acid series were synthesized by Mitsunobu reaction[78]. These include the 4-piperidinyloxy (26a), 3-methoxy-4-piperidinyloxy (26b) and 3,5-bis piperidinyloxy derivatives (26c). These compounds

were synthesized to study their ion-pairing interactions of the piperidinyl N-atom with acidic regions and van der Waals interactions of substituents at 3-position with second pocket. The Mitsunobu reaction and subsequent ester hydrolysis are outlined in scheme 5.3.

Scheme 5.3 Synthesis of 4-piperidinyl oxy benzoic acid derivatives[78]

a - R$_1$= H, R$_2$=OH, R$_3$=H

b - R$_1$= OCH$_3$, R$_2$=OH, R$_3$=H

c - R$_1$=OH, R$_2$=H, R$_3$=OH

a-X$_3$=H, X$_1$= H, X$_2$=

b-X$_3$=H, X$_1$=OCH$_3$, X$_2$=

c-X$_2$= H, X$_1$, X$_3$=

The majority of the N-caps based on the benzoic acid scaffold were designed to incorporate a piperazinemethyl group as a substituent at the 4-position. Synthesis of 4-(piperazin-1-ylmethyl)benzoic acid and its derivatives were carried out by reductive amination reactions in which an aldehyde is converted to amine through reduction of an imine intermediate[79]. This reaction was carried out with 4-formyl benzoic acid precursors and the required amine with sodium triacetoxyborohydride as reducing agent (scheme 5.4 to 5.9). The synthesis of the 4-(piperazin-1-ylmethyl) analogs, 27a and 27b were accomplished using 4-formyl benzoic acid precursors. It was observed that the 3-hydroxyl substitution helped the reaction to go to completion overnight whereas the reaction in 4-formyl benzoic acid required 24 hours to complete (27a-b). The intermediate compound 4-((4-(tert-butoxycarbonyl)piperazin-1-yl)methyl)-3-

hydroxybenzoic acid (27a) was then used as starting material for the synthesis of the derivatives alkylated on the 3-hydroxyl (28a and 28b) (scheme 5.4).
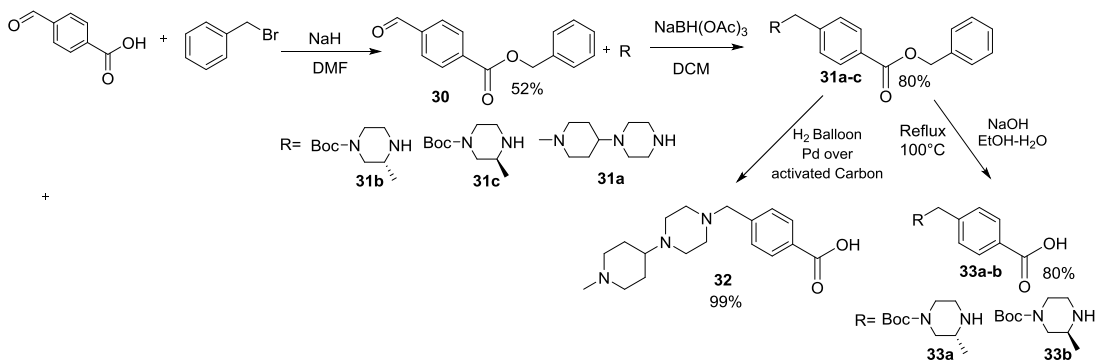
Scheme 5.4 Synthesis of 3-alkoxy-4-piperazinylmethyl benzoic acid derivatives[79,76]
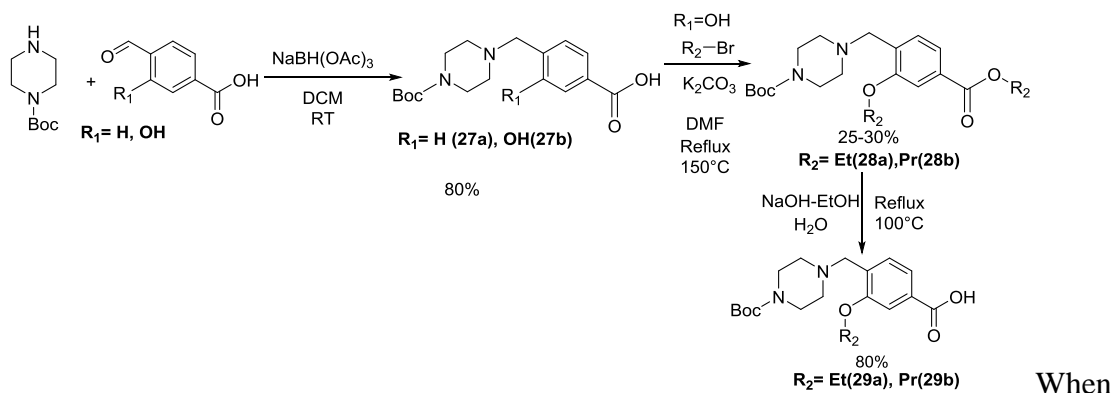

When compounds containing a substituted piperazine (i.e. 4-((4-(1-methylpiperidin-4-yl)piperazin-1-yl)methyl) or (R or S)-4-((4-(tert-butoxycarbonyl)-2-methylpiperazin-1-yl)methyl)) were appended using reductive amination, difficulties occurred in recovery of the resulting product during aqueous work up. Hence the starting material was benzylated with (bromomethyl)benzene using sodium hydride[80]. Using the benzylated precursor, the reductive amination product was easily recovered from the organic layer. To obtain the final product, the benzyl group was removed by hydrogenation[81] (scheme 5.5) however was not successful in every case (i.e. with 33a and 33b), and therefore base hydrolysis was used (scheme 5.5). By way of a similar procedure to the one used for compounds 32 and 33, 4-(((1-(tert-butoxycarbonyl)piperidin-3-yl)(methyl)amino)methyl)benzoic acid and 4-(((1-(tert-butoxycarbonyl)piperidin-4-yl)(methyl)amino)methyl)benzoic acid (35a and 35b) were synthesized by reductive amination of 4-formyl methyl benzoate with the requisite amine followed by base hydrolysis[79]. For the synthesis of 4-((((tert-butoxycarbonyl)(1-(tert-

107

butoxycarbonyl)piperidin-4-yl)amino)methyl)benzoic acid (37), Boc protection of the amine was required (scheme 5.6)[77].
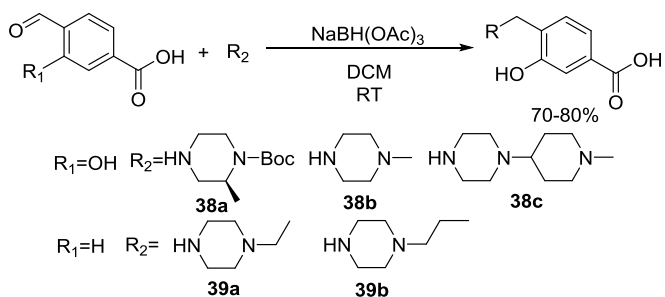
Scheme 5.5 Synthesis of modified piperazinyl benzoic acid derivatives[79,80]

Scheme 5.6 Synthesis of piperidinyl amino methyl benzoic acid derivatives
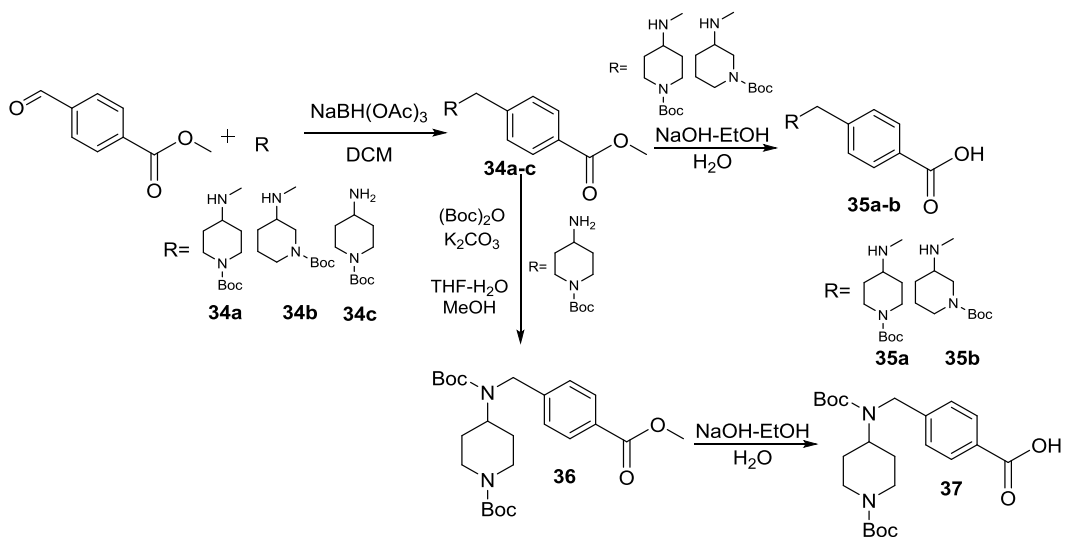

Scheme 5.7 Synthesis of 4- substituted piperazinylmethyl benzoic acid derivatives[79]

Three such derivatives were synthesized from 3-hydroxy-4-formyl benzoic acid by direct reductive amination[79]. The recovery and purification of these compounds were successful and hence the additional derivatives 39a and 39b were synthesized and purified (scheme 5.7). Substituents were included on the piperazine ring to imcreasee the hydrophobicity of the capping groups.

Similar to the N-caps mentioned above, alkyl substituents were incorporated into (S) methyl piperazine analogs to improve binding affinity as well increase the hydrophobicity. Synthesis of (S)-4-((4-alkyl-2-methylpiperazin-1-yl)methyl)benzoic acid was carried out by reductive amination of 4-formylmethyl benzoate with tert-butyl (S)-3-methylpiperazine-1-carboxylate as described previously[79]. Alkylation of the free piperazine nitrogen was acheieved by reductive amination with the requisite aliphatic aldehyde using similar conditions[76]. As before base hydrolysis of the ester liberated the required Ncap product (scheme 5.8).

Scheme 5.8 Synthesis of (S)-4-((4-alkyl-2-methylpiperazin-1-yl)methyl)benzoic acid
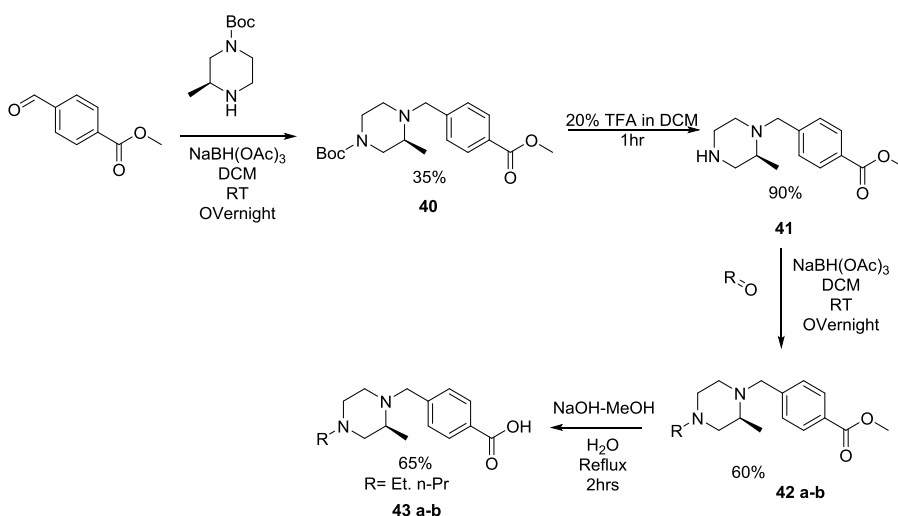
Piperidin-4-ylidenemethyl benzoic acid derivatives were synthesized in the first instance by a Wittig reaction of methyl 4-((diethoxyphosphoryl)methyl)benzoate with

amino piperidone to generate 45a and b (Boc protected and methylated respectively). The resulting ylidene was then base hydrolyzed to obtain the corresponding free benzoic acid, 46a and 46b. The utility of this reaction and the potential SAR information could be further extended by high pressure hydrogenation of the ylidine to reduce the double bond and obtain methyl 4-((1-Bocpiperidin-4-yl)methyl)benzoate (47) which after hydrolysis generated capping group 48 [82](scheme 5.9).

Scheme 5.9 Synthesis of piperidinyl methyl benzoic acid derivatives[82]
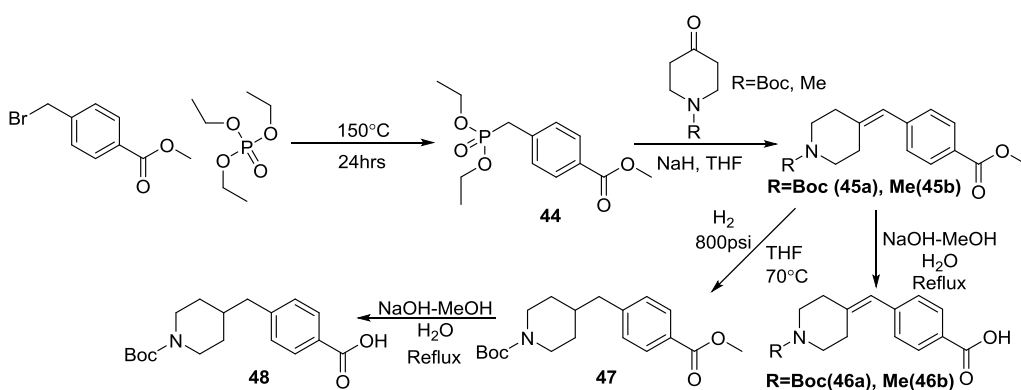
5.2.2 SAR of benzoic acid capped peptides

5.2.2.1 SAR of 3-susbtituted benzoic acid derivatives

As described in chapter 4, the phenylacetic acid capped FLIP, **530** (3,5-diethoxyphenylacetic acid) possessed good affinity for both CDK2/cyclin complexes. Modeling of this analog suggests that the ethoxy group in the 3-position occupies the minor hydrophobic pocket providing a structural basis for its reasonable activity[68]. In order to probe such modifications in the similar benzoic acid derived capping groups, a series of 3-substituted derivatives were docked using the validated LigandFit protocol[55].

Table 5.1 SAR of 3-substitued benzoic acid derivatives for van der Waals interactions
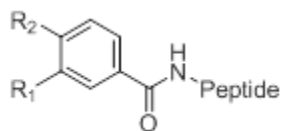
SCCP ID	R1	R2	Peptide	CDK2/A2 IC50 (µM)	CDK4/D1 IC50 (µM)
5857	H	H	RLIF	>100	>100
5835	CH3	H	RLNpfF	>100	>180
5858		H	RLIF	>100	33.9
5844		H	RLIF	>100	>180
5846		H	RLIF	>180	>100
5882		H	RLIF	>100	>100
5883		H	RLIF	>100	>100

The results indicated that the inclusion of alkyl or alkoxy groups at the 3-position provides good complementarity with the secondary pocket as predicted and that the amide carbonyl can form an H-bond with the amide side chain of Gln254. Based on these docking results FLIPs were generated in which RLIF/RLNpfF was N-capped with the described derivatives (Table 5.1). All the FLIPs generated in this series were inactive except **5858** which showed moderate inhibition of CDK4/cyclin D.

5.2.2.2 SAR of 4-Substituted benzoic acid derivatives

Previous investigations (chapter 4), on furoic acid analogs revealed that presence of basic groups resulted in moderate binding activities of CDK2/cyclin A inhibitors targeting the CBG. Furthermore the previously reported CGI compounds incorporated benzoic acids as Ncaps that were substituted with basic functionality[68]. Based on this precedent and the Ncaps described in chapter 4, the design and synthesis of a unique

111

series of benzoic acid derived fragment alternatives was undertaken. These encompassed derivatives reported in this previous study and new variants which were computationally designed. Substituents appended onto the 4-position included piperazinyl (**5850**), piperazin-1ylmethyl (**5566, 5919, 5923, 5920**) and guanidomethyl (**541**). Some of these Ncap derivatives included the 3-(piperidin-4yloxy) group (**5851**) and 3-hydroxy (**5920**). One of the previously reported derivatives incorporated a 4-guanidinomethyl substituent (**541**) and was synthesized for comparison. Each of these N-caps were ligated to RLIF except **5566** and **541** which were N-capped to RLNpfF. The SAR results of these compounds are shown in table 5.2.

In this series the most potent compounds are those ligated to RLNpfF which are 2 fold more potent compared to RRLIF (0.7 μM vs 1.01 μM in CDK2/cyclin A, 2.17 μM vs 25.12 μM in CDK4/cyclin D). The FLIP molecule **541** is the most effective compound (CDK2/cyclin A 0.69 μM and CDK4/cyclin D - 15.32 μM) and where the N-capping group is a benzoic acid substituted with guanidinomethyl group at the 4-position. Incorporation of 4-(piperazine-1ylmethyl)benzoic acid as an N-cap (**5566**) resulted in comparable activity to the 35DCPT triazole Ncaps described in chapter 3 with a binding IC_{50} to CDK2/cyclin A of 5.3 μM and to CDK4/cyclin D of 12.87 μM. The 4-(piperidin-1yloxy)benzamide (**5851**-31.34μM) and the 4-(piperazine-1yl)benzamide (**5850**-35.16μM) FLIPs showed nearly equal potencies in binding to cyclin A in its CDK2 complex. The piperidinyloxy FLIP **5851** (8.52μM) is 4 fold more potent than its piperazinyl counterpart (**5850**- 23.82 μM) in binding to CDK4/cyclin D. Varying the peptide sequence in the 4-piperazinylmethyl benzamide context was undertaken. ALIF (**5923**) is inactive and RLIF (**5919**) is slightly 2 fold less potent than RLNpfF (**5566**) in

cyclin A. Comparison of **5919** and **5566** again confirmed that the difference in activity is because of the more potent peptide sequence RLNpfF.

**Table 5.2 SAR of 3/4 mono and 3,5-disubstituted benzoic acid derivatives for ion-pairing interactions**
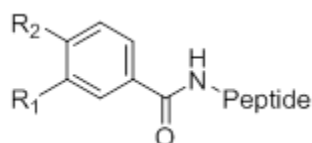
SCCP ID	R1	R2	PeptideSequence	CDK2/Cyclin A IC50 (µM)	CDK4/D1 IC50 (µM)
5851		H	RLIF	31.34±15.71	8.52±4.43
5850	H		RLIF	35.16±10.17	23.82
5566	H		RLNpfF	5.30±0.99	12.87±1.67
541	H		RLNpfF	0.69±0.34	15.32±5.09
5919	H		RLIF	12.89±2.99	11.70±5.92
5923	H		ALIF	>100	51.49±21.34
5920	OH		RLIF	4.56±0.74	10.41±0.61

5.2.3 SAR of benzoic acid FLIPs capable of ion-pairing and van der Waals interactions

In order to further extend the SAR of these 4-(piperazine-1yl)benzoic acid derivatives and to exploit the unoccupied secondary pocket in this context, alkyl substitution of the 3-position was undertaken. The addition of and role of the 3-subsitution was examined through testing of **5896** (3-methoxy, 4-piperidinyloxybenzoic acid) and comparison with its mono 4-substituted counterpart **5851**. The potency of the bis substituted benzamide FLIP increased significantly in binding to CDK2/cyclin A (22 µM vs 31 µM in cyclin A) but was essentially equipotent towards CDK4/cyclin D (9 µM vs 8 µM). Addition of a 3-hydroxyl to this series (**5920**) results in a 2 fold potency

113

enhancement compared to **5919** for CDK2/cyclin A (IC$_{50}$ - 4.56 µM) however does not significantly improve activity towards CDK4/cyclin D (CDK4/cyclin D, IC$_{50}$ -10.41 µM). Incorporation of a 3-ethoxy substituent into the FLIP (**5922**) resulted in similar activity compared to **5920** in cyclin A and 2 fold better activities in cyclin D. Methylation of the free piperizinyl N-atom (**5921**) resulted in slightly diminished potency compared to 5920. Further benzoic acid derived capping group modifications were investigated in the RβLNMeF context described in chapter 5 so as to improve compound stability and cell permeability. In this series (table 5.3), the 4- (piperidin-4yl)oxybenzoic acid derivative (**5965**) is less active in the binding assay compared to the same N-cap ligated to RLIF (**5851**) in CDK2/cyclin A(40 µM (**5965**) vs 31 µM (**5851**)). Comparable results are seen for 5966 (RbLNMeF-NH$_2$) vs 5920 (RLIF) in both cyclins where the N-cap is 3-hydroxy-4-(piperazin-1-ylmethyl)benzamide. The RβLNMeF counterpart (**5968**) to the 3-ethoxy, 4-(piperazin-1yl)benzamide Ncap (5968) has diminished potency for both cyclin A (22.61µM) and D (18.64 µM). Among FLIPs containing modified versions of the piperazine ring system, **5967** (4-((4-(1-methylpiperidin-4-yl)piperazin-1-yl)methyl)benzamide is the most potent followed by **5970** ((S)-4-((2-methylpiperazin-1-yl)methyl) benzamide) and **5969** ((R)-4-((2-methylpiperazin-1-yl)methyl) benzamide). These compounds are unique in this series as they have respectable potency, lower activity towards CDK4/cyclin D and incorporate more drug-like features. The results are shown in table 5.3.

Table 5.3 SAR of benzoic acid FLIPs capable of ion-pairing and van der Waals interactions
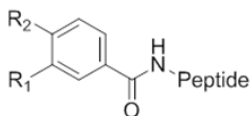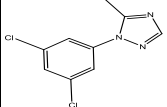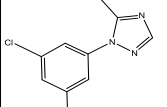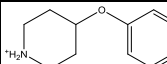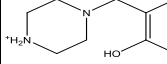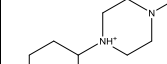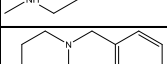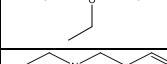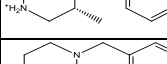

SCCP ID	R1	R2	Peptide Sequence	CDK2/Cyclin A IC50 (µM)	CDK4/D1 IC50 (µM)
5922			RLIF	5.95±2.53	5.14±1.47
5921	H		RLIF	7.92±1.39	11.31±1.48
5896	OCH₃		RLIF	22.42±9.66	9.36±6.56
5965		H	RbLNMeF-NH₂	40.38±17.76	30.99±1.18
5966	OH		RbLNMeF-NH₂	7.42±1.69	11.76±1.01
5968			RbLNMeF-NH₂	22.61±1.89	18.64±9.72
5967	H		RbLNMeF-NH₂	8.32±0.36	48.89±40.36
5969	H		RbLNMeF-NH₂	22.28±5.22	45.45±0.47
5970	H		RbLNMeF-NH₂	13.39±4.35	>100

Due to the introduction of the non-natural C-terminus and more drug-like Ncaps, several FLIPs from this series (Table 5.4) were tested for anti-proliferative activity in U2OS and DU145 cells[52,54]. So as to assess their drug-like character and to predict which modifications might lead to optimization of pharmaceutical properties, their clog P and tPSA were calculated. The resulting parameters were then compared with **5963** (35DCPT RβLNMeF) and **5964** (35DCPT- RβL3-TA) which were both shown to have respectable growth inhibitory activity. For the most part the benzoic acid derived FLIPs were inactive with the exception of **5970** which exhibited very weak anti-proliferative activity. The N-caps in **5969** and **5970** had total low polar surface area (tPSA) of 3.35 (<140 for orally available drug molecules) and a positive value of clog P (2.71) [65,66] (table 6.4). Due to its

115

weak cellular activity, it was hypothesized that modifications that increase hydrophobicity would potentially improve cellular permeability and potency. Therefore derivatives of 4-piperidin-1ylmethylbenzoic acid were designed based on addition of alkyl groups to increase the lipophilicity. The clogP values were used as a guideline to assess effective modifications. The clog P values for the 35DCPT N-capped FLIP (5964) were used as a target value for further modification of N-caps.

Table 5.4 Cellular activity and PSA and clogP of selected
benzoic acid derivatives

Ncap	ID	CDK2/Cyclin A(µM)	U2OS(µM)	PSA	clog P
	5963	6.49±0.27	30.7±2.7	27.96	2.9
	5964	7.91±5.08	18.3±1.5	27.96	2.9
	5965	31.08±14.4	>100	25.84	2.13
	5966	9.22±6.15	>100	40.08	1.47
	5967	10.45±3.58	>100	12.12	3.13
	5968	22.48±1.33	>100	29.08	2.64
	5969	18.42±4.59	>100	19.85	2.71
	5970	4.85	67.3	19.85	2.71

Additional benzoic acid derivatives were designed based on clog P and PSA using the corresponding values of 35DCPT as a reference. The 4-substituents incorporated were piperazinylmethyl or piperidinyl derivatives, were ligated to RβL3-TA and tested in the binding assay and for anti-tumor activity on DU145 cancer cell lines. These

compounds showed good to moderate activity against CDK2/cyclin A but none of them were active in the cellular assay. The results are shown in table 5.5.
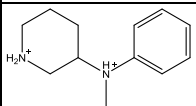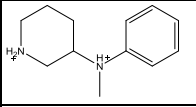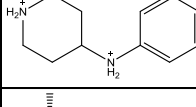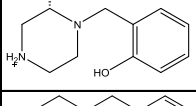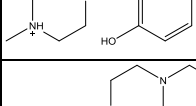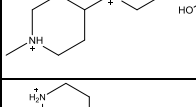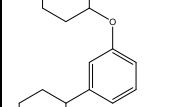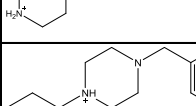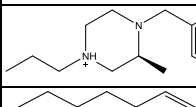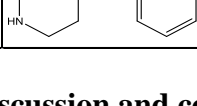
Table 5.5 Benzoic acid derivatives tested in cancer cells.
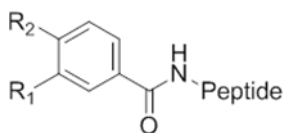
SCCP ID	R1	R2	PeptideSequence	CDK2/Cyclin A IC50 (μM)	CDK4/D1 IC50 (μM)	Du145 IC50 (μM)
6033	H		R-bL-3TA	17.44±13.39	74.28±4.45	>100
6034	H		R-bL-3TA	6.78±2.72	45.60±13.69	>100
6031	H		R-bL-3TA	9.16±8.74	>100	>100
6032	H		R-bL-3TA	26.02±7.13	69.91±7.07	>100

Several other N-caps were designed based improved binding results and calculated physicochemical properties (clogP and PSA) in order to optimize drug-likeness (table 5.6). FLIPs containing the capping groups NC-8, 9 and 10 were designed on the basis that improved hydrophobicity will result in greater cell permeability and anti-tumor activity.

117

Table 5.6 Benzoic acid derivatives designed to improve cell permeability.

ID	N-cap	PSA	clogP
NC-1		21.05	2.29
NC-2		21.05	2.29
NC-3		33.22	2.95
NC-4		40.08	1.99
NC-5		27.91	2.03
NC-6		32.35	2.41
NC-7		32.35	2.41
NC-8		7.68	2.41
NC-9		7.68	4.32
NC-10		16.61	3.33

5.3 Discussion and conclusions

Several N-capping groups scaffolds have been identified however non are optimal in terms of mimicking the majority of the interactions of N-terminal tetrapeptide of HAKRRLIF. Even 35DCPT, the most effective N-cap only practically interacts with this region and hence there is a need for improvement. A previously published study described benzoic acid capped peptides with a chlorophenylcyclohexylamine replacement

118

for the phenylalanine. These derivatives included basic substituents which when incorporated into cyclin groove inhibitors resulted into potent compounds when tested in CDK2/cyclin A ELISA using retinoblastoma protein as substrate for competitive binding[75] (Figure 5.2). This suggested that the benzoic acid scaffold would be an effective one for the presentation of the required functionality to interact more completely with the cyclin groove by including contacts with the secondary pocket while also making ion-pairing interactions with the acidic residues. As described in chapter 3, previous studies demonstrated that FLIP molecules containing 3,4 diethoxyphenylacetamido group as N-cap (**530**) were good inhibitors of CDK2/cyclin A (6.5µM) and CDK4/cyclin D (25.5µM). Incorporation of basic substituents including piperazinyl and alkyl amines onto heterocyclic scaffolds (5-((4-methylpiperazin-1-yl)methyl)furan-2-carboxamide-RLIF, **5589**, 5-((diethylamino)methyl)furan-2-carboxamide-RLIF - **5581**) resulted in moderate activity in both CDK2/cyclin A and CDK4/cyclin D[68]. Supportive docking results suggest that ion-pairing interactions with the negatively charged residues contributed to binding. Based on this result and literature reviews, benzoic acid derivatives were explored as N-capping groups. It was hypothesized that through effective substitutions on the 3,4 positions of benzoic acid core structure, ion-pairing, hydrogen bonding and van der Waals interactions might be retained.
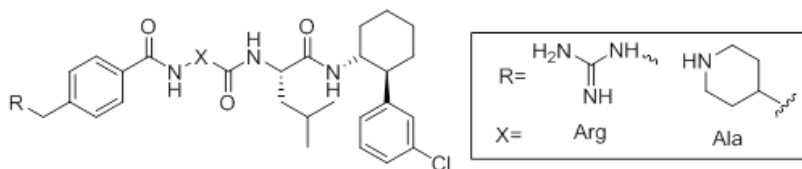
Figure 5.2 CDK2/cyclin A inhibitors developed by Genentech Inc.

In the first steps to exploiting the potential of the benzoic acid scaffold, 3-alkoxy derivatives were designed so as to build on the success of 3,5-diethoxyphenylacetic acid as an Ncapping group. Although docking studies were undertaken with 3- alkyloxy or aryl oxy substituted benzoic acids (Overlays of 3-substituted benzoic acid derivatives are shown in figure 5.3), none of these FLIPs had significant activity in the FP binding assay with the exception of 3-ethoxybenzamido substituted FLIP which had marginal affinity for CDK4/cyclin D. The observed inactivity of this FLIP series could be because of weaker van der Waals interactions resulting from too much flexibility of the groups without the ion-pairing interactions to stabilize binding. For sufficient activity, N-capped peptides require more extensive interactions that are made by the potent CGI peptides including ion-pairing and H-bond contacts. In order to improve the affinity of these Ncapped peptides, and due to the synthetic versatility of the benzoic acid scaffold, additional substituents were appended at the 4 position to include groups capable of ion-pairing with the cyclin groove.
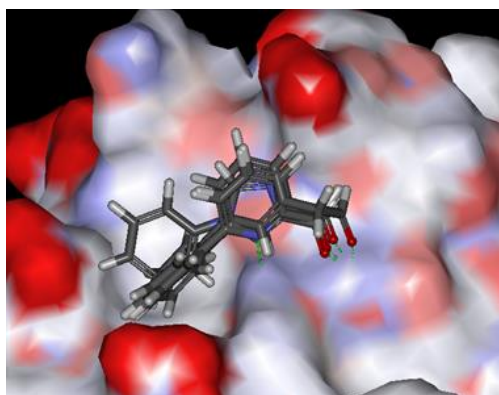
**Figure 5.3 Overlays of 3-susbtituted
benzoic acid derivatives**

**Overlay of docked poses of 3-susbtituted benzoic acid shows van der Waals
interaction at the secondary pocket and hydrogen bonding with Gln 254.**

In the first instance, single 4-substituted benzoic acids were generated for incorporation as capping groups. Inclusion of basic groups (guanidomethyl (**541**), piperazin1-yl (**5850**), piperidin-4yloxy (**5851**) and 4-methylpiperazin-1ylmethyl (**5919**) shown in table 6.1 resulted in significant improvement in the activity compared to the 3-alkyl analogs. The guanidinomethyl substitution which has been previously reported, was generated as a RLNpfF FLIP and was the highest potency cyclin groove inhibitor in this series (0.69μM). The effectiveness of this compound is due to its very strong electrostatic interaction of the positively charged guanidine with the acidic region (Glu220, Glu224). Both the piperidin-4yloxymethyl (**5851**) and piperazinyl (**5850**) are similarly potent in binding to cyclin A in complex with CDK2 however **5851** exhibits higher activity for CDK4/cyclin D. The better activity in cyclin D could due to the proximity of piperidinyl group with Glu70 and GLu66. RRLNpfF is a better CBG inhibitor compared to RRLIF by 2 fold increased potency. The p-fluoro substituent on the phenylalanine ring enables increased hydrophobic contacts in the primary pocket[69]. The increased binding of the RLNpfF peptide was confirmed by the comparison of **5566** and **5919** since both of these FLIPs have (4-piperazin-1ylmethyl)benzoic acid as N-cap. When ligated to RLNpfF (**5566**) has 2.5 fold better potency in cyclin A compared to the one ligated to RLIF (**5919**). Incorporation of a methoxy or a hydroxyl substituent at 3 position in **5896** and **5920** improves cyclin A activity compared to the mono substituted counterparts (**5851, 5919**) (figure 5.4). Alkoxy or hydroxyl substitution provides additional hydrophobic complementarity with secondary pocket in addition to H-bonding interactions of the OH with Trp217. The activity profiles of these two compounds confirms the hypothesis that having a basic group at 4 position and an alkyl group at 3 position improves the activity

of benzamide FLIPs through ion-pairing and van der Waals interactions. Based on improvement in the activity profiles of 3,4-disubstituted benzoic acid N-caps, **5896** and **5920**, next generation fragment alternatives included modifications on the piperazine moieties for additional hydrophobic interactions. These compounds were designed with alkoxy or hydroxyl substituents at 3-position and piperazine with additional alkyl groups at the 4 position of benzoic acid as shown in scheme 5.10.

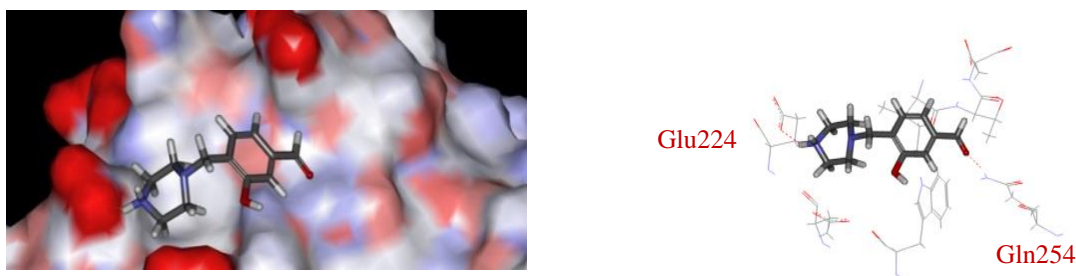**Figure 5.4 Docked pose of 5920 in CDK2/cyclin A**

Examination of the binding mode of 5920 reveals that N4 of the piperazine-1ylmethylbenzoic acid Ncap forms ion-pairing interactions with Glu224, the carbonyl contributes to an H-bond with Gln 254 and 3-hyrdoxyl can H-bond to Trp217.

Scheme 5.10 Design and optimization of benzoic acid derivatives for interaction with the secondary hydrophobic pocket.
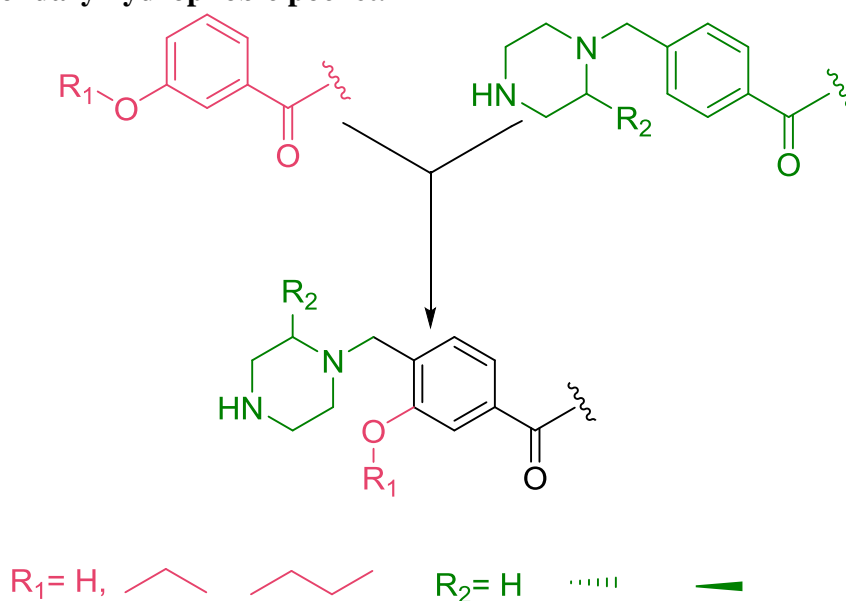
Docking studies were carried out on a series of benzoic acid derivatives with 3-alkoxy-4-(piperazine-1ylmethyl) groups. The docked poses were prioritized based on their PLP1 score and further based on expected complementarity with the key acidic residues of the CBG (Glu220, Glu224), and with the secondary pocket. For the most part, results obtained in testing the synthesized FLIP compounds were in accordance the highly ranked docked poses. The design hypothesis was confirmed in that 3,4-disubstituted benzamido FLIPS and those with a modified piperazine ring possess improved activity compared to previous series. The presence of an ethoxy group at 3-position provides increased van der Waals contacts however the complementarity of the propoxy substitution is more optimal as was observed through increased binding observed with **5922** and **5968**. As described in chapter 4, FLIPs **5963** (35DCPT-RβLNMeFNH$_2$) and **5964** (35DCPT- RβL3TA) provided proof of concept for cell permeability and therefore this sequence was employed in the context of benzoic acid Ncap modification to compare activities with 35DCPT and examine cell permeability. Modifications to the piperazine ring (**5967**, **5969** and **5970**) results in decreased binding to CDK4/cyclin D and shows selectivity for CDK2/cyclin A. Since these contain modified piperazine groups that have increased size, they can be more easily accommodated in the cyclin A groove relative to cyclin D which has a narrower secondary pocket. Although **5969** and **5970** are stereoisomers there is a significant difference in their activity. This can be explained through structural analysis where it was observed that the piperazine-2-methyl group of **5969** points out of the minor pocket however in **5970**, the methyl group interacts efficiently with the secondary pocket resulting in the increased binding affinity for this analog (figure 5.5).

5969   5970
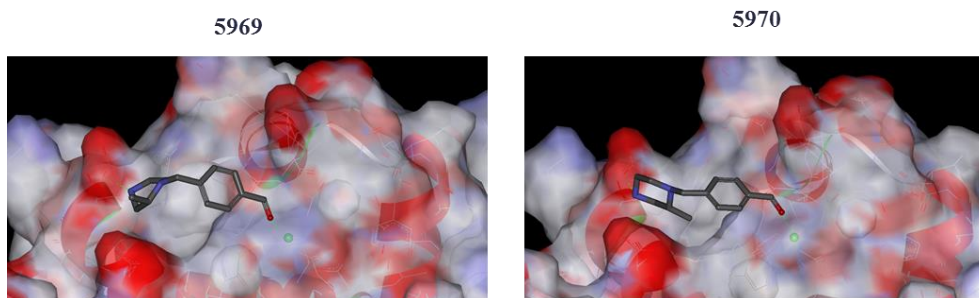
Figure 5.5 Binding modes of 5969 and 5970.

Docked poses of 5969 and 5970 showing the orientation of 3-methyl substituent of piperazine. In 5969 it is pointing above the second pocket and in 55970 it is contacting with the second pocket

As the FLIP molecules in this series were considered to potentially have more drug-likeness and stability they were tested for anti-tumor activity in a MTT assay. For the most part this series were inactive in both U2OS and DU145 cell lines with the exception of 5970 which showed marginal activity. To determine the lack of cellular activity compared to 5964, the physicochemical properties that determine drug likeness (including hydrophobicity and polar surface area) were calculated for these compounds to compare with the 35DCPT capping group. An additional series of benzoic acid derivatives were designed based on the FP results and physicochemical properties of 35DCPT. Further experiments will examine the effects of increased hydrophobicity on cellular anti-proliferative activity.

The main objective of the work described in this chapter was to more completely mimic of the interactions of CGI peptides through optimization of benzoic acid based N-caps. From the SAR results obtained, this objective has been achieved with appropriately modified FLIPs in which the ion-pairing, hydrophobic and hydrogen bonding interactions were retained. Based on the physicochemical properties of 35DCPT, several analogs

were designed to have similar hydrophobicity and PSA characteristics. Although the initial analogs were in active in cellular studies, further analogs were proposed to address this issue and improve drug-like characteristics. In summary, the extensive SAR data obtained for optimized benzoic acid Ncapped peptides further validates REPLACE strategy and suggests how these FLIPS can be further modified and improved for the development non-ATP competitive CDK inhibitors.

5.4 Experimental section

5.4.1 Materials and methods

All solvents and reagents were used as obtained. ^{1}H NMR and ^{13}C NMR spectra were recorded with a Varian Mercury 300 and 400 Spectrometer, respectively. Mass spectra were measured with Micromass QTOF: Tandem quadruple-time of flight mass spectrometer electrospray ionization (ESI) and VG 70S: Double-focusing magnetic sector mass spectrometer (EI). Analytical purities of evaluated compounds were >95% unless stated otherwise. The following analytic method (unless stated otherwise) was used on a Waters Alliance 2695 HPLC with a 2996 diode-array detector and equipped a C18 (2) 100 A, 250 x 4.6mm, 5μ column (Phenomenox Luna). A gradient from 100% water (0.1% trifluoroacetic acid) to 60% acetonitrile (0.1% trifluoroacetic acid) was run over 30 mins and held for 4 mins. The chromatograms were extracted at 226 and 254 nm.

Synthesis of 3-alkoxy benzoic acid derivatives[76]

Step 1: Synthesis of ethyl 3-ethoxybenzoate (20a)

3-hydroxy benzoic acid (0.69g, 5mmol), ethoxy bromide (0.25g, 23mmol) and potassium carbonate (0.13g, 16.5mmol) were refluxed in 5ml of DMF for 12-18hrs. The reaction was monitored by TLC (Ethylacetate: Hexanes= 35:65), after the reaction was

complete, the reaction mixture was cooled to room temperature; water was added to dissolve potassium carbonate. The aqueous layer was extracted with ethyl acetate and the combined organic layers were washed with saturated sodium bicarbonate, brine, dried over sodium sulfate and evaporated to get reddish oil (0.29g, 30%).

ethyl 2-(3-ethoxyphenyl)acetate: 1H NMR (dimethyl sulfoxide-D6, 300MHz) δ (ppm) 7.18(s,1H), 7.13 (t. J=7.71Hz, 1H), 6.75-6.78 (d, J=8.88Hz, 2H), 6.70-6.73 (d, J=8.67Hz, 2H), 1.31 (t, J=7.11Hz, 3H), 1.16 (t, J=7.29Hz, 3H) GC MS- 208

Step 2: Synthesis of 3-ethoxybenzoic acid (21a)

The ethyl 3-ethoxybenzoate (0.97g, 5mmol) obtained from step 1 was treated with sodium hydroxide (2.8g, 70mmol) and a solution of 15ml ethanol and 15ml water. The reaction mixture was refluxed for two hours and the reaction was monitored by TLC (35% ethyl acetate in hexanes). After the completion of reaction, the reaction mixture was cooled, the alcohol was evaporated and diluted with water. The reaction mixture was acidified with 1N hydrochloric acid and stirred to precipitate the product as white solid (0.67g, 81.2%)

2-(3-ethoxyphenyl)acetic acid :^{1}H NMR (chloroform-D3, 500MHz) δ (ppm) 7.256 (t, J=7.75Hz, 1H) 6.8753 (d, J=7.65Hz, 1H), 6.8507(s, 1H), 6.8319 (d, J=2.2Hz, 1H), 4.0636 (q, J=7.0Hz, 2H), 3.636 (s, 1H), 1,4296 (d, J=55.57Hz, 3H)

^{13}C NMR (chloroform-D3, 500MHz) δ (ppm) 177.15, 159.14, 134.61, 129.6, 121.55, 115.65, 113.41, 63.41, 41.01, 31.16, 14.80 GC MS-108

Synthesis of 3-((1-(tert-butoxycarbonyl)piperidin-4-yl)oxy)benzoic acid and 4-(4-(tert-butoxycarbonyl)piperazin-1-yl)benzoic acid (22)[77]

To a solution of 3-(piperidin-4-yloxy) benzoic acid (0.12g, 0.5 mmol) and potassium carbonate (0.13g, 1mmol) in 1mL of water di-*tert*-butyl dicarbonate (0.11g, 0.5 mmol) was added as a solution in 0.6ml tetrahydrofuran, dropwise at 0 °C. After the addition was completed, the reaction mixture was allowed to come to room temperature and stirred for 4 h. THF was removed in vacuum and the aqueous phase was washed with ether. The aqueous phase was separated and adjusted to pH 2 with 1 N hydrochloric acid, and extracted with ethyl acetate. The combined organic extracts were concentrated to get 3-((1-(tert-butoxycarbonyl)piperidin-4-yl)oxy)benzoic acid (0.15 g, 49.5%) as a white solid.

1H NMR (chloroform-D3, 400MHz) δ (ppm) 7.70 (d, J=7.17Hz, 1H), 7.61(s,1H), 7.37(t, J=8.34Hz, 1H), 7.15 (d, J=8.64, 1H), 4.55 (s,1H), 3.70(q, 2H), 3.36(q, 2H), 1.93(q, 2H). 1.77(q, 2H), 1.46 (s,9H)

^{13}C NMR (chloroform-D3, 400MHz) δ (ppm) 170.89, 157.29, 154.89, 130.65, 129.74, 122.94, 122.26, 116.69, 79.75, 72.45, 28.45

ES+344

Synthesis of 4-(4-(tert-butoxycarbonyl)piperazin-1-yl)benzoic acid (23)[77]

To a solution of sodium salt of 4-(piperazin-1-yl)benzoic acid (0.36g, 1.5 mmol) and potassium carbonate (0.20g, 1.5mmol) in 3mL of water di-*tert*-butyl dicarbonate (0.32g, 1.5 mmol) was added as a solution in 1.8ml tetrahydrofuran, dropwise at 0 °C. After the addition was completed, the reaction mixture was allowed to come to room temperature and stirred for 4 h. THF was removed in vacuum and the aqueous phase was

washed with ether. The aqueous phase was separated and adjusted to pH 2 with 1 N hydrochloric acid, and extracted with ethyl acetate. The combined organic extracts were concentrated to get 4-(4-(tert-butoxycarbonyl)piperazin-1-yl)benzoic acid (0.13 g, 45%) as a white solid.

1H NMR (chloroform-D3, 400MHz) δ (ppm) 7.98(d, J=8.10Hz, 2H), 6.87(d, J=8.67Hz, 2H), 3.58(s, 4H), 3.33 (s,4H), 1.48 (2,9H)

13C NMR (chloroform-D3, 400MHz) δ (ppm) 170.86, 154.68, 154.44, 132.03, 118.92, 113.78, 80.21, 47.35, 28.42

ES+307

Synthesis of 4-((1-(tert-butoxycarbonyl)piperidin-4-yl)oxy)benzoic acid[78]

Step 1. Synthesis of 3-methoxybenzoic acid methyl ester (24)[76]

To a solution of vanilic acid (0.67g, 4mmol) in 9ml of anhydrous methanol 0.25ml of Conc. Sulfuric acid (3.0 mL) was added and the mixture was refluxed overnight. The reaction mixture was cooled to room temperature, the solvent was evaporated and the residue was dissolved in ethyl acetate. The organic layer was washed with 5% sodium bicarbonate, water and brine. Then it was dried over sodium sulfate, filtered, and concentrated to get a white solid (0.49 g, 68.2%)

Step 2: Synthesis of tert-butyl 4-(4-(methoxycarbonyl)phenoxy)piperidine-1-carboxylate (25a)[78]

4-Hydroxymethylbenzoate (0.30g, 2mmol) and triphenylphosphine (2.62g, 10mmol) were dissolved in 30 mL of dry THF at 0 °C. To the stirred mixture a solution of N-(*tert*butyloxycarbonyl)piperidin-4-ol (1.15g, 10mmol) and DIAD(2.02g, 10mmol) 20 mL of dry THF was added drop wise over a period of 2 h,. The reaction mixture was

stirred for 5 days at room temperature and monitored by TLC (Ethylacetate: Hexanes-35:65) to see the consumption of starting material. After the reaction was completed, the reaction mixture was diluted with 50 mL of ethyl acetate. The organic phase was washed with saturated aqueous sodium bicarbonate solution, dried over sodium sulfate and concentrated to give a semisolid. This material was suspended in 100-200 mL of hexane/ethyl acetate (9:1), stirred, and filtered to remove triphenylphosphine oxide. Evaporation of the filtrate under reduced pressure yielded oil that was purified by Flash column (hexane/ethyl acetate 6.5:3.5) to give oil that solidified on standing (0.23g, 70%).

^{1}H NMR (chloroform-D3, 300MHz) δ (ppm) 7.97(d, J=8.7Hz, 2H), 6.9 (d, J=8.7Hz, 2H), 4.55(m, 1H), 3.88(s,3H), 3.68(m,2H), 3.36(m,2H), 1.92(m,2H), 1.77(m,2H), 1.46(s,9H)

EI+335

di-tert-butyl 4,4'-((5-(methoxycarbonyl)-1,3-phenylene)bis(oxy))bis(piperidine-1-carboxylate) (25c)

^{1}H NMR (methanol-d4, 300 MHz) δ (ppm) 7.16(s, 2H), 6.78(s, 1H), 4.59(s, 2H), 4.09(q, J= 7.35Hz, 2H), 3.88(s, 3H), 3.69(s, 3H), 3.36(s, 3H), 1.92(s, 2H), 1.66(s, 2H), 1.46(s, 18H) ES+535

Step 3: Synthesis of 4-((1-(tert-butoxycarbonyl)piperidin-4-yl)oxy)benzoic acid (26a)

^{1}H NMR (chloroform-D3, 500MHz) δ (ppm) 8.03 (d, J=8.73Hz, 2H), 6.93(d, J=9.0Hz, 2H), 5.58(m,1H), 3.69(m, 2H), 3.73(m,2H), 1.93(m,2H), 1.85(m,2H), 1.47(s,9H)

EI+321

4-((1-(tert-butoxycarbonyl)piperidin-4-yl)oxy)benzoic acid (26b)

^{1}H NMR (chloroform-D3, 300MHz) δ (ppm) 7.71 (d, J=8.4Hz, 1H). 7.6(s, 1H), 6.93 (d, J=8.49Hz, 1H), 4.56(m,1H), 3.78(m,2H), 3.292(m,2H), 1.95(m,2H), 1.81(m,2H), 1.46(s,9H)

EI+365

^{13}C NMR (chloroform-D3, 400MHz) δ (ppm) 171.22, 154.84, 151.48, 150.06, 124.21, 122.28,114.45, 113.37, 79.77, 73.90, 56.09, 28.45

EI+351

3,5-bis((1-(tert-butoxycarbonyl)piperidin-4-yl)oxy)benzoic acid (26c)

1H NMR (methanol-d4, 300 MHz) δ (ppm) 7.16(s, 2H), 6.65(s, 1H), 4.63-4.51(m, 2H), 4.09(d, J=12.3Hz, 1H), 3.77-3.65(m, 4H), 3.39-3.32(m, 3H), 2.79(s, 1H), 1.91(s, 3H), 1.73-1.57(m, 4H), 1.46(s, 18H) ES+521

Synthesis of 4-((4-(tert-butoxycarbonyl)piperazin-1-yl)methyl)-3-hydroxybenzoic acid[23](27a)[79]

To a solution of 4-Formyl-3-hydroxy benzoic (0.16g, 1mmol) and 1-Boc-Piperazine (0.18g, 1mmol) in 25ml of dichloromethane was added sodium triacetoxy borohydrate (0.21g, 1.4mmol). The reaction mixture was stirred overnight at RT and the reaction was monitored by TLC (ethylacetate:hexanes-35:65). After the reaction was completed the reaction mixture was quenched with 2N sodium hydroxide and the reaction mixture was stirred for 10mins. The reaction mixture was diluted with dichloromethane and 2N sodium hydroxide. The layers were separated; the aqueous layer was acidified to pH4 to precipitate the product. The product was filtered off to get a white solid (0.33g, 80.2%).

^{1}H NMR (chloroform-D3, 300MHz) δ (ppm) 7.69 (d, J=7.17Hz, 1H), 7,64(s,1H), 7.31(d, J=7.74Hz, 1H), 4.34(s,2H), 4.25(d, J=15.33, 2H), 3.67(d, J=10.95Hz), 3.43(m,2H), 2.98(m,2H), 1.48(s,9H)

ES+ 337

tert-butyl 4-(2-ethoxy-4-(ethoxycarbonyl)benzyl)piperazine-1-carboxylate (28a)

^{1}H NMR (chloroform-D3, 300MHz) δ (ppm) 7.61(d, J=7.47Hz, 1H), 7.5 (s,1H), 7.45(d, J=8.13Hz, 1H), 4.36(q, J=6.27, 2H), 4.09(q, J=7.68Hz, 2H), 3.63(s,2H), 3.45(s,3H), 2.65(s,2H), 2.46(s, 3H), 1.44(s,9H), 1.42-1.35(m,6H)

EI+392

tert-butyl 4-(2-propoxy-4-(propoxycarbonyl)benzyl)piperazine-1-carboxylate (28b)

^{1}H NMR (chloroform-D3, 300MHz) δ (ppm) 7.63(d, J=5.31Hz, 1H), 7.52(s,2H), 4.27(t, J=5.91Hz, 2H), 4.0(t, J=6.87Hz, 2H), 3.75(s, 4H), 3.52(s, 4H), 2.55(s,4H), 1.87-1.75(m, 4H), 1.44(s,9H), 1.04(q, J=7.74Hz, 6H)

EI+420

4-((4-(tert-butoxycarbonyl)piperazin-1-yl)methyl)-3-ethoxybenzoic acid (29a)

^{1}H NMR (Dimethyl sulphoxide- D6, 300MHz) δ (ppm) 7.67(s, 2H), 7.62(s, 1H), 4.4(s, 2H), 4.22(q, J=6.39Hz), 4.07(s,2H), 3.41(s,2H), 3.16(s,4H), 1.46(s,9H), 1.30-1.22(m,3H), EI+365

4-((4-(tert-butoxycarbonyl)piperazin-1-yl)methyl)-3-propoxybenzoic acid (29b)

^{1}H NMR (chloroform-D3, 300MHz) δ (ppm) 7.57(s, 2H), 7.53(s,1H), 4.01(t, J=6.69Hz, 2H), 3.89(s,2H), 3.65(s,4H), 2.81(s,4H), 1.84(q, J=8.01Hz, 2H), 1.44(s, 9H), 1.05(t, J=7.32Hz, 3H),

ES+379

Synthesis of 4-((4-(1-methylpiperidin-4-yl)piperazin-1-yl)methyl)benzoic acid/(R) and (S)-4-((4-(tert-butoxycarbonyl)-2-methylpiperazin-1-yl)methyl)benzoic acid

Step 1: Synthesis of benzyl 4-formylbenzoate[76] (30)

To a sample of 4-Formyl benzoic acid (0.75g, 5mmol) dry dimethyl formamide (15 mL) was slowly added with stirring 60 wt % NaH in mineral oil (0.14g, 6mmol). The reaction solution was stirred for 45 min, benzyl bromide (0.10g, 6 mmol) was added dropwise, and the reaction solution was stirred for an additional 5 h and monitored by TLC (ethylacetate:hexanes-35:65 with few drops of acetic acid). After the completion of the reaction, and the reaction solution was poured into 1N HCl (27mL) and extracted with ethyl acetate. The combined organic extracts were washed with saturated sodium bicarbonate and brine, dried over sodium sulfate, and concentrated to get a crude a yellow oil which was purified by flash chromatography (Biotage SP4) using a SNAP 100g column with a gradient run starting from 6% ethylacetate: 94% hexanes to 35% ethyl acetate and 65% hexanes over 15 column volumes to yield a white solid (0.62g, 51.6%).

^{1}H NMR (chloroform-D3, 300MHz) δ (ppm) 10.1(2,1H), 8.23(d, J=8.04Hz), 2H), 9.95(d, J=7.922Hz, 2H), 7.47-7.311(m, 5H), 5.39(s,2H)

EI+240

Step 2: Synthesis of benzyl 4-((4-(1-methylpiperidin-4-yl)piperazin-1-yl)methyl)benzoate (31c)[79]

To a solution of benzyl 4-Formyl benzoate (0.24g, 1mmol) and 1-(1-methylpiperidin-4-yl)piperazine (0.18g, 1mmol) in 25ml of dichloromethane was added sodium triacetoxy borohydrate (0.21g, 1.4mmol). The reaction mixture was stirred overnight at RT and the reaction was monitored by TLC (ethylacetate:hexanes-35:65).

After the reaction was completed the reaction mixture was quenched with 2N sodium hydroxide and the reaction mixture was stirred for 10mins. The reaction mixture was diluted with dichloromethane and 2N sodium hydroxide. The layers were separated; the organic layer was evaporated to get the crude product. The crude material was then purified by flash chromatography (Biotage SP4) using a SNAP 25g column with a gradient run starting from 6% ethylacetate: 94% hexanes to 25% ethyl acetate and 75% hexanes over 10 column volumes to yield a white solid (0.34g, 85.3%).

^{1}H NMR (chloroform-D3, 300MHz) δ (ppm) 8.01(d, J=7.80Hz, 2H), 7.45-7.33(m, 7H), 5.35(s,2H), 3.53(s,2H), 2.89(s,3H), 2.57(s,3H), 2.47(s,3H), 2.24(s,3H), 1.91(t, J=10.98Hz, 2H), 1.78(d, J=12.78, 2H), 1.64-1.50(m, 4H)

ES+408

(R)-tert-butyl 4-(4-((benzyloxy)carbonyl)benzyl)-3-methylpiperazine-1-carboxylate (31a)

^{1}H NMR (chloroform-D3, 300MHz) δ (ppm) 8.02(d, J=7.77Hz, 2H), 7.48-7.29(m, 7H), 5.35(s,2H), 4.01(d, J=14.28Hz,1H), 3.74(s, 1H), 3.62(d, 15.09Hz, 1H), 3.24(d, J=12.95Hz, 1H), 3.07(t, J=11.10Hz, 1H), 2.87(s,1H), 2.59(d, 12.72Hz, 1H), 2.43(s, 1H), 2.09(d, J=12.7Hz, 1H), 1.44(s,9H), 1.10(d, J=6.3Hz, 3H)

ES+425

(S)-tert-butyl 4-(4-((benzyloxy)carbonyl)benzyl)-3-methylpiperazine-1-carboxylate (31b)

^{1}H NMR (chloroform-D3, 300MHz) δ (ppm) 8.07-8.00(m, 2H), 7.45-7.33(m, 7H), 5.35(s,2H), 3.99(d, J=13.53Hz, 1H), 3.61(d, J=13.53Hz, 1H), 3.23(d, J=13.53Hz, 1H), 3.07(d, J=12.78Hz, 1H), 2.92(d, J=8.25Hz, 1H), 2.75(d, J=9.03Hz, 1H), 2.59(d, J=12.03Hz, 1H), 2.49-2.30(m,1H), 1.76(s,1H), 1.44(s,9H), 1.09(d, 6.09Hz, 3H)

ES+425

Step 3a: Synthesis of Synthesis of 4-((4-(1-methylpiperidin-4-yl)piperazin-1-yl)methyl)benzoic acid (32)[80]

The product obtained from step 1 (0.24g, 0.5mmol) was treated with Palladium over activated carbon (24mg, 10%) in the presence of methanol. The reaction mixture was stirred while hydrogen gas was passed from a balloon. The reaction was continued for 12 hours and monitored by TLC (ethylacetate:hexanes-35:65). After the reaction was completed, methanol was evaporated and the reaction mixture was dissolved in water. The palladium catalyst was filtered off using 0.45u filter. The aqueous layer was evaporated to get the desired product as white solid (0.15g, 99%).

^{1}H NMR (methanol-d4, 400 MHz) δ (ppm) 8.18(s,2H), 7.72(s,2H), 3.97(s,2H), 3.76(s,2H), 2.23(t, J=13.68Hz, 2H), 3.09(s,3H), 2.98(d, J=19..3Hz, 9H), 2.45(d, J=16.01Hz, 2H, 2.08-1.92(m, 2H)

^{13}C NMR (methanol-d4, 400 MHz) δ (ppm) 130.18, 129.0, 61.75, 58.74, 53.94, 52.06, 48.20, 43.21, 25.89

ES+318

Step 3b: Synthesis of (R)-4-((4-(tert-butoxycarbonyl)-2-methylpiperazin-1-yl)methyl)benzoic (33 a)[76]

The SM (0.44g, 1.1mmol), 4ml of 1N NaOH, 3ml of water and 3ml of alcohol were refluxed at 100°C for 2 hours. The reaction was monitored by TLC (ethylacetate:hexanes-35:65). After the completion of reaction, the aqueous solution was evaporated completely. The residue was dissolved in methanol, white solid that was not soluble in methanol was filtered off. The methanol was evaporated to get a reddish brown solid (0.27g, 73.5%).

(R)-4-((4-(tert-butoxycarbonyl)-2-methylpiperazin-1-yl)methyl)benzoic acid (33a)

^{1}H NMR (methanol-d4, 400 MHz) δ (ppm) 7.61(d, J=8.32Hz, 2H), 7.13(d, J=7.52Hz, 2H) 3.92(d, J=17.6Hz, 2H), 3.25-3.12(m, 4H), 3.10-2.98(m, 1H), 2.94-2.80(m, 2H), 1.29(s, 9H), 1.14(d, J=6.44Hz, 3H)

^{13}C NMR (dimethylsulfoxide-D6, 500MHz) δ (ppm) 170.84, 168.96, 142.41, 134.18, 129.56, 79.7, 60.24, 57.48, 54.74, 28.51,

ES+335

(S)-4-((4-(tert-butoxycarbonyl)-2-methylpiperazin-1-yl)methyl)benzoic acid (33b)

^{1}H NMR (chloroform-D3, 300MHz) δ (ppm) 7.96(d, J=8.04Hz, 2H), 7.43(d, J=8.04Hz, 2H), 4.077(d, J=13.5Hz, 2H), 3.80-3.53(m,2H), 3.12(t, J=22.74Hz, 2H), 2.9(s, 1H), 2.73-2.62(m, 1H), 2.50(s,1H), 2.15(t, J=10.11Hz, 1H), 1.44(s,9H), 1.16(d, J=6.57, 3H)

^{13}C NMR (dimethylsulfoxide-D6, 500MHz) δ (ppm) 172.78, 169.26, 154.23, 142.99, 141.21, 136.43, 129.47, 128.48, 128.38, 127.06, 126.87, 79.14, 63.33, 57.54, 54.70, 28.67

ES+335

Synthesis of 4-(((1-(tert-butoxycarbonyl)piperidin-4-yl)(methyl)amino)methyl)benzoic acid (16a) and 4-((((tert-butoxycarbonyl)(1-(tert-butoxycarbonyl)piperidin-4-yl)amino)methyl)benzoic acid (37)

Step1: tert-butyl 4-((4-(methoxycarbonyl)benzyl)(methyl)amino)piperidine-1-carboxylate (34a)

^{1}H NMR (chloroform-D3, 300MHz) δ (ppm) 7.98(d, J=8.19Hz, 2H), 7.39(d, J=7.92Hz, 2H), 4.16(s,2H), 3.9(s,3H), 3.67(s,2H), 2.71-2.56(m,3H), 2.21(s,3H), 1,81(d, J=12.39Hz, 2H), 1.56-1.50(m,2H), 1.44(s,9H) ES+363

tert-butyl 4-((4-(methoxycarbonyl)benzyl)amino)piperidine-1-carboxylate (34c)

^{1}H NMR (methanol-d4, 300 MHz) δ (ppm) 7.99(d, J=7.86Hz, 2H), 7.40(d, J=8.43Hz, 2H), 4.03(s,2H), 3.90(s,5H), 3.59(s,2H), 2.80(s,1H), 2.03(s,1H), 1.86(d, J=12.15Hz, 2H), 1.44s, 9H) ES+349

Step 2: Synthesis of 4-(((1-(tert-butoxycarbonyl)piperidin-4-yl)(methyl)amino)methyl)benzoic acid (35a)[76]

The SM (0.24g, 0.648 mmol), 4ml of 1N NaOH, 3ml of water and 3ml of alcohol were refluxed at 100°C for 2 hours. The reaction was monitored by TLC (ethylacetate:hexanes-35:65). After the completion of reaction, the aqueous solution was evaporated completely to get a white solid (0.1g, 80%). The crude mixture was purified by semi-prep HPLC[22].

^{1}H NMR (methanol-d4, 300 MHz) δ (ppm) 7.99(d, J=7.68Hz, 2H), 7.47(d, J=8.19Hz, 2H), 4.22(d, J=13.34Hz, 2H), 4.08(s, 2H), 3.13(t, J=10.68Hz, 1H), 2.78(t, J=14.01, 2H), 2.50(s, 3H), 2.02(d, J=14.01Hz, 2H), 1.63(q, J=12.0Hz, 2H), 1.45(s, 9H) ES+349

Step 2a: Synthesis of tert-butyl 4-((tert-butoxycarbonyl)(4-(methoxycarbonyl)benzyl)amino)piperidine-1-carboxylate (36)[77]

The starting material (0.34g, 1.16mmol), and potassium carbonate (0.13g, 1.16mmol) were dissolved in water and methanol to get a clear solution. The reaction mixture was stirred in an ice bath. The di-tert-butyl dicarbonate (0.50g, 2.32mmol) was dissolved in THF and added drop wise into the reaction mixture. The reaction mixture was allowed to come to room temperature and then it was stirred overnight. The consumption of the starting material was monitored by TLC (100% Ethylacetate). After the reaction was completed, the solvents were evaporated and the crude mixture was

separated by flash chromatography using a gradient of 12-100% Ethylacetate in 5 column volumes. The product was obtained as a white solid (0.4g, 77%) [20].

^{1}H NMR (methanol-d4, 300 MHz) δ (ppm) 7.97(d, J=7.92Hz, 2H), 7.35(d, J=8.67Hz, 2H) 4.47(s, 2H), 4.09(d, J=11.85Hz, 2H), 3.34(s,3H), 2.74(s,2H), 1.61(s,4H), 1.41(s, 18H) ES+449

Step 3: Synthesis of 4-((((tert-butoxycarbonyl)(1-(tert-butoxycarbonyl)piperidin-4-yl)amino)methyl)benzoic acid (37)[76]

The SM (0.44g, 1mmol), 3ml of 1N NaOH, 3ml of water and 3ml of alcohol were refluxed at 100°C for 2 hours. The reaction was monitored by TLC (ethylacetate:hexanes-35:65). After the completion of reaction, the organic solvents were evaporated completely. The aqueous layer was neutralized to pH 7.0 with 1N NaOH to get a white solid which was filtered off (0.3g, 69.0%).

^{1}H NMR (methanol-d4, 300 MHz) δ (ppm) 7.95(d, J=7.80Hz, 2H), 7.31(d, J=7.29Hz, 2H), 4.47(s,2H), 4.09(d, J=13.89Hz, 2H), 2.72(s,2H), 1.61(s,5H), 1.42(18H) ES+435

Synthesis of (S)-4-((4-(tert-butoxycarbonyl)-2-methylpiperazin-1-yl)methyl)-3-hydroxybenzoic acid (38a-c, 39a-b)[79]

To a solution of 4-Formyl-3-hydroxy benzoic (0.16g, 1mmol) and (S)-tert-butyl 2-methylpiperazine-1-carboxylate (0.45g, 2mmol) in 25ml of dichloromethane was added sodium triacetoxy borohydrate (0.59g, 2.8mmol). The reaction mixture was stirred for 2 days at RT and the reaction was monitored by TLC (ethylacetate:hexanes-35:65). After the reaction was completed the reaction mixture was quenched with water and the reaction mixture was stirred for 10mins. The layers were separated; the aqueous layer was evaporated to get the crude product which was purified by flash chromatography.

¹H NMR (methanol-d4, 300 MHz) δ (ppm) 7.45(d, J=7.83Hz, 1H), 7.38(s,1H), 7.17(d, 8.52, 1H), 4.27(d, J=14.07Hz, 1H), 3.75-3.60(m,3H), 3.52(s,1H), 3.09(s,1H), 2.85(d, J=12.39Hz, 1H), 1.45(s,9H), 1.21(d, J=6.03Hz, 3H) ES+351

3-hydroxy-4-((4-methylpiperazin-1-yl)methyl)benzoic acid (38b)

¹H NMR (methanol-d4, 300 MHz) δ (ppm) 7.42(d, J=8.01Hz, 1H), 7.38(s,1H), 7.16(d, J=7.89Hz, 1H), 3.80(s, 2H) 2.79(d, J=25.89Hz, 8H), 2.51(s, 3H) ES+251

3-hydroxy-4-((4-(1-methylpiperidin-4-yl)piperazin-1-yl)methyl)benzoic acid (38c)

¹H NMR (methanol-d4, 300 MHz) δ (ppm) 7.44(d, J=8.13Hz, 1H), 7.41(s, 1H), 7.34(d, J=8.13Hz, 1H, 4.32(s,2H), 3.52(d, J=12.0, 2H), 3.42(s, 4H), 3.27(s, 4H), 2.95(t, J=12.45, 2H), 2.73(s, 3H), 2.24(d, J=12.87Hz, 2H), 1.75(q, J=20.97Hz, 2H) ES+334

4-((4-ethylpiperazin-1-yl)methyl)benzoic acid (39a)

¹H NMR (methanol-d4, 300 MHz) δ (ppm) 7.91(d, J=6.78Hz, 2H), 7.35(d, J=7.08Hz, 2H), 3.65(s, 2H), 3.02(s, 3H), 2.92(q, J=5.10, 3H), 2.68(s, 4H), 1.24(t, J=6.87, 3H), ES+248.33

4-((4-propylpiperazin-1-yl)methyl)benzoic acid (39b)

¹H NMR (chloroform-D3, 300 MHz) δ (ppm) 7.86(d, J=7.47, 2H), 7.21(d, J=8.04Hz, 2H), 3.77(s, 2H), 2.91(s, 3H), 2.71(s, 4H), 2.60(m, 3H), 1.68(m, 2H), 0.90(t, J=6.75Hz, 3H) ES+262.35

Synthesis of (S)-tert-butyl 4-(4-(methoxycarbonyl)benzyl)-3-methylpiperazine-1-carboxylate

Step 1: Synthesis of (S)-tert-butyl 4-(4-(methoxycarbonyl)benzyl)-3-methylpiperazine-1-carboxylate (40)[79]

To a solution of 4-Formyl methylbenzoate (0.16g, 1mmol) and (S)-tert-butyl 3-methylpiperazine-1-carboxylate (0.20g, 1mmol) in 25ml of dichloromethane was added sodium triacetoxy borohydrate (0.21g, 1.4mmol). The reaction mixture was stirred overnight at RT and the reaction was monitored by TLC (ethylacetate:hexanes-35:65). After the reaction was completed the reaction mixture was quenched with 2N sodium hydroxide and the reaction mixture was stirred for 10mins. The reaction mixture was diluted with dichloromethane and 2N sodium hydroxide. The layers were separated; the organic layer was evaporated to get the crude product. The crude material was then purified by flash chromatography (Biotage SP4) using a SNAP 25g column with a gradient run starting from 6% ethylacetate: 94% hexanes to 25% ethyl acetate and 75% hexanes over 10 column volumes to yield a white solid (0.34g, 85.3%).

Step 2: Synthesis of (S)-methyl 4-((2-methylpiperazin-1-yl)methyl)benzoate (41)[56]

The product from step 1 (S)-tert-butyl 4-(4-(methoxycarbonyl)benzyl)-3-methylpiperazine-1-carboxylate (0.35g, 1mM) was stirred with 20% trifluoroacetic acid in 5ml of dichloromethane for 2hrs. The reaction was monitored by TLC (ethylacetate:hexanes-35:65). After the reaction was completed the reaction mixture was evaporated and the concentrated crude material was purified by flash chromatography (Biotage SP4) using a RP SNAP 10g column with a gradient run starting from 0%

Acetonitrile : 60% water over 10 column volumes to yield a reddish semi solid (0.22g, 90%).

^{1}H NMR (chloroform-D3, 300MHz) δ (ppm) 8.50(d, J=7.92Hz, 2H), 7.90(d, J=7.17Hz, 2H), 4.41(s,3H) 3.74(q, J=12.51Hz, 2H), 3.58(t, J=11.74Hz, 3H), 3.43(m,2H), 3.319m, 1H), 3.04(t, J=11.79Hz, 1H), 1.75(s, 3H) ES+248.15

Step 3: (S)-methyl 4-((4-ethyl-2-methylpiperazin-1-yl)methyl)benzoate (42a)[79]

To a solution of (S)-methyl 4-((2-methylpiperazin-1-yl)methyl)benzoate (0.24g, 1mmol) and acetaldehyde (0.44g, 10mmol) in 25ml of dichloromethane was added sodium triacetoxy borohydrate (0.21g, 1.4mmol). The reaction mixture was stirred overnight at RT and the reaction was monitored by TLC (ethylacetate:hexanes-35:65). After the reaction was completed the reaction mixture was quenched with 2N sodium hydroxide and the reaction mixture was stirred for 10mins. The reaction mixture was diluted with dichloromethane and 2N sodium hydroxide. The layers were separated; the organic layer was evaporated to get the crude product. The crude material was then purified by flash chromatography (Biotage SP4) using a RP SNAP 10g column with a gradient run starting from 0% acetonitrile: 25% water, to 25% acetonitrile:75% water for 3 column volumes, the gradient was held at 25% acetonitrile:75% water for 5 column volumes and then proceeded till 100% acetonitrile over 4column volumes to yield a white semi solid (0.16g, 60%).

^{1}H NMR (chloroform-D3, 300MHz) δ (ppm) 7.92(d, J=7.17Hz, 2H), 7.30(d, J=7.65Hz, 2H), 3.84(s, 3H), 3.33(d, J=12.48Hz, 2H), 3.13(m,2H), 2.96(q, J=5.25Hz, 2H), 2.86(s, 1H), 2.68(m,2H), 2.50(m,2H), 1.26(t, J=7.41Hz, 3H), 1.16(d, J=5.94Hz, 3H) ES+276.18

(S)-methyl 4-((4-propyl-2-methylpiperazin-1-yl)methyl)benzoate (42b)

^{1}H NMR (chloroform-D3, 300MHz) δ (ppm) 7.98 (d, J=7.74Hz, 2H), 7.37(d, J=7.98Hz, 2H), 3.91(s,3H), 3.31(d, J=10.59Hz, 2H), 3.17(d, J=13.89Hz, 1H), 2.88(m,1H), 2.76(m,3H), 2.52(m,4H), 1.72(m, 2H), 1.20(d, J=7.26, 3H), 0.96(t, J=8.82, 3H) ES+290.41

Synthesis of (S)-4-((4-ethyl-2-methylpiperazin-1-yl)methyl)benzoic acid (43a)[76]

Step 4: (S)-methyl 4-((4-ethyl-2-methylpiperazin-1-yl)methyl)benzoate (0.27g, 1mmol), 4ml of 1N NaOH, 3ml of water and 3ml of alcohol were refluxed at 100°C for 2 hours. The reaction was monitored by TLC (ethylacetate:hexanes-35:65). After the completion of reaction, the aqueous solution was evaporated completely. The residue was purified flash chromatography (Biotage SP4) using a RP SNAP 10g column with a gradient run starting from 0% acetonitrile: 25% water over 10 column volumes, the gradient was held at 25% acetonitrile:75% water for 3column volumes and then proceeded till 60% acetonitrile over 4column volumes to yield a white solid (0.17g, 65%)

^{1}H NMR (chloroform-D3, 300MHz) δ (ppm) 7.89(d, J=7.50Hz, 2H), 7.32(d, J=7.08Hz, 2H), 2.89(m,2H), 2.75(m,2H), 2.52(m,4H), 2.23(m,2H), 2.08(m,1H), 1.21(d, J=7.20Hz, 3H), 1.11(t, J=7.20Hz, 3H) ES+262.17

(S)-4-((2-methyl-4-propylpiperazin-1-yl)methyl)benzoic acid (43b)

^{1}H NMR (chloroform-D3, 300MHz) δ (ppm) 8.00(d, J=7.86Hz, 2H), 7.40(d, J=8.22Hz, 2H), 3.92(s,2H), 3.44(s, 1H), 3.22(m,2H), 2.91(m,3H), 2.78(m, 3H), 1.77(m,2H), 1.29(d, J=6.81Hz, 3H), 0.97(t, J=7.23Hz, 3H) ES+276.38

Synthesis of 4-((1-substituted piperidin-4-ylidene)methyl)benzoic acid[82]

Step 1: Synthesis of methyl 4-((diethoxyphosphoryl)methyl)benzoate (44)

A mixture of methyl 4-(bromomethyl)benzoate (1.39 g, 5mmol) and triethyl phosphite (1.08g, 5.5 mmol) were stirred at 150°C for 24 h in an oil bath. The mixture was purified by reverse phase flash chromatography with a gradient of 100% water, 0% acetonitrile for 3 column volumes, the gradient was slowly changed to 40% water in 2 column volumes and held at 40% water for 2 column volumes. Then the gradient was slowly chaged to 0% water, 100% acetonitrile in 3 column volumes. The product was obtained as a colorless oil (yield-1.11 g, 78%).

^{1}H NMR (chloroform-D3, 300MHz) δ (ppm) 7.96(d, J=8.22Hz, 2H), 7.34(d, J=7.98Hz, 2H), 3.99 (t, J=7.14Hz, 2H), 3.88(s,3H), 3.21(s,1H), 3.14(s,1H), 1.21(t, J=6.42Hz, 6H) ES+286.28

Step 2: methyl 4-((1-methylpiperidin-4-ylidene)methyl)benzoate (45a) [82]

The product 25 (0.29g, 1 mmol) step 1obtained from step 1 is stirred with THF (1.7 ml) in an ice bath. To this 15-crown-5 (0.018 g, 0.08 mmol) and NaH (60% in oil, 0.04g) was added and stirred for 30 mins at 0°C. a solution of 1-methylpiperidin-4-one (0.09 g, 0.83 mmol) dissolved in about 1ml of THF was added drop by drop to ice cold stirring mixture for about 20 mins while maintaining the temperature of the mixture at 0°C. After the addition of 1-methylpiperidin-4-one, the reaction was stirred at room temperature. Reaction was monitored with TLC (50% Ethylacetate: 50% Hexanes) for completion. After the reaction is complete the reaction mixture was poured in ice water and further partitioned with ethylacetate. Ethylacetate layer was collected and washed with saturated sodium bicarbonate followed by brine and finally dried over magnesium sulfate. The

crude product was purified in purified by flash chromatography (Biotage SP4) using a SNAP 100g column with a gradient 0% to 40% ethylacetate for 5 column volumes, the concentration of ethyl acetate at 40% was kept constant for 2 column volumes and then increased to 100% in 5 column volume. The purified product was obtained as white powder (yield- 0.23g, 94%).

^{1}H NMR (chloroform-D3, 300MHz) δ (ppm) 7.97(d, J=7.83Hz, 2H), 7.26(d, J=2.978Hz, 2H), 6.30(s, 1H) 3.90(s,3H), 3.21(s,1H), 2.51(m,4H), 2.40(m,4H), 2.29(s, 3H)

ES+245.14

tert-butyl 4-(4-(methoxycarbonyl)benzylidene)piperidine-1-carboxylate (45b)

^{1}H NMR (chloroform-D3, 300MHz) δ (ppm) 7.98(d, J=7.92Hz, 2H), 7.24(d, J=6.60Hz, 2H), 6.36(s, 1H) 3.90(s,3H), 3.51 (t, J=5.97Hz, 2H), 3.40 (J=5.43, 2H), 2.45(t, J=5.40Hz, 2H), 2.35(t, J=2.28Hz, 2H), 1.47(s, 9H)

ES+331.41

4-((1-methylpiperidin-4-ylidene)methyl)benzoic acid (46a)

^{1}H NMR (D$_2$O, 300MHz) δ (ppm) 7.95(d, J=7.53Hz, 2H), 7.27(d, J=7.53Hz, 2H), 6.57(s,1H), 3.30(s,2H), 3.20(s,1H), 2.85(s,3H), 2.78(t, J=5.55Hz, 2H), 2.70(t, J=5.58Hz, 2H) ES+231.29

4-((1-(tert-butoxycarbonyl)piperidin-4-ylidene)methyl)benzoic acid (46b)

^{1}H NMR (chloroform-D3, 300MHz) δ (ppm) 8.54(d, J=7.86Hz, 2H), 7.77(d, J=7.328Hz, 2H), 6.87(s, 1H), 4.01(t, J=6.21Hz, 2H) 3.91(t, J=6.66Hz, 2H), 2.96(t, J=2.88Hz, 2H), 2.85(t, J=6.18Hz, 2H), 1.96 (s, 9H) ES+331.41

tert-butyl 4-(4-(methoxycarbonyl)benzyl)piperidine-1-carboxylate (47) [82]

The product 26b (0.31 g, 1 mmol) was dissolved in MeOH/THF (1:1, 3 mL) and hydrogenated at 780 psi over 10% Pd/C(water 50%, 0.02 g) at 70°C for 18 h. The reaction mixture was filtered to remove Pd/C and concentrated in rotatory evaporator and dried. The residue was purified by flash chromatography (Biotage SP4) using a SNAP 100g column with a gradient 0% to 60% ethylacetate for 5 column volumes, the concentration of ethyl acetate at 60% was kept constant for 2 column volumes and then increased to 100% in 5 column volume. The purified was product obtained as white powder (yield- 0.32g, 98%)

^{1}H NMR (chloroform-D3, 300MHz) δ (ppm) 7.88(d, J=8.16Hz, 2H), 7.13(d, J=8.13Hz, 2H), 4.02(m, 2H), 3.83(s,3H), 2.52(m, 4H), 1.52(s,4H), 1.37(s, 9H), 1.10 (m,2H) ES+233.31

4-((1-(tert-butoxycarbonyl)piperidin-4-yl)methyl)benzoic acid (48)

^{1}H NMR (chloroform-D3, 300MHz) δ (ppm) 8.36(d, J=8.07Hz, 2H), 7.58(d, J=9.18Hz, 2H), 4.42(d, J=14.58Hz, 2H) 2.96(m, 4H), 1.94(d, J=13.86Hz, 2H), 1.79 (s, 9H) ES+319.40

5.4.2 Fluorescence Polarization Binding Assay

CDK4D1 FP assay: This assay was performed using black 384-well plates using a previously described procedure[55] with the following modifications. To each well were added: 5 µl CDK4D1 (0.3 µg/well purified recombinant human kinase complex from Invitrogen), 5 µl compound solution, 5 µl 30 nM fluoresceinyl-Ahx-Pro-Val-Lys-Arg-Arg-Leu-(3ClPhe)-Gly tracer peptide. Compounds and kinase complexes were diluted using assay buffer (25 nM HEPES pH 7, 10 nM NaCl, 0.01% Nonidet P-40, 1mM

dithiothretiol (DTT). Plate was centrifuged for 1 min at 500 rpm and then incubated with shaking for 45 min at room temperature. Fluorescence polarization was read on DTX880 multimode detector (Beckman Coulter, Brea, CA) fitted with 485 nm/535 nm excitation/emission filters and a dichroic mirror suitable for fluorescein. Relative mp was calculated for each concentration tested using the equation showing below. IC$_{50}$ values were determined by logarithmic regression by correlating relative mp and testing concentrations.

$$\text{Relative mp} = \frac{\text{mP(compound)-mP(DMSO, protein, tracer)}}{\text{mP(DMSO, protein)-mP(DMSO, protein, tracer)}}$$

CDK2A2 FP assay This assay was performed using black 384-well plates. To each well were added: 5 µl CDK2A2 (0.3 µg/well purified recombinant human kinase complex), 5 µl compound solution, 5 µl 30 nM fluoresceinyl-Ahx-Pro-Val-Lys-Arg-Arg-Leu-Phe-Gly tracer peptide. Compounds and kinase complexes were diluted using assay buffer (25 nM HEPES pH 7, 10 nM NaCl, 0.01% Nonidet P-40, 1mM dithiothretiol (DTT). Plate was centrifuged for 1 min at 500 rpm and then incubated with shaking for 45 mins at room temperature. Fluorescence polarization was read on DTX880 multimode detector (Beckman Coulter, Brea, CA) fitted with 485 nm/535 nm excitation/emission filters and a dichroic mirror suitable for fluorescein. Relative mp was calculated for each concentration tested using the equation showing below. IC$_{50}$ values were determined by logarithmic regression by correlating relative mps and testing concentrations.

5.4.3 Docking[55]

All the N-capping groups were docked in the cyclin A/CDK2 crystal structure (PDB ID 2UUE) using 1-(3,5- dichlorophenyl)-5-methyl-1H-1,2,4-triazole-3-carbaldehyde as control ligand. The parameters of the LigandFit (Discovery Studio 3.0,

Accelrys) were PLP1 energy grid, minimization sphere "on", number of poses 10. All the docked poses analyzed with PLP1 scoring function, hydrogen bonding and were subjected to visual analysis for complementarity with second pocket.

5.4.4 Cell culture[79]

U2OS osteosarcoma cells and DU145 human prostate cancer cells were obtained from ATCC (Manassas, VA). All cells were grown in Dulbecco's modified Eagle's medium (DMEM , Fisher Scientific) supplemented with 10% Fetal Bovine Serum (FBS, USA Scientific) and 100µg/ml of Streptomycin (strep)/ 100 U/ml of Penicillin (pen). Cells were incubated at 37ºC with 5% CO_2.

5.4.5 Viability assay

Cells were seeded in 96-well plates at (2×10^3 cells/ml) and allowed to adhere overnight in DMEM growth media containing 10% NU serum and 1% Pen/Strep. The compounds **5965**, **5966, 5967, 5968** and **5970** were dissolved in DMSO and added in a dose dependent manner (1 µM to 100 µM). The diluted compounds were added to the cells in triplicate and incubated for 72 hours at 37ºC with 5% CO_2. The cell viability was determined using MTT (3-(4,5-Dimethylthiazol-2YI)-2,5-Diphenyl tetrazolium Bromide) assay[4]. Absorbance readings were obtained using a DTX880 multimode detector fitted with 595nm filter. Cell viability results were represented as the ratio of the absorbance reading in treated vs. untreated cells. IC_{50} values were obtained using a nonlinear regression line with 5.0 Graghpad Prism. Experiments performed in triplicates.

CHAPTER 6

OUTLOOK FOR THE FUTUTRE DVELOPMENT OF NON-ATP COMPETITVE COMPOUNDS AS CELL CYCLE SPECIFIC CDK INHIBITORS

CDK inhibitors comprise an important class of anticancer agents. CDKs play a critical role in cell cycle and CDKs are deregulated in majority of human tumors[40]. Although there are several drugs in development in this category with interesting preclinical activity none have yet been approved by the FDA for clinical use[41]. For the most part, CDK inhibitors that have been investigated in clinical studies lack selectivity towards cell cycle CDK targets and have side effects as a result of their cross-reactivity[42]. The main goal of this project is to develop non-ATP competitive inhibitors targeting cell cycle CDKs. This is achieved by targeting CBG which is unique to cyclin A, D and E so as to avoid inhibition of transcriptional CDKs. Antagonizing protein-protein interactions at this site leads to selective inhibition of CDK2 and CDK4 that form complexes with the cyclins A, D and E which can lead to tumor specific killing of cancer cells with deregulated CDK/Cyclin/Rb/E2F1 pathways. Potent peptidic inhibitors have been identified in cell permeable forms that have significant anti-tumor activity. In this study, a novel strategy called REPLACE has been exploited to iteratively convert optimized peptidic inhibitors which in general do not make good drugs of CDK2/cyclin A as pharmaceutically appropriate compounds. Targeting protein-protein interactions (PPI) in drug discovery is highly challenging as these typically involve a large shallow contact

interface comprised ofnumerous and diffuse contacts[83]. Furthermore, peptidic compounds which inhibit PPI's that are amenable to drug discovery are problematic due to their metabolic instability, cell permeability and poor bioavailability[48]. Current strategies that have been applied for the development of PPI inhibitors include design of proteomimetics and fragment based design[84,85]. REPLACE is an iterative strategy comprised of computational prediction, synthetic organic chemistry and biological evaluation used to convert peptidic inhibitors into FLIPs and ultimately non-peptidic drug-like compounds. Using REPLACE, fragment alternatives are designed and identified to mimic the interactions of binding determinants of a peptidic inhibitor. The combination of structural analysis along with synthetic methodologies and biological evaluation results in the efficient design of molecules that interact with hot spots (sites of critical interaction) and complement the large contact surface area of the PPI binding site. REPLACE overcomes the disadvantages of conventional fragment based design since the peptide acts as an affinity and solubility scaffold. Also the iterative nature of REPLACE means that the inhibitor is gradually converted in several steps therefore minimizing the possibility of complete potency loss through conformation change. PLAs are optimized in the context of the peptide prior to further truncation. In this study REPLACE has been exploited to generate more drug-like inhibitors that selectively inhibit cell cycle CDK/cyclin complexes and possess significant anti-proliferative activity. Capped peptides have been identified as more drug-like mimics of the lead octapeptide. Key fragment alternatives discovered include N-caps based on (i) phenyl heterocyclic carboxylic acids[63], (ii) furan and thiazole carboxylic acids substituted with alkylamino

148

groups[68] and (iii) pyridine carboxylic acids modified with alkoxy or basic groups[68], (iv) phenylacetic acid derivatives[68] and (v) benzoic acid derivatives.

The first stage of the REPLACE[49] strategy was identification of fragment alternatives for key peptide determinants using high-throughput docking. LigandFit[55], a shape based docking method was employed for evaluating binding of fragments in the cyclin groove. LigandFit[55] generates poses that have high complementarity with a binding site through the use of Monte Carlo conformational search methods in conjunction with a shape based comparison filter. Use of a LigandFit protocol with the PLP1 energy grid and a minimization step to refine generated poses, was shown to reproduce known binding modes of previously determined N-capping groups. An accurate prediction of the binding affinity of the generated poses was provided by using the PLP1 scoring function which was shown to obtain the best results since it takes into account hydrogen bonding between the ligand and receptor. Specific H-bonds and ion-pairing interaction of CGI ligands with the cyclin groove have been shown to be important determinants of high affinity binding. Potential fragment alternatives for the N-terminus were synthesized or obtained from commercial sources and then used to generate FLIP molecules through coupling to an assembled peptide on a solid support[56]. The ability of FLIPs to recapitulate the affinity of the native peptide is determined in a competitive binding assay using a known cyclin groove inhibitory peptide which is fluorescently labeled[57]. This assay has an important advantage which shows the inhibition of CDK2/cyclin A and CDK4/cyclin D complexes through specific binding of FLIPs on target (CBG). After confirmation of the ability of FLIPs to bind with sufficient avidity to the CBG, the potency of the peptide-fragment hybrids can then be further refined through

149

modifications to the N-capping groups. Initial studies examined the SAR of phenyl heterocyclic carboxylic acids as N-capping groups with these being designed to retain H-bond interactions (Trp217 and Gln 254) and hydrophobic complementarity with secondary pocket[63]. Subsequent to this, additional Ncap scaffolds were pursued in order to provide charge-charge interactions with the acidic regions of CBG in addition to the H-bond and minor pocket complementarity. To achieve this furoic and picolinic acid based derivatives were exploited and found to be moderately effective[68]. Benzoic acid based N-caps easy to synthesize and were used to generate diverse SAR providing interactions with multiple subsites of CBG with the aim of improving previously developed scaffolds. Through the N-cap development and optimization critical interactions important for binding at the CBG was studied. The critical N-terminal residue Arg was replaced so as to reduce the charge of the overall compound and also to improve metabolic stability of the FLIP molecule.

After identification of more optimal Ncaps, in order to make the rest of the peptidic cyclin groove inhibitor more drug-like, REPLACEments for C-terminal motif interacting with the major hydrophibic pocket were investigated. Non-natural residues (β-Leu for Leu and Ile, NMePh/3TA for Phe) were incorporated to improve metabolic stability of the FLIPs along with retaining interactions at the primary pocket[71,72]. Along with metabolic stability, modification with a C-terminal amide functionality improved physicochemical properties such as clogP and polar surface area that contribute to drug like characteristics. After identifying a more optimal C-terminal motif, these were then combined with the most effective Ncap to generate FLIPS which should have greater metabolic stability and cell permeability. After confirming their binding activity, the

more drug like inhibitors were further tested for their anti-proliferative activity in cancer cell lines that harbor deregulated CDK/Cyclin/Rb/E2F1 pathways[52,54]. The effects on cell cycle distribution for the lead CGI compound, SCCP5964 were determined by FACS analysis and revealed that this molecule induces a G1 arrest, an observation consistent with the inhibition of cell cycle CDKs.

Overall significant progress has been achieved in further validating the REPLACE strategy in the generation of more drug-like cyclin groove inhibitors that are cell permeable and have anti-proliferative activity. These are the first reported CGI compounds that are innately drug-like and have anti-tumor activity. These compounds therefore form a novel class of CDK inhibitors with their unique capability to specifically inhibit cell cycle specific CDKs unlike clinically investigated compounds that target ATP binding pocket. The REPLACE strategy has been successfully employed in the iterative conversion of peptidic inhibitors into more drug like compounds with anti-tumor activity consistent with on target inhibition demonstrating their potential for drug development. These compounds therefore have significant potential for further development as anti-tumor therapeutics that show specificity towards cancer cells and potentially reduce the toxicities observed with ATP competitive compounds.

REFERENCES

1. http://www.cancer.gov/cancertopics/cancerlibrary/what-is-cancer

2. Rebecca, S.; Deepa, N.; Ahmedin, J. Siegel, R.; Naishadham, D.; Jermal, A.; Cancer Statistics. *CA-Cancer J*. **2012**, *62*, 10-29.

3. Are, C.; Rajaram, S.; Are, M.; Raj, H.; Anderson, B.; Swamy, C.R.; Vijayakumar, M.; Song, T,; Pandey, M.; Edney, J.A,; Cazap, E.L.; A Review of Global Cancer burden: Trends, Challenges. Strategies and a Role for Surgeons, *J. Surg. Oncol*. **2013**, *107*, 221-226.

4. http://www.cancer.org/research/cancerfactsstatistics/cancerfactsfigures2014

5. http://www.cancer.org/treatment/treatmentsandsideeffects/treatmenttypes/

6. http://www.fda.gov/Drugs/InformationOnDrugs/ApprovedDrugs/ucm279174.htm

7. DeVita, V.T.; Chu, E.; A History of Cancer Chemotherapy. *Cancer Res*. **2008**, *68*, 8643-8653.

8. Chabner, B.A.; Thomas G. Roberts, T.G.; Chemotherapy and the war on cancer. *Nat. Rev. Cancer*. **2005**, *5*, 65-72.

9. Gilman, A.; The initial clinical trial of nitrogen mustard. *Am. J. Surg.* **1963**, *105*, 574–578.

10. Wills, L.; Clutterbuch, P.; Evans, B. D. F.; A new factor in the production and cure of macrocytic anaemias and its relation to other haemopoietic principles curative in pernicious anaemia. *Biochem. J.* **1937**, *31*, 2136–2147

11. Wright, J. C.; Prigot, A.; Wright, B.P.; Weintraub, S; Wright, L.T.; An evaluation of folic acid antagonists in adults with neoplastic diseases. A study of 93 patients with incurable neoplasms. *J. Natl. Med. Assoc*. **1951,** *43*, 211–240.

12. Meyer, L.M.; Miller, F.R.; Rowen, M.J.; Bock, G.; Rutzky, J.; Treatment of Acute Leukemia with Amethopterin (4-amino, 10-methyl pteroyl glutamic acid). *Acta Haematol*. **1950,** *4*, 157–67.

13. Ravi, R.T.; Zhang, Zhiquan, Z.; Lynn, M; Mary, D.;, Stephen, J.B; Gordon G.H.; Interaction of dihydrofolate reductase with methotrexate: Ensemble and single-molecule kinetics. *Proc. Natl. Acad. Sci.* **2002**, *99,* 13481–13486.

14. Bensch, K. G., Malawista, S. E.; Microtubule crystals: a new biophysical phenomenon induced by Vincaalkaloids. *Nature*. **1968**, *218*, 1176–1177.

15. Moxley, J. H.; De Vita, V. T.; Brace, K.; Frei, E.; Intensive combination chemotherapy and X-irradiation in Hodgkin's disease. *Cancer Res*. **1967**, *27*, 1258–1263.

16. Devita, V. T.; Serpick, A. A.; Carbone, P. P.; Combination chemotherapy in the treatment of advanced Hodgkin's disease. *Ann. Intern. Med*. **1970,** *73*, 881–895.

17. Rodriguez, V.; Hart, J.; Freireich, E.; Bodey, G.; Mccredie, K.; POMP combination chemotherapy of adult acute leukemia, *Cancer,* **1973**, *32*, 69-75.

18. Adams, J.D.; Flora, K.P.; Goldspiel, B.R.; Wilson, J.W.; Arbuck, S.G.; Finley, R.; Taxol: a history of pharmaceutical development and current pharmaceutical concerns. *J. Natl. Cancer. Inst. Monogr.* **1993,** *15,*141-147.

19. Martin, V.; Overview of paclitaxel (TAXOL). *Seminars in Oncology nursing,* **1993**, 2-5.

20. Lokich, J.; Anderson, N.; Carboplatin versus cisplatin in solid tumors: an analysis of the literature. *Ann. Oncol.* **1998**, *9,* 13-21.

21. Douglas, H.; Robert A.W.; The Hallmarks of Cancer. *Cell*. **2000**, *100*, 57–70.

22. Douglas, H,; Robert A.W.; The Hallmarks of Cancer: Next generation. *Cell*. **2011**, *144*, 646-674.

23. Shepard, H.M.; Jin, P.; Slamon, D.J.; Pirot. Z.; Maneval, D.C.; Herceptin. *Handb. Exp. Pharmacol.* **2008**, *181*,183-219.

24. Capdeville, R.; Buchdunger, E.; Zimmermann, J.; Matter, A.; Glivec (STI571, Imatinib), A rationally developed, targeted anticancer drug. *Nat. Rev. Drug Discov.* **2002,** *1*, 493-502.

25. Zhang, J.; Yang, P.L.; Gray, N.S.; Targeting cancer with small molecule kinase inhibitors. *Nat. Rev. Cancer*. **2009**, *9*, 28-39.

26. http://www.cancer.gov/cancertopics/factsheet/Therapy/targeted

27. Dancey, J.; Sausville, E.A.; Issues and progress with protein kinase inhibitors for cancer treatment. *Nat. Rev. Drug Discov.* **2003***, 2*, 296-313.

28. Manning, G.; Whyte, D.B.; Martinez, R.; Hunter, T.; Sudarsanam, S.; The protein kinase complement of the human genome. *Science.* **2002**, *298*, 1912-1934.

29. Niedner, R.H.; Buzko, O.V.; Haste, N.M.; Taylor, A.; Gribskov, M.; Taylor, S.S. Protein kinase resource: an integrated environment for phosphorylation research. *Proteins*. **2006**, *63*, 78-86.

30. Cohen, P.; Protein kinases - the major drug targets of the twenty-first century?. *Nat. Rev. Drug Discov.* **2002**, *1*, 309-315.

31. Zwick, E.; Bange. J.; Ullrich, A.; Receptor tyrosine kinase signalling as a target for cancer intervention strategies. *Endocr-Relat Cancer.* **2001**, *8,* 161-173.

32. McInnes, C.; Recent Advances in the Structure-Guided Design of Protein Kinase Inhibitors, *Frontiers in drug discovery.* **2007**, *3*, 145-170.

33. Lapenna, S.; Giordano, A.; Cell cycle kinases as therapeutic targets for cancer. *Nat. Rev. Drug Discov.* **2009**, *8*, 547- 566.

34. Shappiro, G.I.; Cyclin-Dependent Kinase Pathways as Targets for Cancer Treatmen. *J. Clin. Oncol.* **2006**, *24*, 1770-1783.

35. David, O.M.; Principles of control Chapter 3. *The Cell cycle.* **2007**, 12-25.

36. David, O.M.; Principles of CDK regulation. *Nature.* **1995,** *374,* 131-134.

37. George Kontopidis, G.; McInnes, C.; Pandalaneni, S.R.; McNae, I.; Gibson, D.; Mezna, M.; Thomas,M.; Wood, G.; Wang, S.; Walkinshaw, M.D.; Fischer, P.M.; Differential binding of inhibitors to active and inactive CDK2 provides insights for drug design. *Chem. Biol.* **2006**, *13*, 201-211.

38. Reynisdottir, I.; Polyak, K.; Lavarone, A.; Massague, J.; Kip/Cip anf Ink4 Cdk inhibitors cooperate to induce cell cycle arrest in response to TGF-beta. *Genes and Dev*. **1995**, *9*, 1831-1845.

39. Ray, A.; James, M.K.; Larchelle, S.; .Fischer, R.P.; Blain, S.W.; p27Kip1 inhibits cyclin D- cyclin-dependent kinase 4 by two independent modes. *Mol. Cell Biol*. **2008**, *29*, 989-999.

40. Sielecki, T.M.; Boylan, J.F.; Enfield, P.A.; Trainor,G.; Cyclin dependant kinase inhibitors: Useful targets in cell cycle regulation. *J. Med. Chem*. **2000**, *43,* 1-18.

41. Sausville, E.A.; Complexities in the development of cyclin-dependent kinase inhibitor drugs. *Trends. Mol. Medicine*. **2002**, *8*, S32-S37.

42. Fischer, P.M.; Gianella, B.A.; CDK inhibitors in clinical development for the treatment of cancer. *Expert Opin. Investig.* **2003**, *12*, 955–970.

43. Musgrove, E.A,; Elizabeth Caldon, E.; Barraclough, J.; Stone, A.; Sutherland, R.L.; Cyclin D as a therapeutic target in cancer. *Nat. Rev. Cancer*. **2011**, *11*, 558-572.

44. McInnes,C.; Fischer, P.M.; Strategies for the Design of Potent and Selective Kinase Inhibitors. *Curr. Pharm Design*. **2005**, *11*, 1845-1863.

45. Orzaez, M.; Gorat, A.; Mondragon, L.; Bachs, O.; Perez-Paya, E.; ATP Non-competitive inhibitors of CDK-cyclin complexes. *ChemMedChem.* **2009,** *4*, 19-24.

46. Zheleva, D.I.; McInnes, C.; Gavine, A.L.; Zhelev, N.Z.; Fischer, P.M.; Lane, D.P.; Highly potent p21WAF1-derived peptide inhibitors of CDK-mediated pRb phosphorylation: Delineation and structural insight into their interactions with cyclin A. *J. Pept. Res*. **2002**, *60*, 257–27.

47. Erez, E.; Fass, D.; Bibi, E.; Cell cycle, CDKs and cancer changing paradigm. *Nat. Rev. Cancer.* **2009,** *9*, 153-166.

48. Elinor, E.; Deborah, F.; Eitan, B.; How intramembrane proteases bury hydrolytic reactions in the membrane. *Nature.* **2009***, 459*, 371-378.

49. Andrews, M.J.; Kontopidis, G.; McInnes, C.; Plater, A.; Innes, L.; Cowan, A.; Jewsbury, P.; Fischer, P.M.; REPLACE: A Strategy for Iterative Design of Cyclin-Binding Groove Inhibitors. *ChemBioChem*. **2006**, *7*, 1909 – 1915.

50. McInnes, C.; Andrews, M.J.; Zheleva, D.I.; Lane, D.P.; Fischer, P.M.; Peptidomimetic Design of CDK Inhibitors Targeting the Recruitment Site of the Cyclin Subunit. *Curr. Med. Chem. - Anti-Cancer Agents.* **2003**, *3*, 57-69.

51. Ball, K.L.; Lain, S.; Fåhraeus, R.; Smythe, C.; Lane, D.P.; Cell-cycle arrest and inhibition of Cdk4 activity by small peptides based on the carboxy-terminal domain of p21. *Curr. Biol.* **1997**, *7*, 71–80.

52. Mendoza, N.; Fong, S.; Marsters, J.; Hartmut, Ralph Schwall, H.R.; Wickramasinghe, D.; Selective cyclin dependent kinase 2/cyclin A antagonists that differ from ATP site inhibitors block tumor growth. *Cancer Res.* **2003**, *63*, 1020-1024.

53. Liu, S.; Bolger, J.; Kirkland, L.; Premnath, P.N.; McInnes, C.; Structural and Functional Analysis of Cyclin D1 Reveals p27 and Substrate Inhibitor Binding Requirements. *ACS Chem. Biol*. **2010**, *5*, 1169–1182.

54. Ying-Nan, P.C.; Sushil, K. S.; Timothy, M. R.; Li, J.; Mary, S.M.; Kayla, B.; Peter, D.A.; Kenneth, W. B.; William, G. K.; Selective killing of transformed cells by cyclin/cyclin-dependent kinase 2 antagonists. *Proc. Natl. Acad. Sci.* **1999**, *96*, 4325-4329.

55. Venkatachalam, M.; Jiang, X.; Oldfield, T.; Waldman,M.; LigandFit: a novel method for the shape-directed rapid docking of ligands to protein active sites. *J. Mol. Graph Model.***2003,** *21*, 289-307.

56. Kontopidis, G.; Andrews, M. J.; McInnes, C.; Plater, A.; Innes, L.; Renachowski, S.; Cowan, A.; Fischer, P. M. Truncation and optimization of peptide inhibitors of cyclin-dependent kinase 2-cyclin a through structure-guided design. *ChemMedChem.* **2009**, *4*, 1120−1128.

57. Andrews, M. J.; McInnes, C.; Kontopidis, G.; Innes, L.; Cowan, A.; Plater, A.; Fischer, P. M. Design, synthesis, biological activity and structural analysis of cyclic peptide inhibitors targeting the substrate recruitment site of cyclin-dependent kinase complexes. *Org. Biomol. Chem.* **2004**, *2*, 2735−2741.

58. Pfefferkorn, J. A.; Choi, C.; Larsen, S. D.; Auerbach, B.; Hutchings, R.; Park, W.; Askew, V.; Dillon, L.; Hanselman, J. C.; Lin, Z.;Lu, G. H.; Robertson, A.; Sekerke, C.; Harris, M. S.; Pavlovsky, A.;Bainbridge, G.; Caspers, N.; Kowala, M.; Tait, B. D. Substituted pyrazoles as hepatoselective HMG-CoA reductase inhibitors: Discovery of (3R,5R)-7-[2-(4-fluorophenyl)-4-isopropyl-5-(4-methylbenzylcarbamoyl)- 2H-pyrazo l-3-yl]-3,5-dihydroxyheptanoic acid (PF-3052334) as a candidate for the treatment of hypercholesterolemia. *J. Med. Chem.* **2008**, *51*, 31−45.

59. Wang, L.-Y.; Tseng, W.-C.; Lin, H-Y.; Wong, F. F. An effective nitrilimine cycloaddition for the synthesis of 1,3,5-trisubstituted 1,2,4-triazoles from oximes with hydrazonoyl hydrochlorides. *Synlett.* **2011**, *10*, 1467−1471.

60. Atkinson, R. N.; Drizin, I.; Gregg, R. J.; Gross, M. F.; Kort, M. E.; Shi, L. Pyrazole-amides and sulfonamides as sodium channel modulators. U.S. Patent 2005/0020564, 2005.

61. Prasad, D. J.; Karthikeyan, M. S.; Karegoudar, P. B.; Poojary, B.; Holla, B. S.; Kumari, N. S. Synthesis of some thiadiazolotriazinone derivatives as possible antimicrobial agents. *Phosphorus, Sulfur, Silicon Relat. Elem.* **2007**, *182*, 1083−1091.

62. Sbardella, G.; Mai, A.; Artico, M.; Loddo, R.; Setzu, M. G.; La Colla, P. Synthesis and in vitro antimycobacterial activity of novel 3-(1H-pyrrol-1-yl)-2-oxazolidinone analogues of PNU-100480. *Bioorg. Med. Chem. Lett.* **2004**, *14*, 1537−1541.

63. Liu, S.; P.N.; Bolger, J.; McInnes,C.; Optimization of CDK/cyclin groove Inhibitors through REPLACE mediated Fragment Assembly. *J. Med. Chem.* **2013**, *56*, 1573–1582.

64. Allred, A. L.; Electronegativity values from thermochemical data. *J. Inorg. Nucl. Chem.* **1966**, *17*, 215–221.

65. Lipinski, C. A.; Lombardo, F.; Dominy, B. W.; Feeney, P. J. Experimental and computational approaches to estimate solubility and permeability in drug discovery and development settings. Adv. *Drug Delivery Rev*. **1997**, *23*, 3−25.

66. Ghose, A. K.; Viswanadhan, V. N.; Wendoloski, J. J. A knowledge based approach in designing combinatorial or medicinal chemistry libraries for drug discovery. 1. A qualitative and quantitative characterization of known drug databases. *J. Comb. Chem*. **1999**, *1*, 55−68.

67. Guy, S. Y., P. J.; Jean, M.; A re-investigation of resveratrol synthesis by Perkins reaction. Application to the synthesis of aryl cinnamic acids. *Tetrahedron.* **2003,** *59*, 3315-3321.

68. Premnath, P.N.; Liu, S.; Perkins, T.; Abott, J.; Anderson, E.; McInnes, C.; Furoic and picolinic acid derived isosteres for arginine: towards non-ATP competitive CDK inhibitors. *Bio. Org. Med. Chem.* **2014**, *22*, 616-622.

69. Kontopidis, G.; Andrews, J.M.; McInnes, C.; Plater, A.; Innes, L.; Renachowski, S.; Cowan, A.; Fischer, P.M.; Truncation and optimisation of Peptide Inhibitors of Cyclin-Dependent Kinase 2-Cyclin A Through Structure-Guided Design *ChemMedChem*, **2009**, *4*, 1120 − 1128.

70. Kontopidis, G.; Andrews, M.J.; McInnes,C.; Cowan, A.; Powers, H.; Innes, L.; Plater, A.; Griffiths, G.; Paterson, D.; Zheleva, D.I.; Lane, P.D.; Green, S.; Walkinshaw, M.D.; Fischer, P.M.; Insights into cyclin groove recognition: complex crystal structure and inhibitor design through ligand exchange. *Structure* **2003**, *11*, 1537-1546.

71. Rafi, S.; Hearn, B.; Vedantham, P.; Jacabson, M.; Renslo, A.; Predicting and improving the membrane permeability of peptidic small molecules. *J. Med. chem.* **2012**, *55*, 3163-3169.

72. Chatterjee, J. R. F.; Kessler, H.; N-methylation of peptides and proteins: an important element for modulating biological functions. *Angew Chem Int Ed Engl*. **2013**, *52*, 254-69.

73. Miller, S.M.; Simon, J.R.; Simon N.G.; Zuckermann, R.N.; Kerr, J.M.; Moos, W.H.; Comparison of the Proteolytic Susceptibilities of Homologous L-Amino Acid, D-Amino Acid, and N-Substituted Glycine Peptide and Peptoid Oligomers. *Drug. Dev. Res.* **1995**, *35*, 20-33.

74. Denizot, F.; Lang, R. Rapid colorimetric assay for cell growth and survival. Modifications to the tetrazolium dye procedure giving improved sensitivity and reliability. *J. Immunol. Methods.* **1986**, *89*, 271-277.

75. Castanedo, G.; Clark, K.; Wang, S.; Tsui, V.; Wong, M.; Nicholas, J.; Wickramasinghe, D.; Marsters, J. C., Jr.; Sutherlin, D. CDK2/cyclinA inhibitors: targeting the cyclinA recruitment site with small molecules derived from peptide leads. *Bioorg. Med. Chem. Lett.* **2006**, *16*, 1716-1720.

76. Solladie, G.; Pasturel-Jacope´a, Y.; Maignan, J.; A re-investigation of resveratrol synthesis by Perkins reaction. Application to the synthesis of aryl cinnamic acids *Tetrahedron*, **2003**, *59,* 3315–3321.

77. Klein, S.I.; Molino, B.F.; Czekaj, M.; Gardner, C.J.; Chu, V.; Brown,K.; Sabatino, R.D.; Bostwick, J.S.; Kasiewski, C.; Bentley, R.; Windisch, V.; Perrone, M.; Dunwiddie, C.T.; Robert J. Leadley, R.J.; Design of a New Class of Orally Active Fibrinogen Receptor Antagonists. *J. Med. Chem.* **1998**, *41*, 2492-2502.

78. Picard, F.; Barassin, S.; Mokhtarian, A.; Hartmann, R.W.; Synthesis and Evaluation of 2-Substituted 4-(4-Carboxy- or 4-carboxymethylbenzylidene)-N-acylpiperidines: Highly Potent and in Vivo Active Steroid 5r-Reductase Type 2 Inhibitors. *J. Med. Chem.* **2002**, *45*, 3406-3417.

79. Potashman, M.H.; Bready, J.; Coxon, A.; DeMelfi, T.M.; DiPietro, L.; Doerr, N.; Elbaum, D.; Estrada, J.; Gallant, P.; Germain, J.; Gu, Y.; Harmange, J-G.; Kaufman, S.A.; Design, Synthesis, and Evaluation of Orally Active Benzimidazoles and Benzoxazoles as Vascular Endothelial Growth Factor-2 Receptor Tyrosine Kinase Inhibitors. *J. Med. Chem.* **2007**, *50,* 4351-4373.

80. Wagner, C.E.; Jurutka, P.W.; Marshall, P.A.; Groy, T.L.; Vaart, A.V.; Ziller, J.W.; Furmick, J.K.; Graeber, M.E.; Matro, E.; Modeling, Synthesis and Biological Evaluation of Potential Retinoid X Receptor (RXR) Selective Agonists: Novel Analogues of 4-[1-(3,5,5,8,8-Pentamethyl-5,6,7,8-tetrahydro-2-naphthyl)ethynyl]benzoic Acid (Bexarotene). *J. Med. Chem.* **2009***, 52*, 5950–5966.

81. Monguchi, Y.; Fujita, Y.; Hashimoto, S.; Ina, M.; Takahashi, T.; Ito, R.; Nozaki, K.; Maegaway, T.; Sajiki, H.; Hydrogenation: Palladium on carbon-catalyzed solvent-

free and solid-phase hydrogenation and Suzukie Miyaura reaction. *Tetrahedron.* **2011**, *67*, 8628-8634.

82. Imamura, S.; Ichikawa, T.; Nishikawa, Y.; Kanzaki, N.; Takashima, K.; Niwa, S.; Iizawa, Y.; Baba, M.; Sugihara, Y.; Discovery of a Piperidine-4-carboxamide CCR5 Antagonist (TAK-220) with Highly Potent Anti-HIV-1 Activity. *J. Med. Chem.* **2006**, *49*, 2784-2793.

83. Andrei, A.; Ivanov, F. R. K.; Fu, H.; Targeting protein–protein interactions as an anticancer strategy. *Trend. Pharm. Sci.* **2013,** *34*, 393-400.

84. Yin, H.; Hamilton, A.D.; Strategies for targeting protein-protein interactions with synthetic agents. *Angew Chem. Int. Ed. Engl.* **2005**, *44*, 4130-4163.

85. Jubb, H.; Higueruelo, A. P.; Winter, A.; Blundell, T. L.; Structural biology and drug discovery for protein-protein interactions. *Trends Pharmacol Sci.* **2012**, *33*, 241-248.

APPENDIX A

CHARACTERIZATION DATA OF REPRESENTATIVE N-CAPS
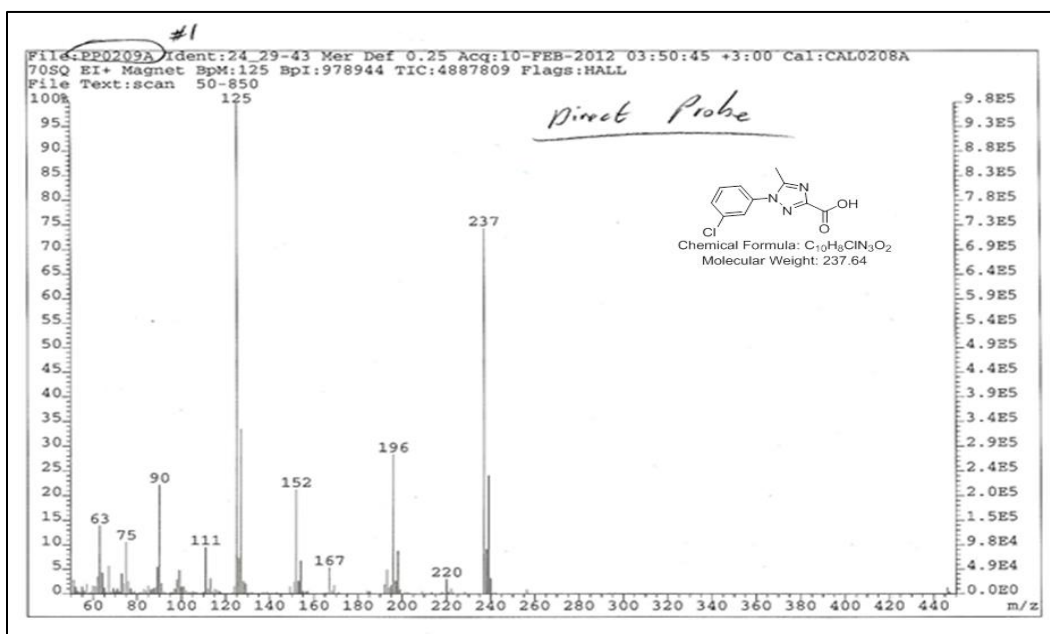
Figure A.1 MS: 1-(3-chlorophenyl)-5-methyl-1H-1,2,4-triazole-3-carboxylic acid
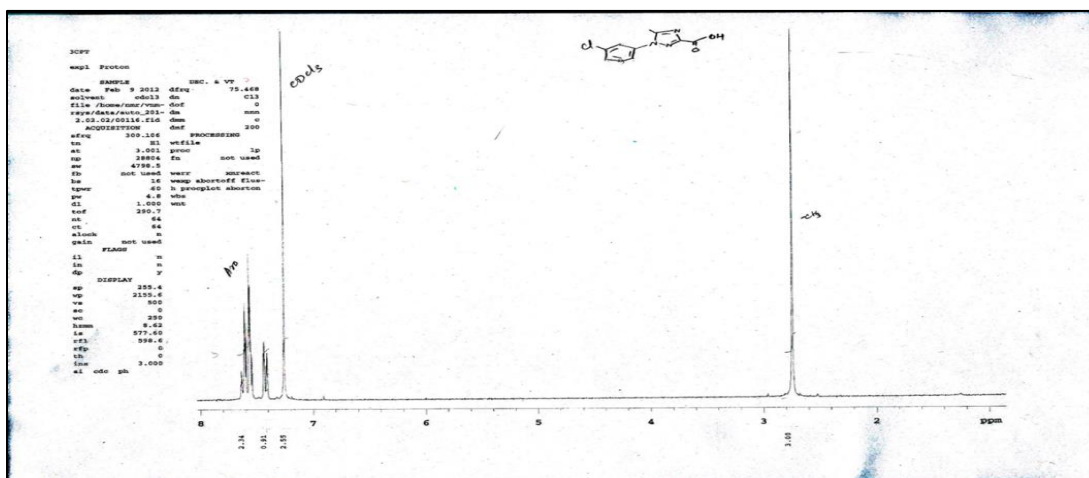
Figure A.2 NMR: 1-(3-chlorophenyl)-5-methyl-1H-1,2,4-triazole-3-carboxylic acid
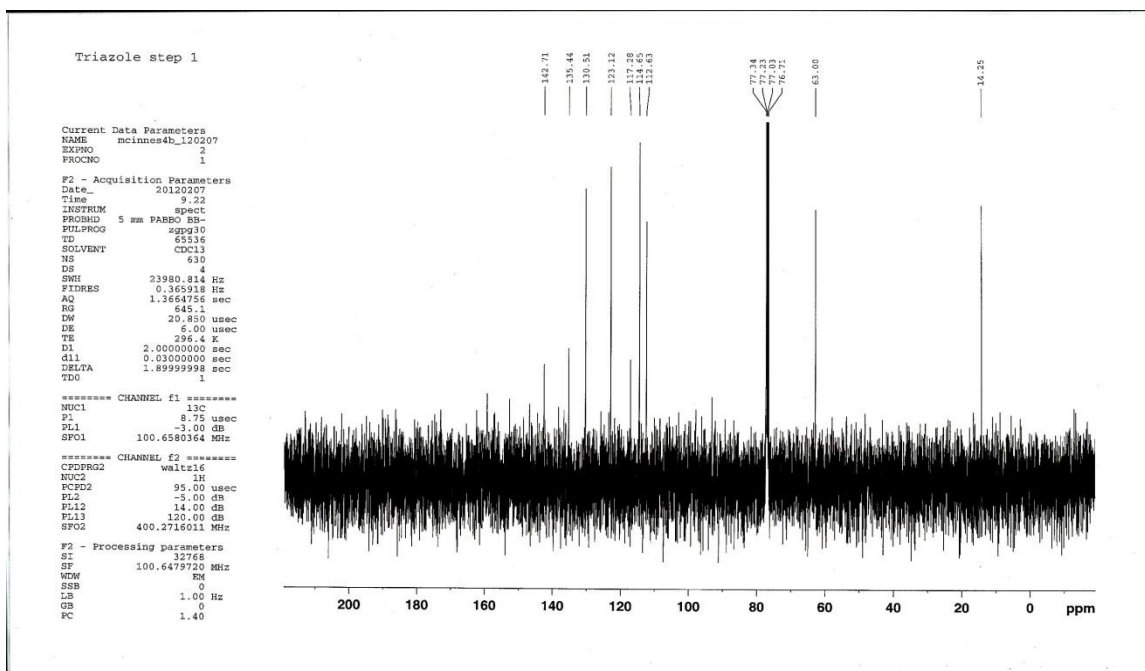
Figure A.3 ¹³CNMR: 1-(3-chlorophenyl)-5-methyl-1H-1,2,4-triazole-3-carboxylic acid
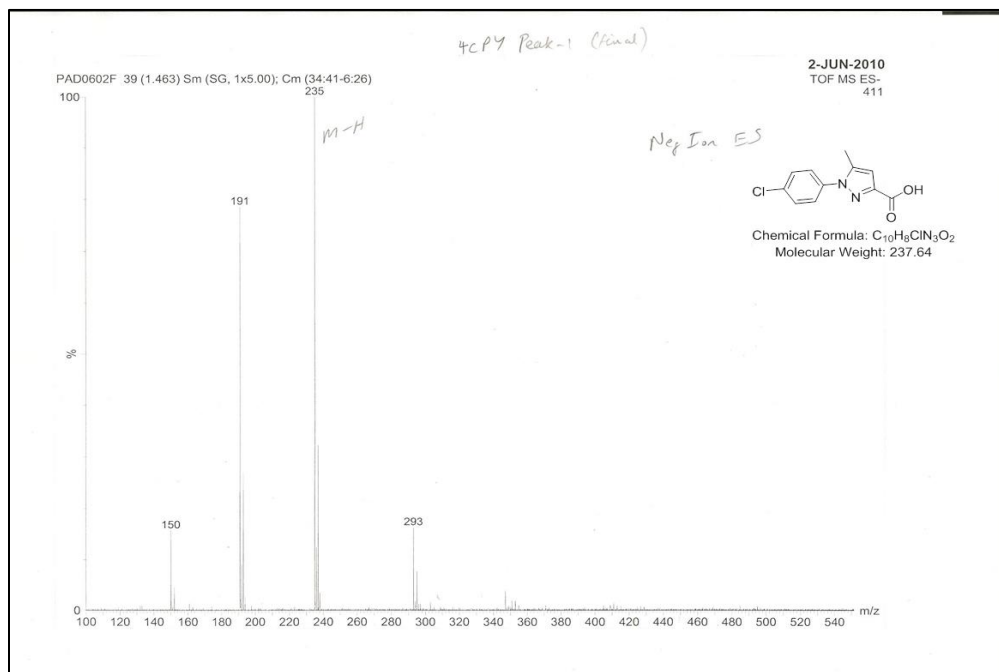
Figure A.4 MS-1-(4-chlorophenyl)-5-methyl-1H-pyrazole-3-carboxylic acid
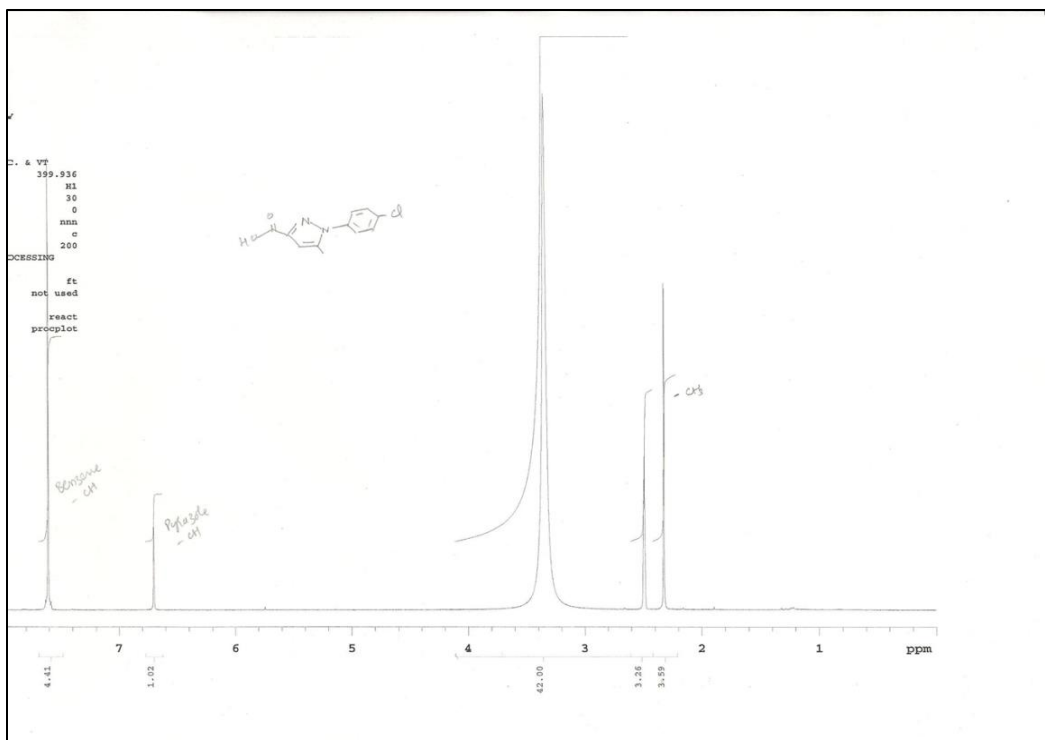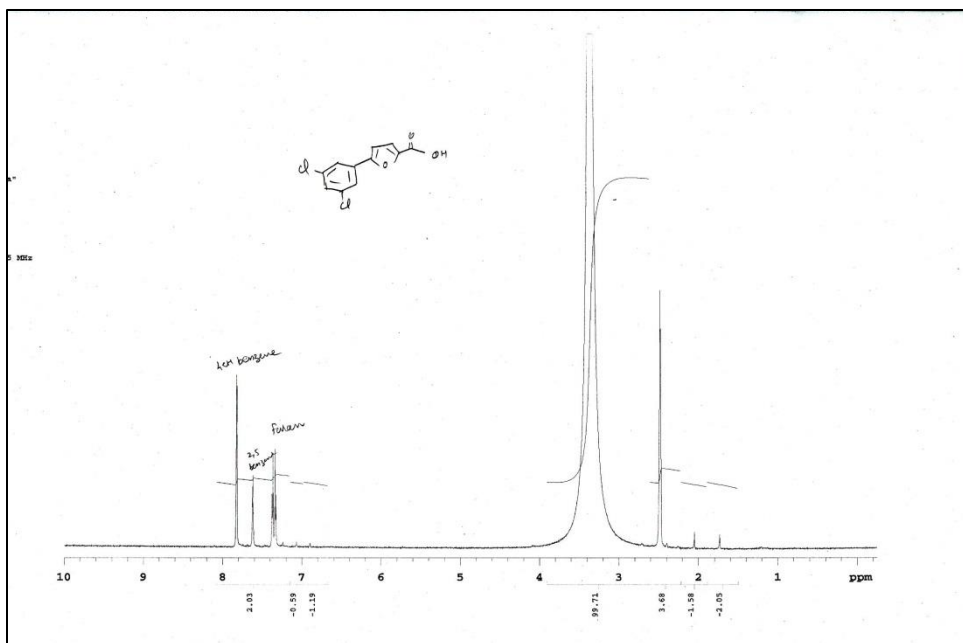
Figure A.5 NMR- 1-(4-chlorophenyl)-5-methyl-1H-pyrazole-3-carboxylic acid
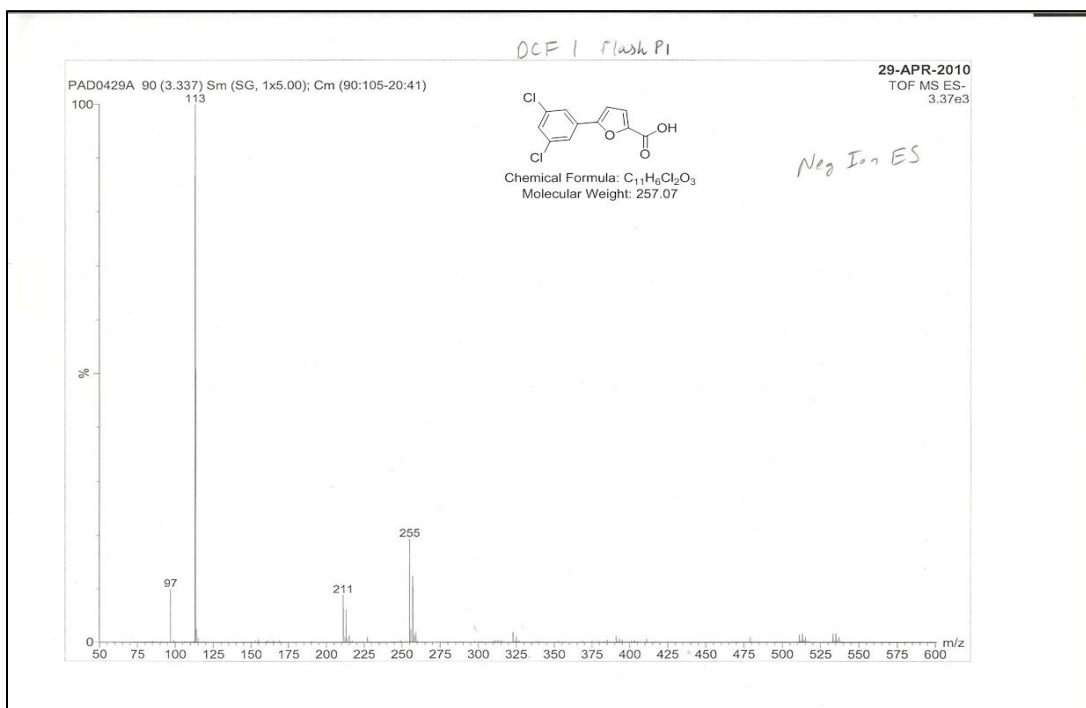
Figure A.6 MS- 5-(3,5-dichlorophenyl)furan-2-carboxylic acid

165

Figure A.7 NMR- 5-(3,5-dichlorophenyl)furan-2-carboxylic acid
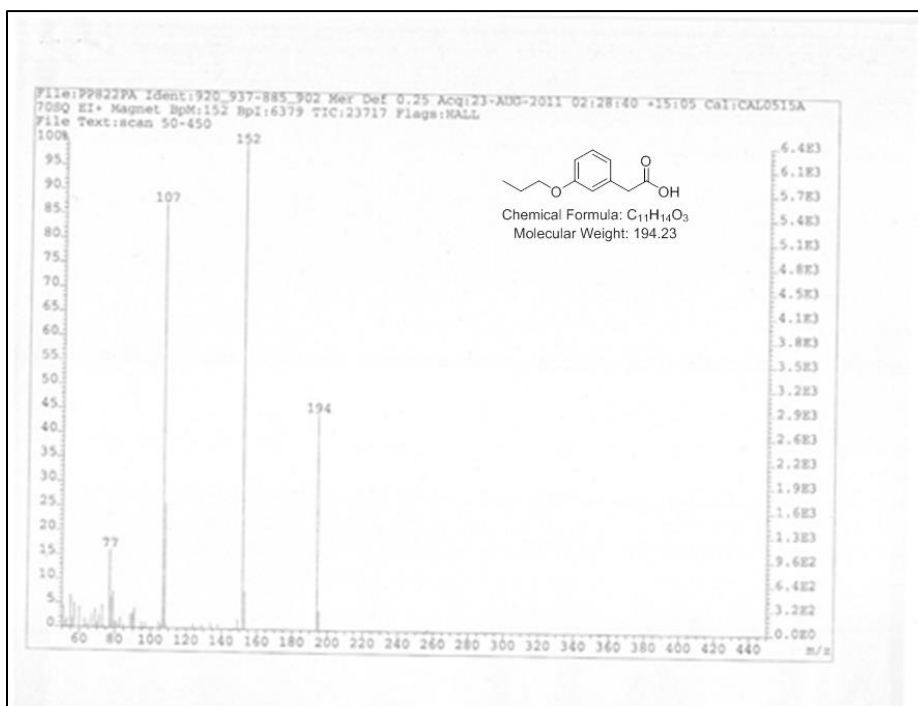
Figure A.8 MS- 2-(3-propoxyphenyl)acetic acid
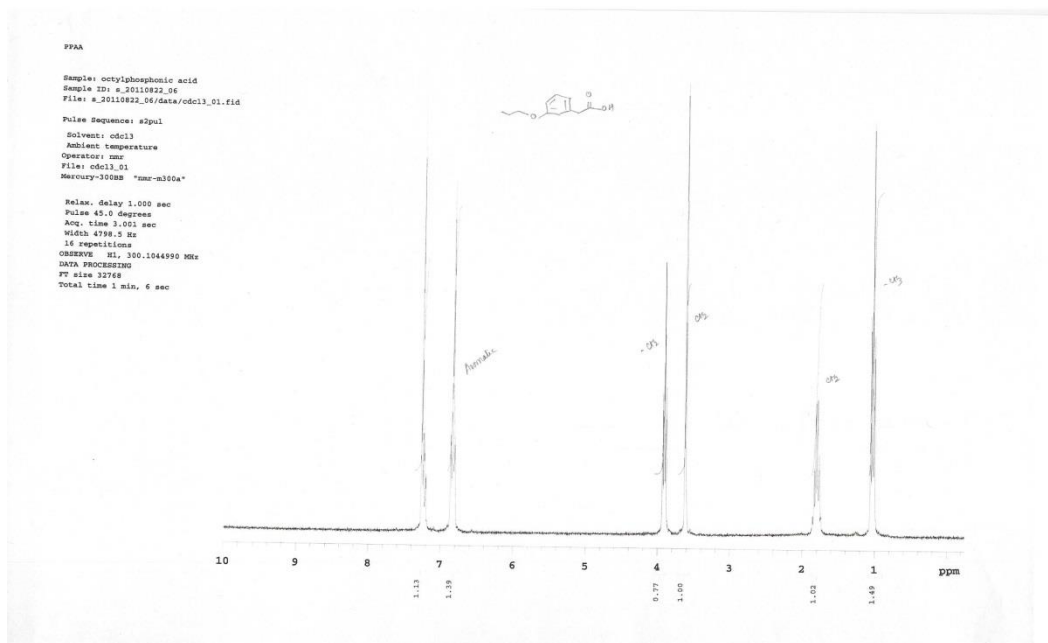
Figure A.9 NMR- 2-(3-propoxyphenyl)acetic acid
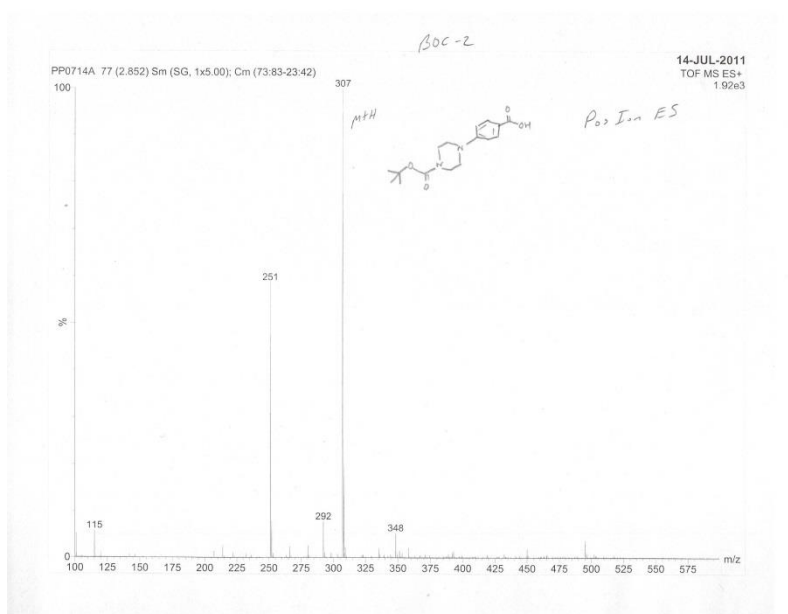
Figure A.10 MS: 4-(4-(tert-butoxycarbonyl)piperazin-1-yl)benzoic acid

167
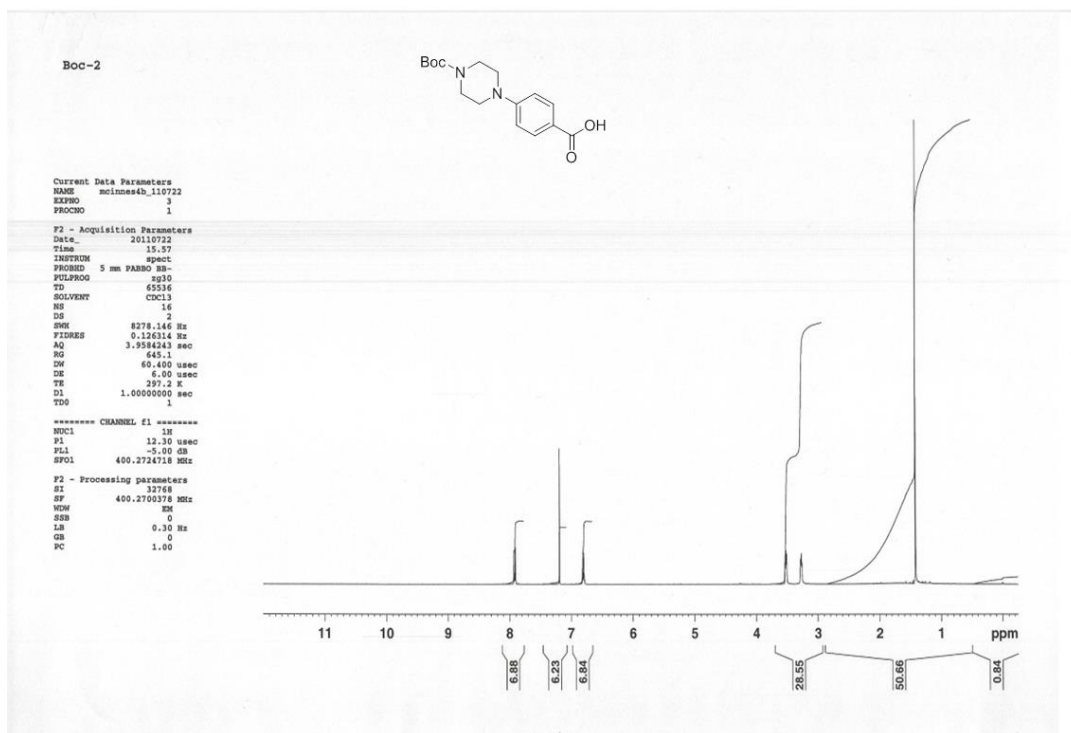
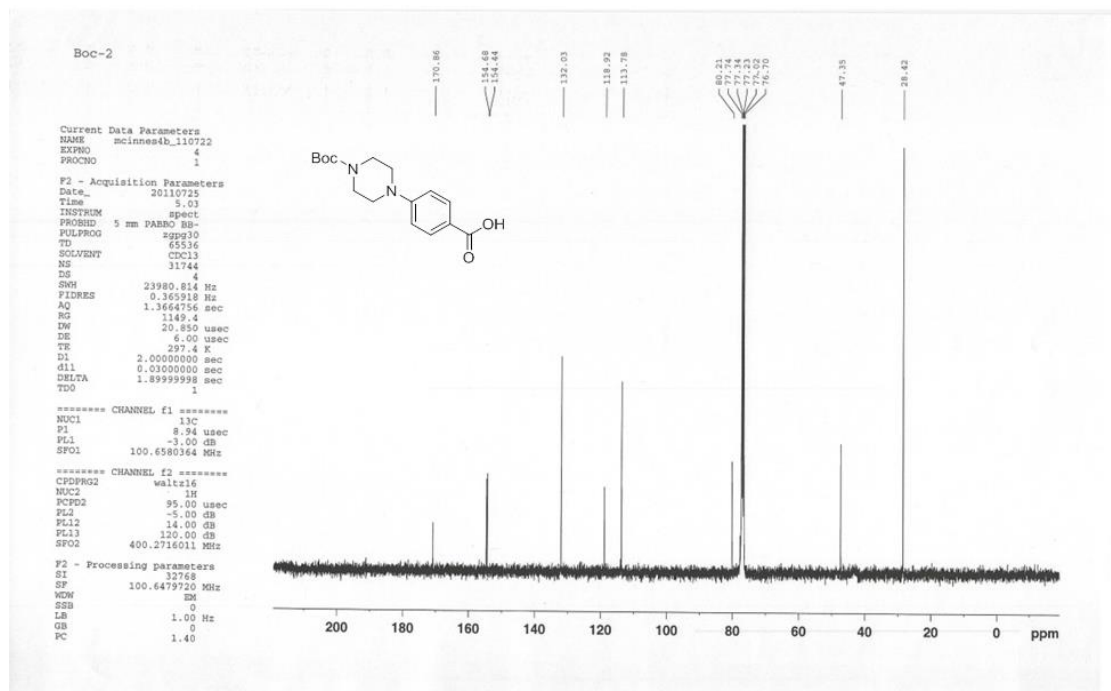Figure A.11 ^{1}HNMR: 4-(4-(tert-butoxycarbonyl)piperazin-1-yl)benzoic acid

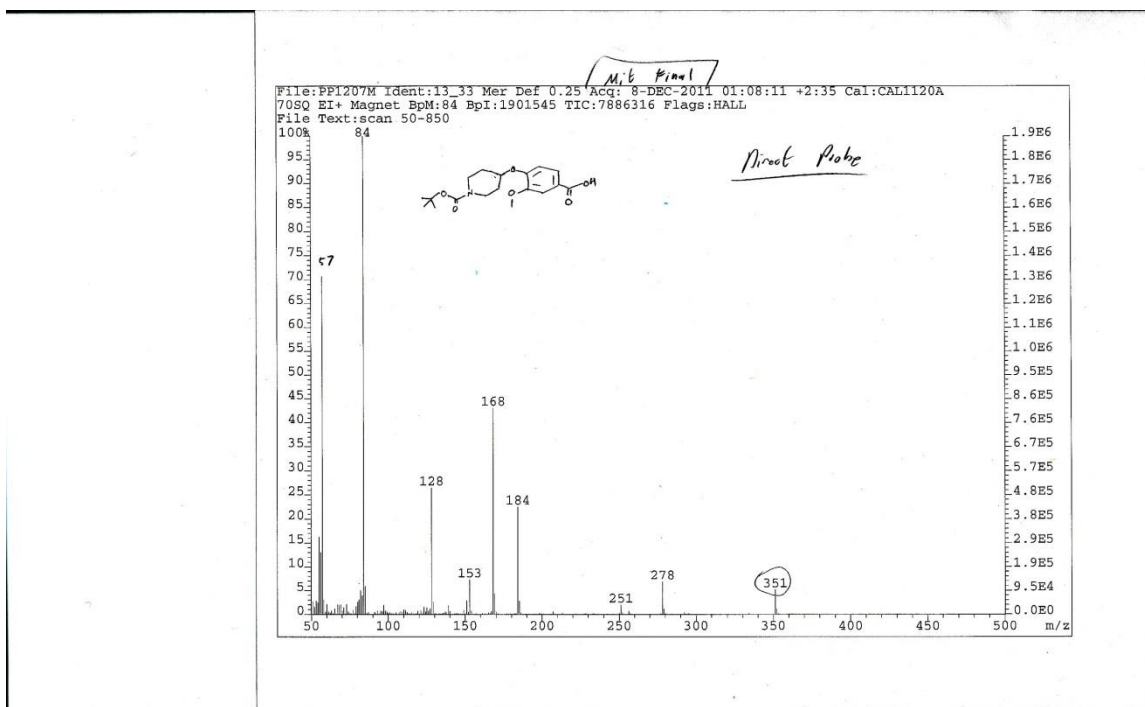Figure A.12 ^{12}CNMR: 4-(4-(tert-butoxycarbonyl)piperazin-1-yl)benzoic acid

168

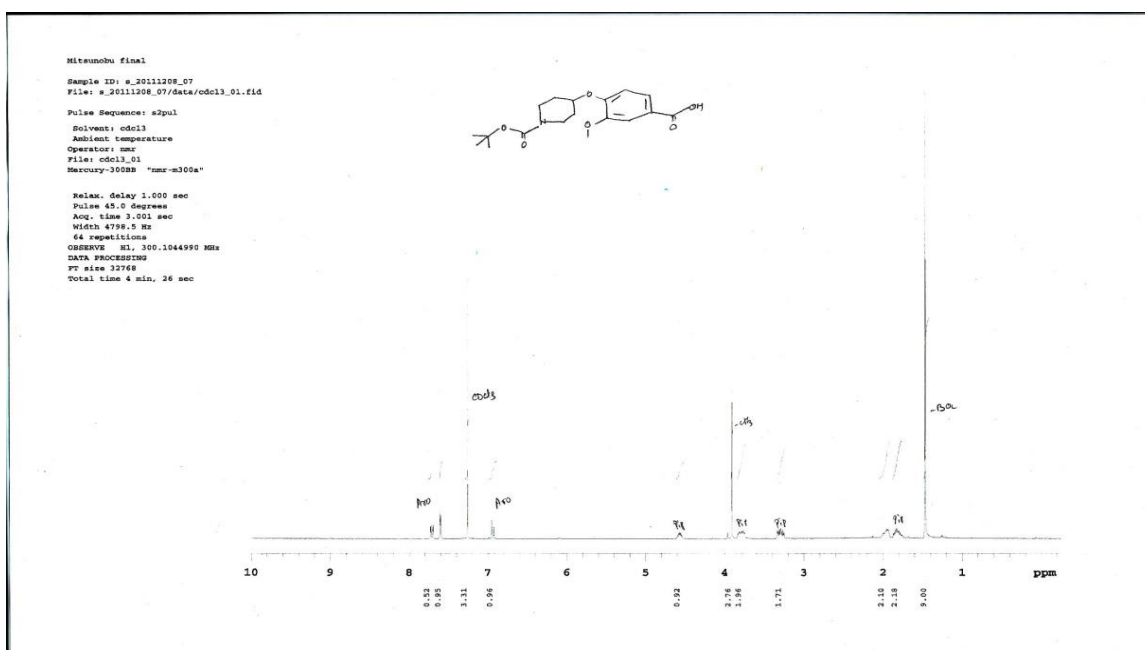Figure A.13 MS:4-((1-(tert-butoxycarbonyl)piperidin-4-yl)oxy)-3-methoxybenzoic acid

Figure A.14 ^{1}HNMR:4-((1-(tert-butoxycarbonyl)piperidin-4-yl)oxy)-3-methoxybenzoic acid
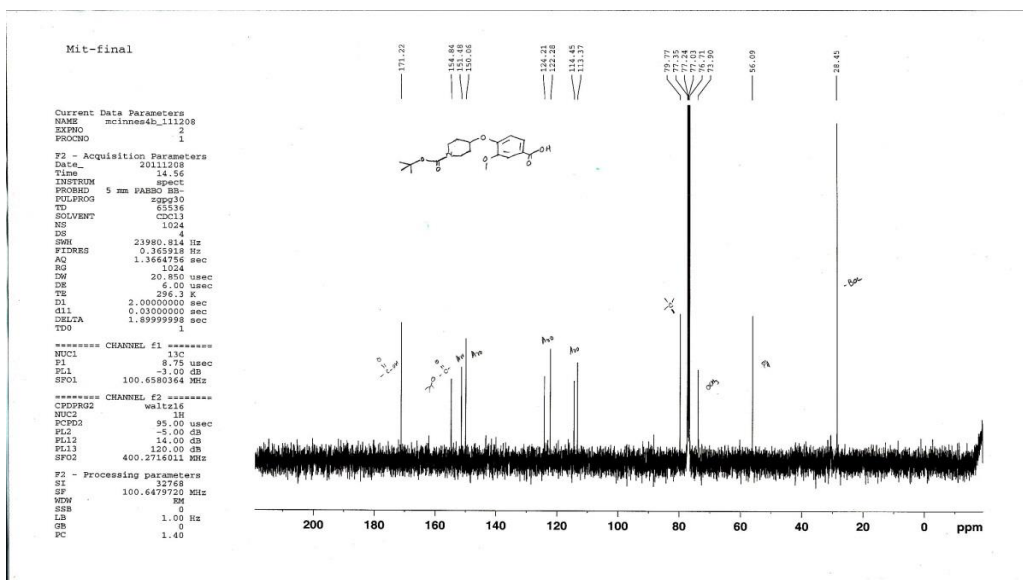
Figure A.15 ^{13}CNMR:4-((1-(tert-butoxycarbonyl)piperidin-4-yl)oxy)
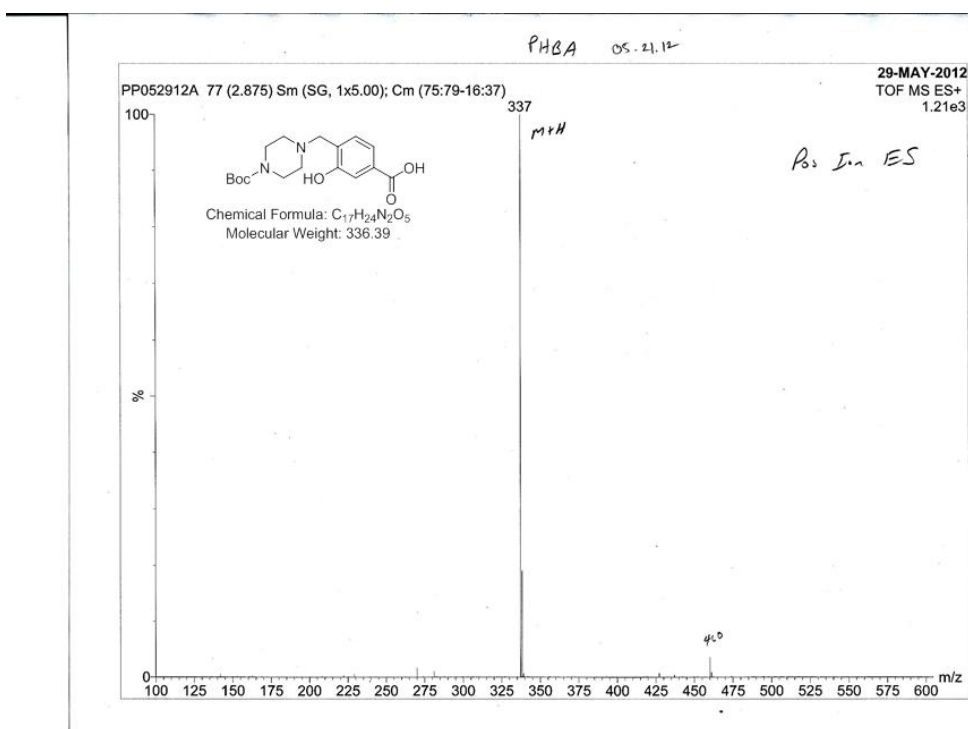-3-methoxybenzoic acid

Figure A.16 MS: 4-((4-(tert-butoxycarbonyl)piperazin-1-yl)methyl)
-3-hydroxybenzoic acid

file: ...\April\cm3_120427_PNP_PHBA.fid\fid block# 1 expt: "s2pul"
transmitter freq.: 300.106300 MHz
time domain size: 28804 points
width: 4798.46 Hz = 15.9892 ppm = 0.166590 Hz/pt
number of scans: 32

freq. of 0 ppm: 300.104499 MHz
processed size: 32768 complex points
LB: 1.500   GF: 0.0000
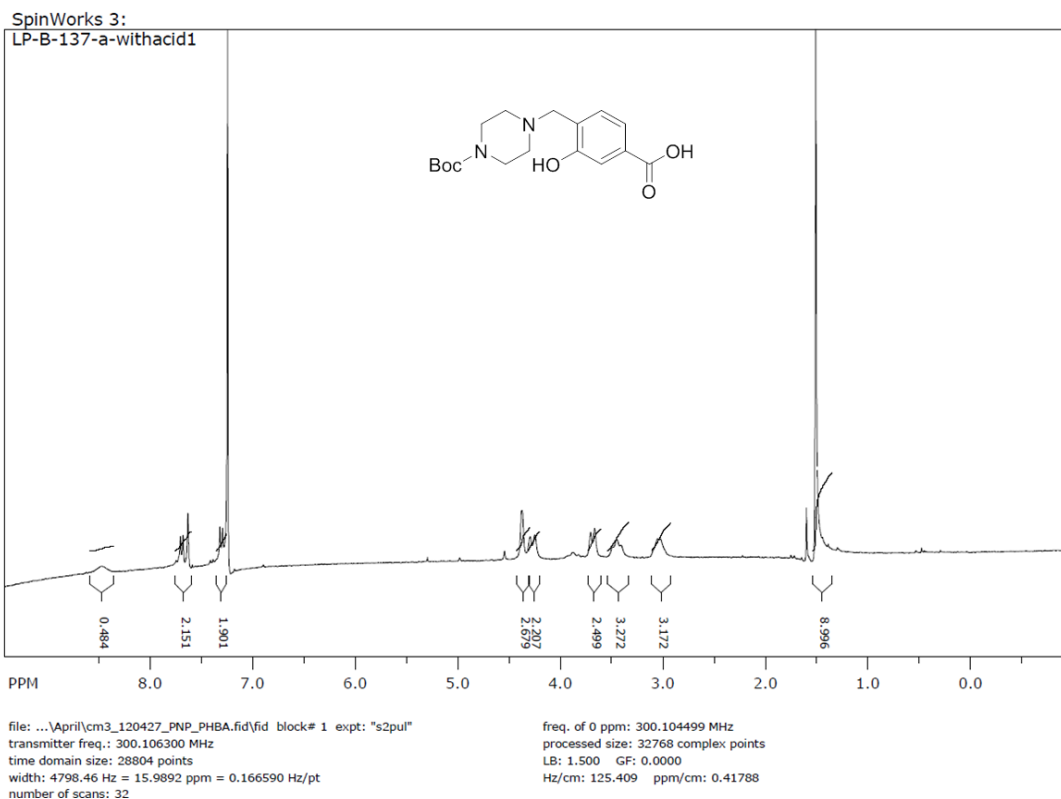Hz/cm: 125.409   ppm/cm: 0.41788

Figure A.17 NMR: 4-((4-(tert-butoxycarbonyl)piperazin-1-yl)methyl)-3-hydroxybenzoic acid
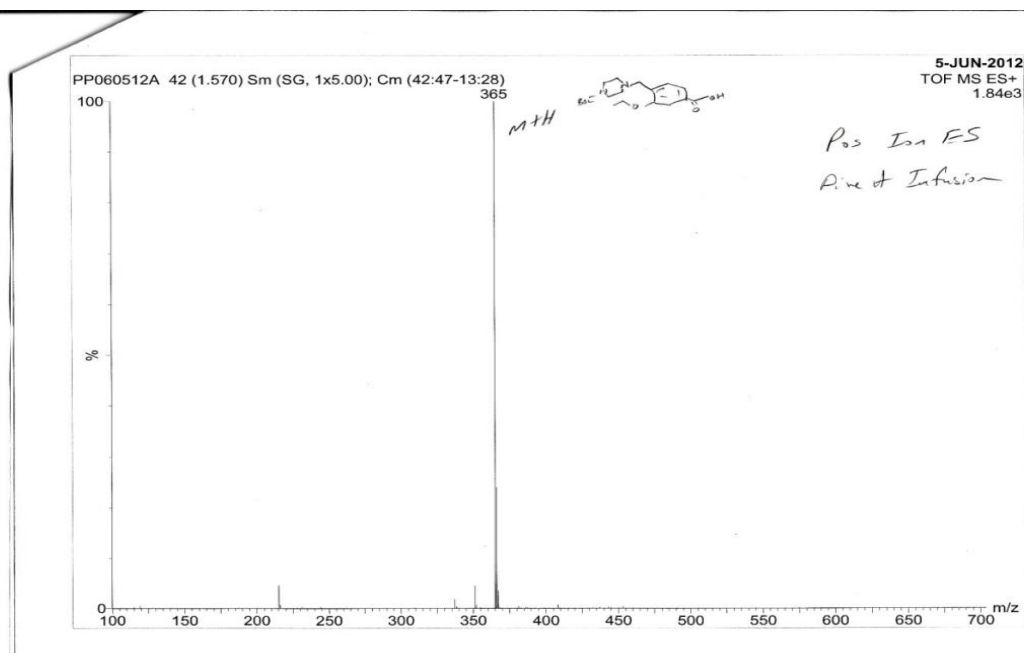

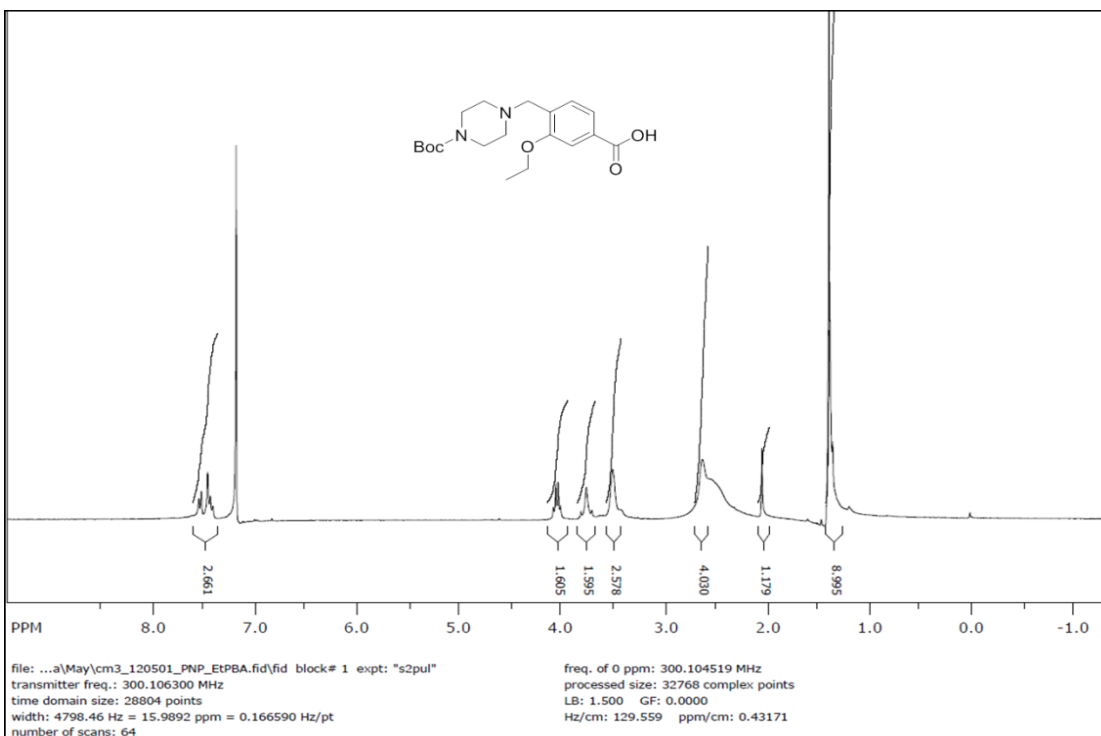Figure A.18 MS: 4-((4-(tert-butoxycarbonyl)piperazin-1-yl)methyl)-3-ethoxybenzoicacid

171

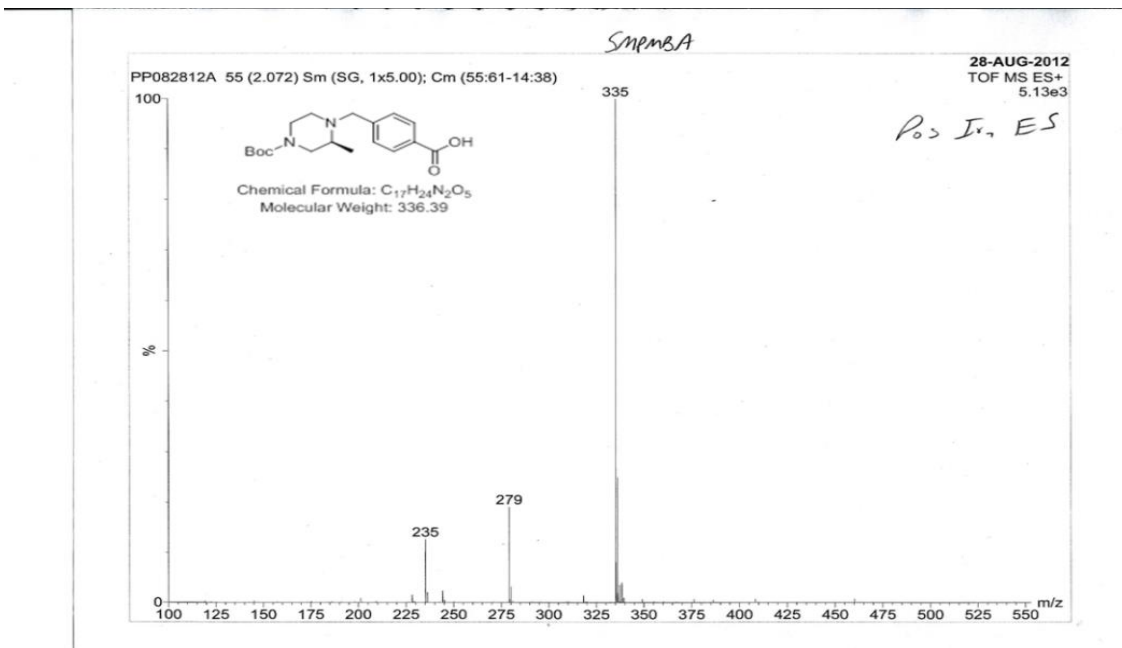Figure A.19 NMR: 4-((4-(tert-butoxycarbonyl)piperazin-1-yl)methyl)-3-ethoxybenzoic acid

Figure A.20 MS:(S)-4-((4-(tert-butoxycarbonyl)-2-methylpiperazin-1-yl)methyl)benzoic acid
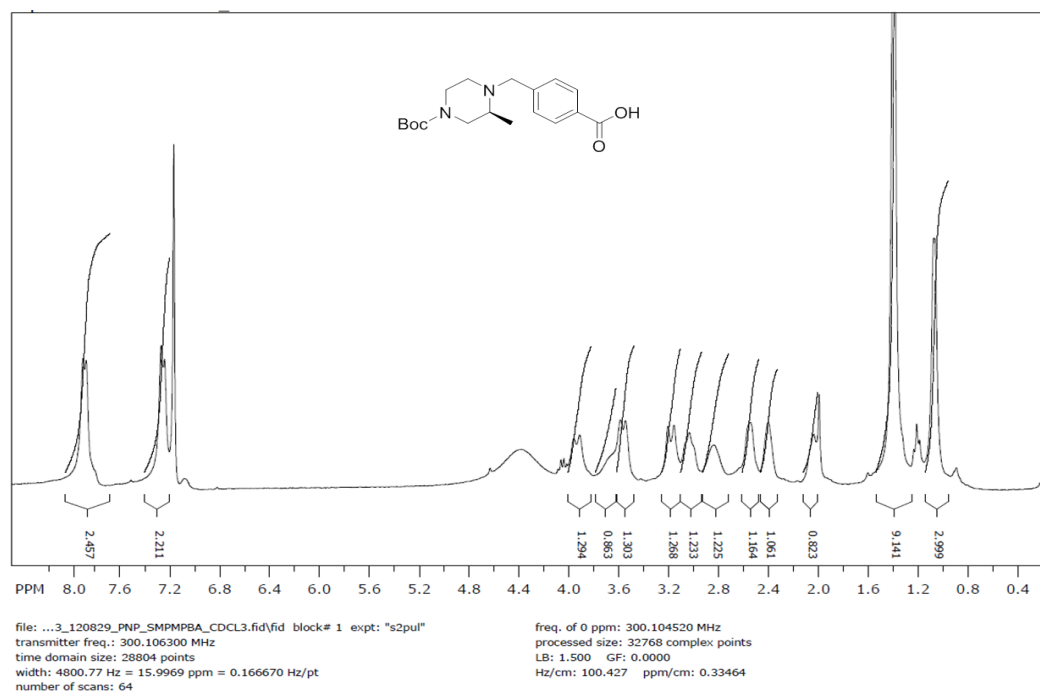
Figure A.21 NMR:(R)-4-((4-(tert-butoxycarbonyl)-2-methylpiperazin-1-yl)methyl)benzoic acid

Figure A.22 MS: 4-(((1-(tert-butoxycarbonyl)piperidin-4-yl)(methyl)amino)methyl)benzoic acid

Figure A.23 NMR: 4-(((1-(tert-butoxycarbonyl)piperidin-4-yl)(methyl)amino)methyl)benzoic acid
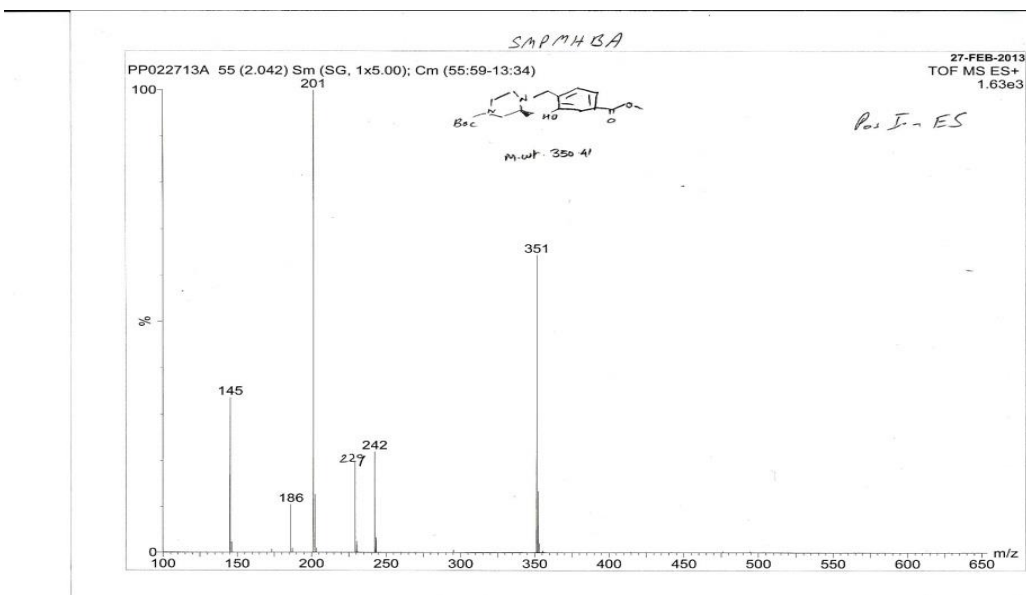
Figure A.24 MS: (S)-4-((4-(tert-butoxycarbonyl)-2-methylpiperazin-1-yl)methyl)-3-hydroxybenzoic acid
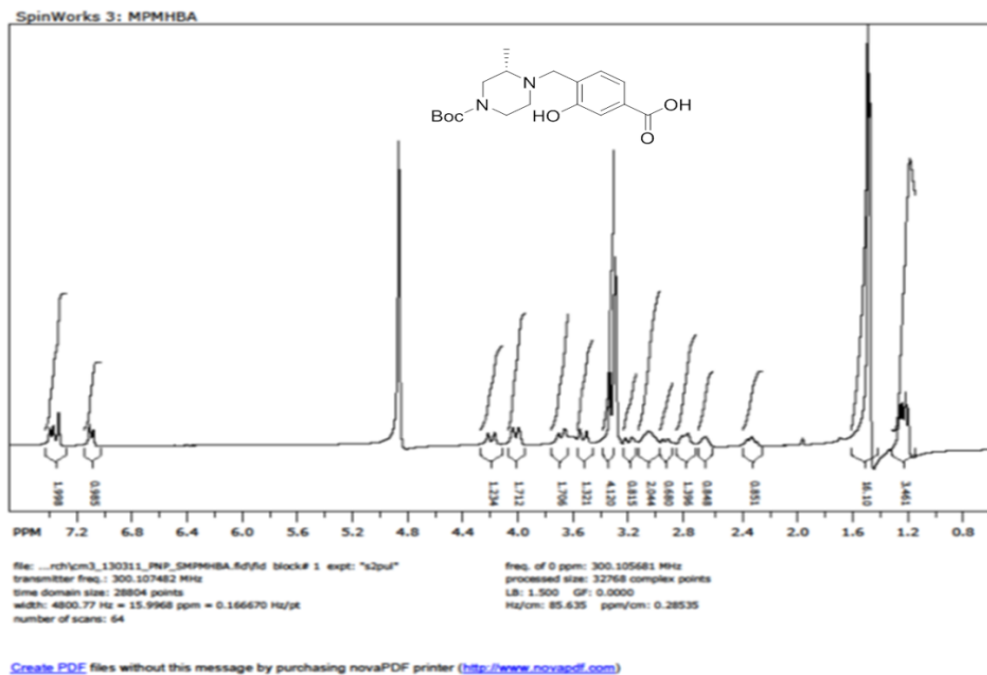
Figure A.25 NMR: (S)-4-((4-(tert-butoxycarbonyl)-2-methylpiperazin-1-yl)methyl)-3-hydroxybenzoic acid
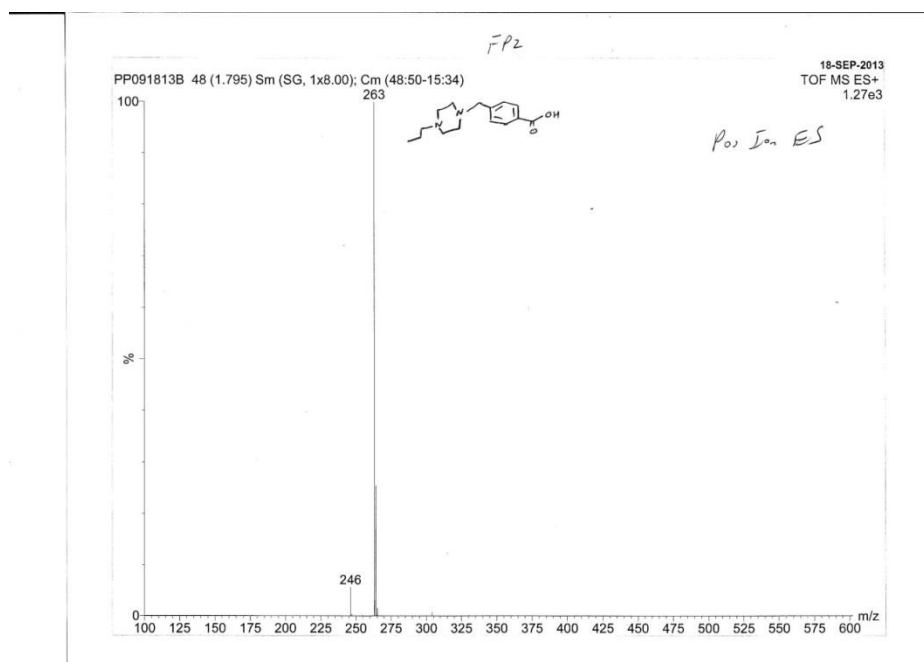
Figure A.26 MS: 4-((4-propylpiperazin-1-yl)methyl)benzoic acid
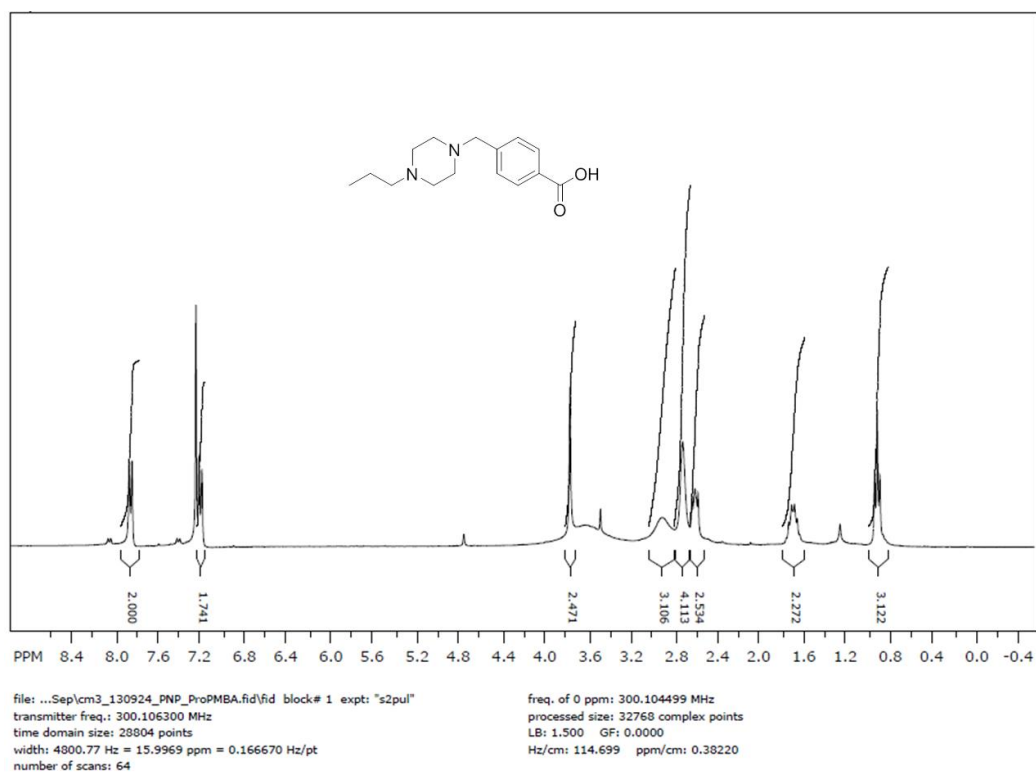
Figure A.27 NMR: 4-((4-propylpiperazin-1-yl)methyl)benzoic acid

Figure A.28 MS (S)-4-((2-methyl-4-ethylpiperazin-1-yl)methyl)benzoic acid

Figure A.29 NMR: (S)-4-((2-methyl-4-ethylpiperazin-1-yl)methyl)benzoic acid

Figure A.30 MS: 4-((1-methylpiperidin-4-ylidene)methyl)benzoic acid
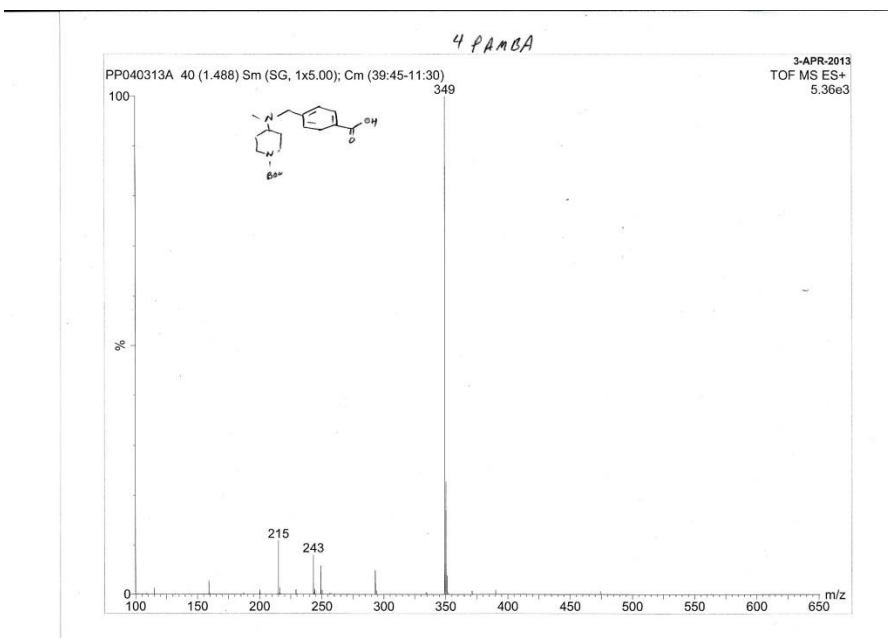
Figure A.31 NMR: 4-((1-methylpiperidin-4-ylidene)methyl)benzoic acid

Figure A.32 MS: 4-((1-(tert-butoxycarbonyl)piperidin-4-yl)methyl)benzoic acid

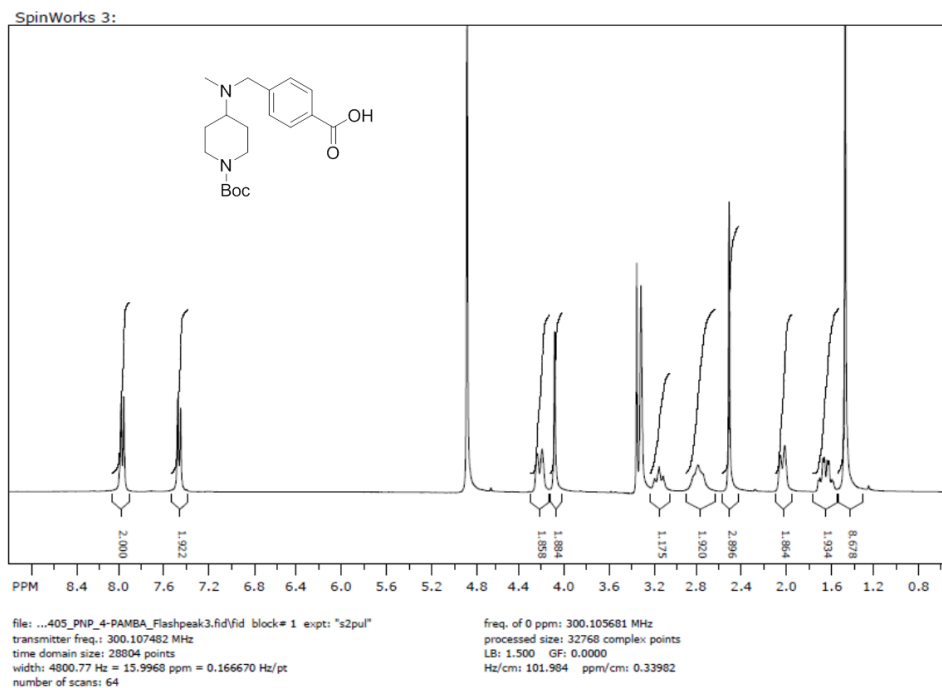Figure A.33 NMR: 4-((1-(tert-butoxycarbonyl)piperidin-4-yl)methyl)benzoic acid

APPENDIX B:

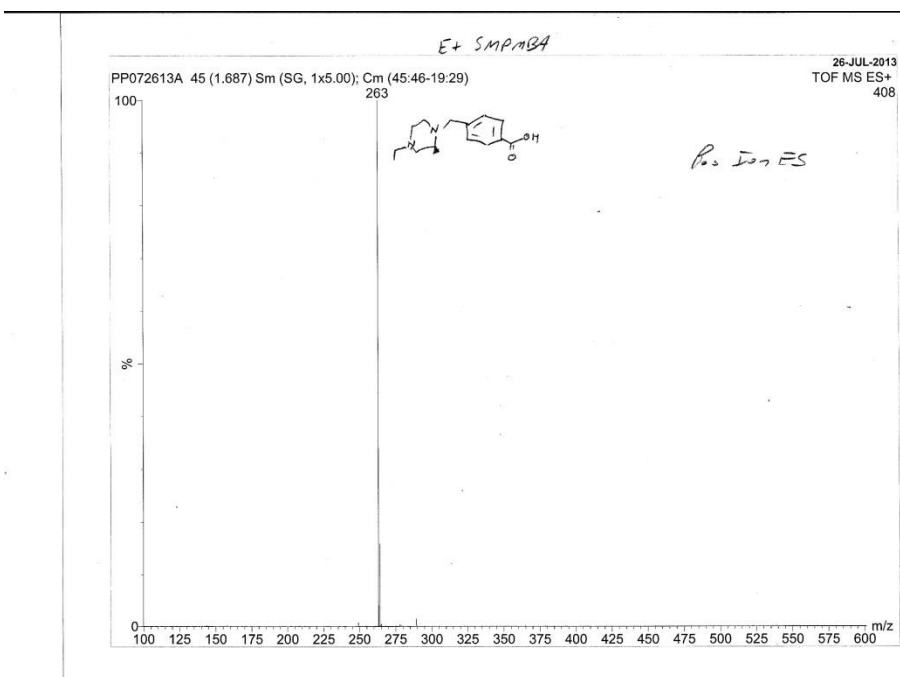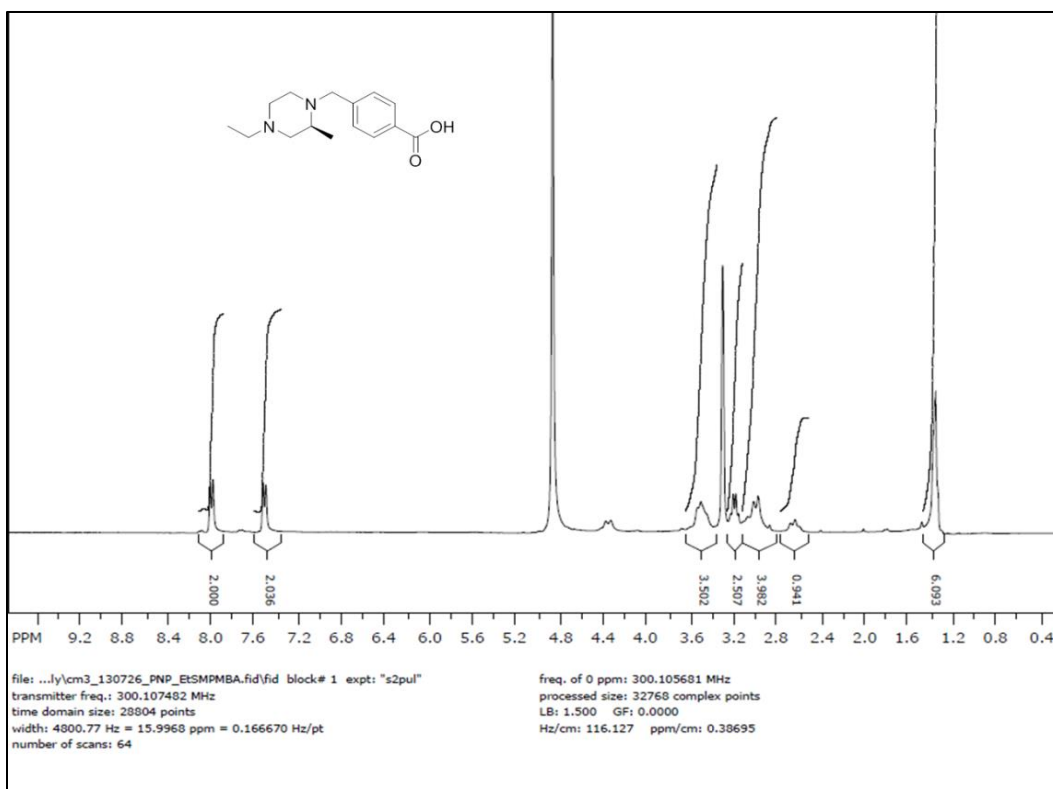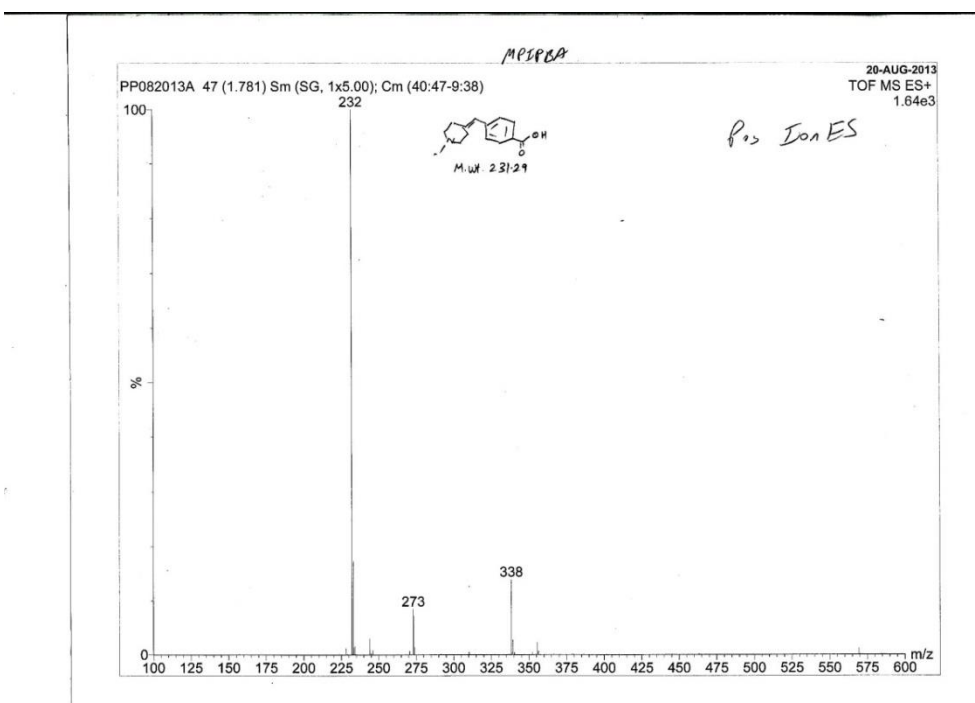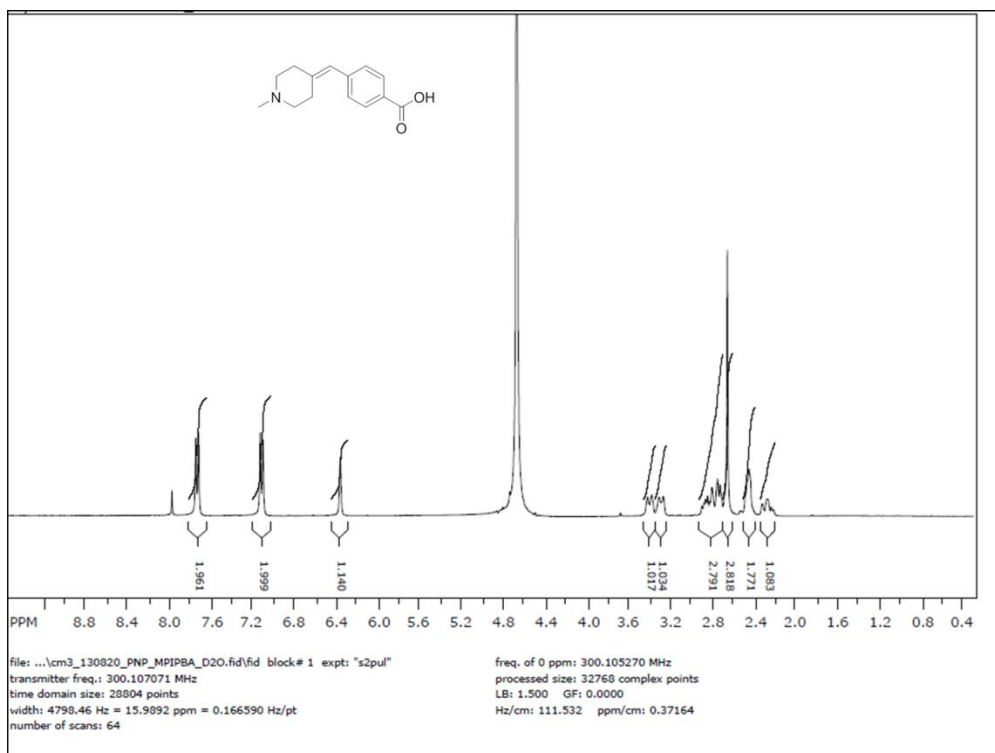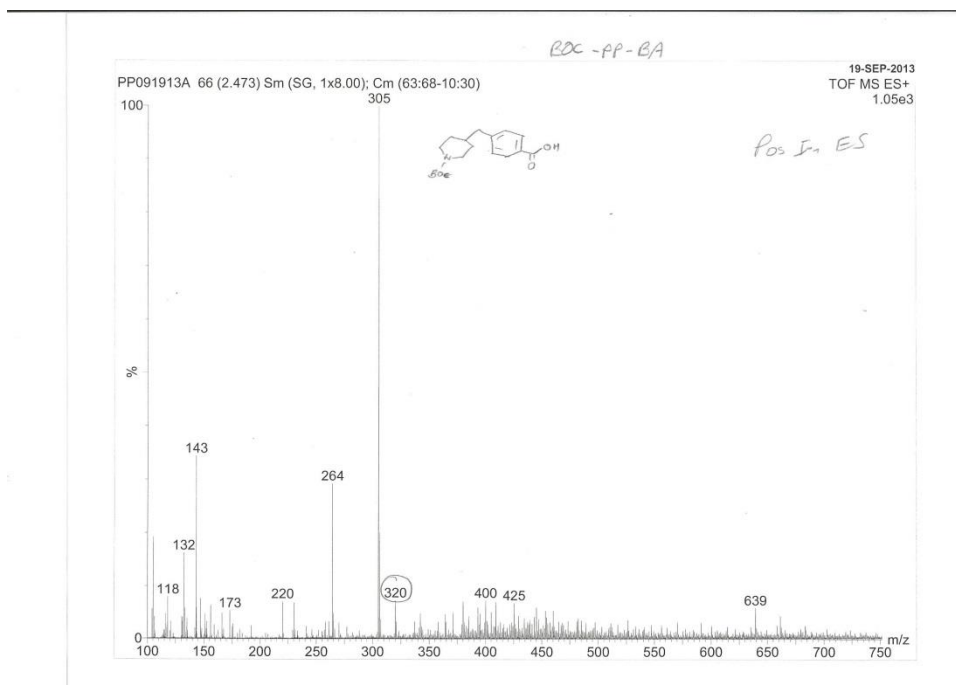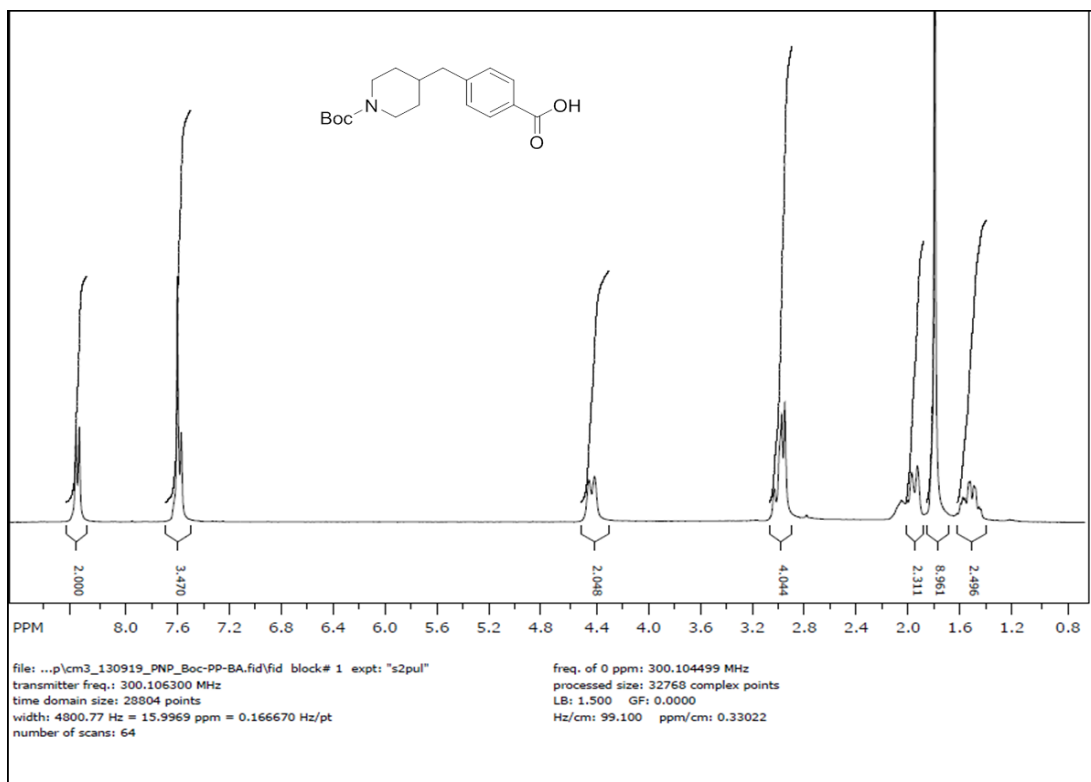## CHARACTERIZATION DATA OF FLIP MOLECULES

Table B.1 Analytical data for FLIPs based on phenyl heterocyclic carboxylic acid derivatives

FLIP	Purity	Column Dimensions	Method	Flow rate	HPLC Retention Time	Theoretical MW	Observed MW
5843	>90%	4.6 × 250 mm	5-65% acetonitrile/water/0.1%TFA	1ml/min	23.9	732	732.6
5773	>90%	4.6 × 250 mm	5-65% acetonitrile/water/0.1%TFA	1ml/min	22.4	801.77	800.55
5774	>90%	4.6 × 250 mm	5-65% acetonitrile/water/0.1%TFA	1ml/min	24.2	767.33	766.5
5762	>90%	4.6 × 250 mm	5-65% acetonitrile/water/0.1%TFA	1ml/min	9.0	731.91	731.65
5763	>90%	4.6 × 250 mm	5-65% acetonitrile/water/0.1%TFA	1ml/min	11.2	800.8	799.5
5764	>90%	4.6 × 250 mm	5-65% acetonitrile/water/0.1%TFA	1ml/min	10.1	766.34	765.55
5771	>90%	4.6 × 250 mm	5-65% acetonitrile/water/0.1%TFA	1ml/min	9.4	749.9	749.6
5765	>90%	4.6 × 250 mm	5-65% acetonitrile/water/0.1%TFA	1ml/min	10.1	766.35	755.65
5766	>90%	4.6 × 250 mm	5-65% acetonitrile/water/0.1%TFA	1ml/min	9.4	761.9	761.55
5767	>90%	4.6 × 250 mm	5-65% acetonitrile/water/0.1%TFA	1ml/min	20.4	761.9	761.55
5776	>75%	4.6 × 250 mm	5-65% acetonitrile/water/0.1%TFA	1ml/min	23.3	785.7	784.55
5775	>90%	4.6 × 250 mm	5-65% acetonitrile/water/0.1%TFA	1ml/min	9.9	751.34	750.45
5768	>90%	4.6 × 250 mm	5-65% acetonitrile/water/0.1%TFA	1ml/min	11.4	786.77	787.55
5769	>90%	4.6 × 250 mm	5-65% acetonitrile/water/0.1%TFA	1ml/min	22.9	752.3	751.55
5772	>90%	4.6 × 250 mm	5-65% acetonitrile/water/0.1%TFA	1ml/min	9.7	735.87	735.65
5770	>90%	4.6 × 250 mm	5-65% acetonitrile/water/0.1%TFA	1ml/min	10.4	752.32	751.55
5588	>90%	4.6 × 250 mm	5-65% acetonitrile/water/0.1%TFA	1ml/min	21.7	747.9	747.4
5587	>90%	4.6 × 250 mm	5-65% acetonitrile/water/0.1%TFA	1ml/min	22.5	731.9	731.4
5760	>90%	4.6 × 250 mm	5-65% acetonitrile/water/0.1%TFA	1ml/min	22.2	731.9	731.6
5852	>90%	4.6 × 250 mm	5-65% acetonitrile/water/0.1%TFA	1ml/min	19.2	735.69	735.4
5583	>90%	4.6 × 250 mm	5-65% acetonitrile/water/0.1%TFA	1ml/min	23.6	769.37	768.3

Table B.2 Analytical data for FLIPs based on thiazole, furan carboxylic acid, picolinic acid, phenylacetic acids

FLIP	Purity	Column Dimensions	Method	Flow rate	HPLC Retention Time	Theoretical MW	Observed MW
5581	>90%	4.6 × 250 mm	5-95% acetonitrile(0.05%TFA)/water(0.065%TFA)	1ml/min	18.58	726.9	727.4
5585	>90%	4.6 × 250 mm	5-95% acetonitrile(0.05%TFA)/water(0.065%TFA)	1ml/min	17.94	721.82	721.45
5584	>90%	4.6 × 250 mm	5-95% acetonitrile(0.05%TFA)/water(0.065%TFA)	1ml/min	21.48	740.95	740.4
5589	>90%	4.6 × 250 mm	5-95% acetonitrile(0.05%TFA)/water(0.065%TFA)	1ml/min	17.82	753.95	753.45
5586	>90%	4.6 × 250 mm	5-95% acetonitrile(0.05%TFA)/water(0.065%TFA)	1ml/min	21.83	721.86	721.35
5582	>90%	4.6 × 250 mm	5-95% acetonitrile(0.05%TFA)/water(0.065%TFA)	1ml/min	21.10	740.95	740.25
5761	>90%	4.6 × 250 mm	5-95% acetonitrile(0.05%TFA)/water(0.065%TFA)	1ml/min	7.21	735.9	735.55
5845	>90%	4.6 × 250 mm	5-95% acetonitrile(0.05%TFA)/water(0.065%TFA)	1ml/min	19.68	666.69	666.55
5856	>90%	4.6 × 250 mm	5-95% acetonitrile(0.05%TFA)/water(0.065%TFA)	1ml/min	19.81	735.69	737.0
5854	>90%	4.6 × 250 mm	5-95% acetonitrile(0.05%TFA)/water(0.065%TFA)	1ml/min	19.85	709.69	709.45
5855	>90%	4.6 × 250 mm	5-95% acetonitrile(0.05%TFA)/water(0.065%TFA)	1ml/min	11.71	737.69	737.45
5853	>90%	4.6 × 250 mm	5-95% acetonitrile(0.05%TFA)/water(0.065%TFA)	1ml/min	22.42	723.69	723.45

Table B.3 Analytical data for peptides and FLIPs derived from p21 and p107

Peptide	Purity	Column Dimensions	Method	Flow rate	HPLC Retention Time	Theoretical MW	Observed MW
540	>90%	4.6X250mm	5-95% acetonitrile(0.05%TFA)/water(0.065%TFA)	1.0ml/min	14.97	722.8	722.4
5811	>90%	4.6X250mm	5-95% acetonitrile(0.05%TFA)/water(0.065%TFA)	1.0ml/min	16.5	703.88	703.8
5812	>90%	4.6X250mm	5-95% acetonitrile(0.05%TFA)/water(0.065%TFA)	1.0ml/min	19.54	704.88	704.45
5831	>90%	4.6X250mm	5-95% acetonitrile(0.05%TFA)/water(0.065%TFA)	1.0ml/min	17.68	704.89	704.9
5832	>90%	4.6X250mm	5-95% acetonitrile(0.05%TFA)/water(0.065%TFA)	1.0ml/min	17.48	644.81	644.45
5833	>90%	4.6X250mm	5-95% acetonitrile(0.05%TFA)/water(0.065%TFA)	1.0ml/min	21.05	618.77	618.4
5871	>90%	4.6X250mm	5-95% acetonitrile(0.05%TFA)/water(0.065%TFA)	1.0ml/min	14.81	647.77	647.9
5873	>90%	4.6X250mm	5-95% acetonitrile(0.05%TFA)/water(0.065%TFA)	1.0ml/min	18.02	604.74	604.45
5874	>90%	4.6X250mm	5-95% acetonitrile(0.05%TFA)/water(0.065%TFA)	1.0ml/min	14.36	590.72	590.45
5875	>90%	4.6X250mm	5-95% acetonitrile(0.05%TFA)/water(0.065%TFA)	1.0ml/min	15.15	604.7	605.1
5876	>90%	4.6X250mm	5-95% acetonitrile(0.05%TFA)/water(0.065%TFA)	1.0ml/min	14.84	661.5	661.55
5941	>90%	4.6X250mm	5-95% acetonitrile(0.05%TFA)/water(0.065%TFA)	1.0ml/min	16.51	618.78	618.25
5925	>90%	4.6X250mm	5-95% acetonitrile(0.05%TFA)/water(0.065%TFA)	1.0ml/min	16.8	716.9	717.4
5930	>90%	4.6X250mm	5-95% acetonitrile(0.05%TFA)/water(0.065%TFA)	1.0ml/min	16.63	618.72	617.9
5918	>90%	4.6X250mm	5-95% acetonitrile(0.05%TFA)/water(0.065%TFA)	1.0ml/min	17.09	703.87	703.4
5877	>90%	4.6X250mm	5-95% acetonitrile(0.05%TFA)/water(0.065%TFA)	1.0ml/min	17.69	675	676
5878	>90%	4.6X250mm	5-95% acetonitrile(0.05%TFA)/water(0.065%TFA)	1.0ml/min	21.22	681	681.4
5879	>90%	4.6X250mm	5-95% acetonitrile(0.05%TFA)/water(0.065%TFA)	1.0ml/min	17.2	689.87	689.6
5815	>90%	4.6X250mm	5-95% acetonitrile(0.05%TFA)/water(0.065%TFA)	1.0ml/min	15.71	934.1	934.6
5814	>90%	4.6X250mm	5-95% acetonitrile(0.05%TFA)/water(0.065%TFA)	1.0ml/min	13.14	940.14	940
5820	>90%	4.6X250mm	5-95% acetonitrile(0.05%TFA)/water(0.065%TFA)	1.0ml/min	11.13	948.12	948.2
5813	>90%	4.6X250mm	5-95% acetonitrile(0.05%TFA)/water(0.065%TFA)	1.0ml/min	13.36	953.14	953.9
5816	>90%	4.6X250mm	5-95% acetonitrile(0.05%TFA)/water(0.065%TFA)	1.0ml/min	17.1	1046.4	1046.4
444	>90%	4.6X250mm	5-95% acetonitrile(0.05%TFA)/water(0.065%TFA)	1.0ml/min	14.84	1040.27	1040.3
5557	>90%	4.6X250mm	5-95% acetonitrile(0.05%TFA)/water(0.065%TFA)	1.0ml/min	15.97	1023.22	1023.2
5558	>90%	4.6X250mm	5-95% acetonitrile(0.05%TFA)/water(0.065%TFA)	1.0ml/min	13.9	891.03	890.5
5559	>90%	4.6X250mm	5-95% acetonitrile(0.05%TFA)/water(0.065%TFA)	1.0ml/min	16.5	980.19	980.1
5564	>90%	4.6X250mm	5-95% acetonitrile(0.05%TFA)/water(0.065%TFA)	1.0ml/min	15.94	1064.31	1064.45

Table B.4 Analytical data for FLIPs based on benzoic acid derivatives

SCCP ID	Purity	Column Dimensions	Method	Flow rate	HPLC Retention Time	Theoretical MW	Observed MW
5857	>90%	4.6 × 250 mm	5-65% acetonitrile/water/0.1%TFA	1ml/min	22.36	651.69	651.4
5858	>90%	4.6 × 250 mm	5-65% acetonitrile/water/0.1%TFA	1ml/min	10.3	681.69	681.4
5844	>90%	4.6 × 250 mm	5-65% acetonitrile/water/0.1%TFA	1ml/min	12.93	723.92	723.6
5846	>90%	4.6 × 250 mm	5-65% acetonitrile/water/0.1%TFA	1ml/min	21.01	743.5	743.55
5882	>90%	4.6 × 250 mm	5-65% acetonitrile/water/0.1%TFA	1ml/min	20.66	695.86	695.5
5883	>90%	4.6 × 250 mm	5-65% acetonitrile/water/0.1%TFA	1ml/min	22.65	709.89	709.5
5851	>90%	4.6 × 250 mm	5-65% acetonitrile/water/0.1%TFA	1ml/min	20.65	749.69	750.45
5850	>90%	4.6 × 250 mm	5-65% acetonitrile/water/0.1%TFA	1ml/min	19..79	734.69	736.4
5896	>90%	4.6 × 250 mm	5-65% acetonitrile/water/0.1%TFA	1ml/min	21.22	779.5	780.55
5919	>90%	4.6 × 250 mm	5-65% acetonitrile/water/0.1%TFA	1ml/min	17.74	749.7	749.4
5923	>90%	4.6 × 250 mm	5-65% acetonitrile/water/0.1%TFA	1ml/min	19.52	664.59	664.29
5920	>90%	4.6 × 250 mm	5-65% acetonitrile/water/0.1%TFA	1ml/min	17.44	765.7	765.1
5922	>90%	4.6 × 250 mm	5-65% acetonitrile/water/0.1%TFA	1ml/min	19.14	808.69	807.5
5921	>90%	4.6 × 250 mm	5-65% acetonitrile/water/0.1%TFA	1ml/min	17.99	763.7	763.2
5965	>90%	4.6 × 250 mm	5-65% acetonitrile/water/0.1%TFA	1ml/min	19.55	665.69	665.5
5966	>90%	4.6 × 250 mm	5-65% acetonitrile/water/0.1%TFA	1ml/min	17.02	680.69	708.5
5968	>90%	4.6 × 250 mm	5-65% acetonitrile/water/0.1%TFA	1ml/min	18.81	708.69	708.5
5967	>90%	4.6 × 250 mm	5-65% acetonitrile/water/0.1%TFA	1ml/min	17.8	760.69	761.6
5969	>90%	4.6 × 250 mm	5-65% acetonitrile/water/0.1%TFA	1ml/min	18.19	678.69	678.75
5970	>90%	4.6 × 250 mm	5-65% acetonitrile/water/0.1%TFA	1ml/min	17.87	679.54	678.55
6033	>90%	4.6 × 250 mm	5-65% acetonitrile/water/0.1%TFA	1ml/min	16.37	683.94	684.4
6034	>90%	4.6 × 250 mm	5-65% acetonitrile/water/0.1%TFA	1ml/min	16.07	697.97	698.3
6031	>90%	4.6 × 250 mm	5-65% acetonitrile/water/0.1%TFA	1ml/min	17.14	653.28	653.2
6032	>90%	4.6 × 250 mm	5-65% acetonitrile/water/0.1%TFA	1ml/min	18.28	722.09	721.25